



Soil moisture dynamics
and land surface-atmosphere interaction

Adriaan J. Teuling

Promotoren

Prof.dr.ir. P. A. Troch

Hoogleraar Hydrologie en Kwantitatief Waterbeheer (1999–2005)
Wageningen Universiteit

Professor of Hydrology and Water Resources
Professor of Civil Engineering and Engineering Mechanics
University of Arizona (Tucson, AZ, USA)

Prof.dr.ir. R. Uijlenhoet

Hoogleraar Hydrologie en Kwantitatief Waterbeheer
Wageningen Universiteit

Samenstelling promotiecommissie

Prof.dr.ir. M. F. P. Bierkens, Universiteit Utrecht

Prof.dr. W. J. Shuttleworth, University of Arizona (Tucson, AZ, USA)

Prof.dr. S. I. Seneviratne, ETH Zurich (Switzerland)

Prof.dr.ir. S. E. A. T. M. van der Zee, Wageningen Universiteit

Dit onderzoek is uitgevoerd binnen de onderzoekschool SENSE

Soil moisture dynamics and land surface-atmosphere interaction

Adriaan J. Teuling

Proefschrift
ter verkrijging van de graad van doctor
op gezag van de rector magnificus
van Wageningen Universiteit,
Prof.dr. M. J. Kropff
in het openbaar te verdedigen
op dinsdag 23 oktober 2007
des namiddags te vier uur in de Aula.

CIP-data Koninklijke Bibliotheek, Den Haag

Soil moisture dynamics and land surface-atmosphere interaction

Teuling, A. J., 2007

PhD thesis, Wageningen University, The Netherlands
With references - with summaries in English and Dutch

ISBN 978-90-8504-736-0

Abstract

This thesis deals with aspects of the spatial and temporal variability of soil moisture in relation to atmospheric conditions. It is first illustrated that the combination of seasonality in atmospheric forcing and non-linearity in the relation between soil moisture and the losses from the soil moisture reservoir result in a bimodal temporal distribution. Next, the impact of root water uptake on the coupled dynamics of soil moisture and evapotranspiration is investigated by a dimensionless analytical model. Subsequently, observations of evapotranspiration are used to study characteristic soil moisture response times under water-limited conditions for different biomes. Typically, these values are in the order of 15–25 days. In order to investigate the accuracy with which areal soil moisture can be estimated from a limited number of point-scale observations, rank stability analysis is applied to different field- or catchment-scale soil moisture datasets. It is shown that temporal changes in the spatial soil moisture distribution prevent perfect rank stability. Covariance analysis of Monte-Carlo simulations reveals that these changes in spatial soil moisture variability are caused by spatially variable root water uptake during drydown, and drainage during (re)wetting. These simulations also reveal that the nonlinear relation between soil moisture and evapotranspiration in combination with climate variability induces hysteresis (i.e., non-uniqueness) in the relation between mean soil moisture and its variability. A linear analytical model is used to characterize space-time variability of surface soil moisture fields in response to minor rainfall events. The results are in good agreement with observations made during a recent field experiment conducted under very dry conditions.

Voorwoord

Voor u ligt mijn proefschrift, het concrete resultaat van mijn promotie-onderzoek. Ondanks het feit dat er vele jaren werk in dit boekje zitten, is het toch een relatief dun boekje geworden. Omgerekend komt dit overeen met ongeveer één pagina inhoud per maand. Compact is niet per se makkelijker om te schrijven, en het gezegde “schrijven is schrappen” is dan ook zeker opgegaan tijdens het schrijven van dit proefschrift. Ik ben me ervan bewust dat het de leesbaarheid niet per se ten goede komt, zeker niet voor mensen die niet bekend zijn met de terminologie van de landoppervlakte-hydrologie. Desalniettemin hoop ik toch dat u dit proefschrift met plezier en interesse zult lezen.

In september 2002 begon ik aan mijn onderzoek, aanvankelijk onder begeleiding van Peter Troch, Eddy Moors en Emiel van Loon. De grotere fysieke afstand tot Eddy bleek helaas al snel een belemmering te zijn voor intensieve samenwerking. Emiel was in de opstartfase een belangrijke vraagbaak, maar hij verruilde Wageningen al snel voor de UvA. Na de zomer van 2005, toen ik net halverwege mijn onderzoek gevorderd was, verruilde Peter Wageningen voor het zonnige Tucson. Hoewel er regelmatig e-mail contact bleef, betekende dit helaas het einde van de vaak uitgebreide en inspirerende discussies.

In de tussentijd was er een groeiende samenwerking met Remko Uijlenhoet op gang gekomen. Na het vertrek van Peter nam Remko dan ook als vanzelfsprekend een belangrijk gedeelte van de dagelijkse begeleiding over. De geringe afstand tot Remko’s werkplek heeft hier zeker een belangrijke rol in gespeeld. De samenwerking met Remko heeft uiteindelijk ook geresulteerd in een gedeeld promotorschap. Dankzij een lang bezoek aan Tucson in het voorjaar van 2007 was Peter toch nog nauw betrokken bij de afronding van mijn onderzoek.

Mede door (of dankzij) de eerder genoemde omstandigheden heb ik zelf richting kunnen en moeten geven aan het onderzoek. Het ontbreken van een vast onderzoekskader had als gunstige bijkomstigheid dat ik kon inspelen op recente publicaties. Zo verscheen in 2003 een paper van John Albertson en Nicola Montaldo in *Water Resources Research*, dat de mathematische achtergrond beschreef van temporele veranderingen in de ruimtelijke variatie van bodemvocht. Hoewel ik toen al bijna een jaar gevorderd was met mijn onderzoek, is dit paper uiteindelijk een belangrijke inspiratiebron gebleken voor de laatste drie hoofdstukken van dit proefschrift. Maar ook heb ik dankbaar gebruik gemaakt van de kans om te reageren op het paper van Paolo D’Odorico en Amilcare Porporato dat in 2004 verscheen in de *Proceedings of the National Academy of Sciences of the United States of America*.

In 2004 werden ikzelf en Hidde Leijnse door Peter betrokken in de organisatie van de tweede CAHMDA workshop, die in oktober van dat jaar plaats had in Princeton bij de groep van Eric Wood. Hoewel de organisatie een forse hoeveelheid tijd kostte, was het een zeer leerzame ervaring. De \LaTeX kennis die ik heb opgedaan met de opmaak van het boek of abstracts is me bij dit proefschrift goed van pas gekomen. Ook ontmoette ik Sonia Seneviratne tijdens CAHMDA. Dit resulteerde in een kort bezoek aan het ETH in Zürich in het najaar van 2005, waar de basis werd gelegd voor een gezamenlijke publicatie.

In het najaar van 2006 kregen Ruud Hurkmans en ik de mogelijkheid om deel te nemen aan NAFE’06, een veldexperiment in Australië dat werd georganiseerd door de groep van Jeff Walker aan de University of Melbourne. Naast een prachtige ervaring leverde NAFE’06 ook een mooie dataset op, waarvan een gedeelte nog in dit proefschrift verwerkt kon worden. Ik ben de Nederlandse Organisatie voor Wetenschappelijk Onderzoek (NWO) erkentelijk voor de financiële steun aan onze deelname in de vorm van twee reisbeurzen. I also thank all NAFE’06 participants for their efforts in collecting the soil moisture data, and Olivier Merlin and Rocco Panciera for rapidly making the data available to me.

In this thesis I have used data from many sources, and I wouldn’t have been able to do this research using only the publicly accessible ones. Several people readily provided me with their data, namely: François Hupet (now at Baxter BioScience, Belgium), John Albertson (Duke University, USA), Mehdi Homaei (University of Tarbiat Modarres, Iran), John Hunt (Landcare Research, New Zealand), Keith Loague (Stanford University, USA), Dirk Schüttemeyer (German National Committee on Global Change Research), Anne Verhoef (University of Reading, UK), Chris Williams (University of Maryland, USA), and Marita Voogt (KNMI). Especially Francois’ data turned out to be an important source of inspiration for several papers. Although our contact went mainly

via e-mail, the collaboration was fruitful. Also, I thank my co-authors and the anonymous reviewers for their efforts in correcting and improving the various papers.

Vooral mijn kamergenoten Emiel, later Shaakeel en nog weer later Hidde, heb ik regelmatig lastigvallen met de meest uiteenlopende, vaak technische, vragen. Ik heb veel gehad aan jullie kennis en behulpzaamheid! Patrick, bedankt voor al de levendige discussies en je hulp met PCRaster. Emiel, Hidde, Remko, Shaakeel en Tessa: koffie was nooit zo goed als op de Nieuwlanden! Henri, bedankt voor je hulp bij het maken van de omslag. Jascha en Hans, bedankt dat jullie als mijn paranimfen op willen treden! Dionne, Olivier, and Ruud: we made a great team! I enjoyed being out with you in the field. If it wasn't for the snakes and spiders, I could still be out there sampling! Verder wil ik iedereen bedanken die ik hier nu vergeten ben, maar die, op wat voor manier dan ook, toch heeft bijgedragen aan de totstandkoming van dit proefschrift.

Mijn lieve Moniek: het is eindelijk af! Bedankt voor al je steun en geduld. Nu is de beurt aan jou! Ik hoop dat ik je kan helpen zoals je mij geholpen hebt!

Ryan Teuling

Zürich, september 2007.

Contents

1. Prologue	1
1.1. About the cover	1
1.2. Problem outline	1
1.3. This thesis	4
2. On bimodality in warm season soil moisture observations	5
2.1. Introduction	5
2.2. Effects of seasonality	5
2.3. Characterizing wet and dry modes	8
2.4. Discussion and Conclusions	9
3. Impact of plant water uptake strategy on soil moisture and evapotranspiration dynamics during drydown	11
3.1. Introduction	11
3.2. A field example	12
3.3. Modeling root water uptake	12
3.4. Evapotranspiration decay	13
3.5. Soil moisture decay	14
3.6. Root zone aggregation	16
3.7. Discussion and Conclusions	16
4. Observed timescales of evapotranspiration response to soil moisture	17
4.1. Introduction	17
4.2. Data	18
4.3. Theory	18
4.4. Results	19
4.4.1. Observations	19
4.4.2. GSWP-2 simulations	21
4.5. Discussion and Conclusions	21
5. Estimating spatial mean root-zone soil moisture from point-scale observations	23
5.1. Introduction	23
5.2. Data	24
5.3. Method	26
5.3.1. Notation	26
5.3.2. Soil moisture distribution	26
5.3.3. Mean soil moisture estimation	26
5.3.4. Mean soil moisture time series estimation	27
5.3.5. A priori site selection	29
5.4. Results	29
5.4.1. Soil moisture distribution	29
5.4.2. Mean soil moisture estimation	29
5.4.3. Mean soil moisture time series estimation	32
5.4.4. A priori site selection	33
5.5. Discussion and Conclusions	33

CONTENTS

6. Improved understanding of soil moisture variability dynamics	35
6.1. Introduction	35
6.2. Data	35
6.3. Modeling variability	36
6.3.1. Point-scale soil moisture dynamics	36
6.3.2. Spatial closure	37
6.3.3. Total simulated variability	38
6.4. Analysis and Results	38
6.5. Discussion and Conclusions	40
7. Dry-end surface soil moisture variability during the National Airborne Field Experiment 2006	41
7.1. Introduction	41
7.2. Data	41
7.3. Temporal dynamics	42
7.4. Mean versus variability	45
7.5. Steady state distribution	45
7.6. Discussion and Conclusions	46
8. Climate variability effects on spatial soil moisture dynamics	47
8.1. Introduction	47
8.2. Data	47
8.3. Model	48
8.4. Analysis and Results	49
8.5. Discussion and Conclusions	52
9. Epilogue	53
9.1. General discussion	53
9.2. Directions for further research	54
A. Time integration of gravitational drainage	55
B. Integration of double exponential with linear term	56
C. Integration of double exponential without linear term	57
D. Regression results for GSWP-2 simulations	58
E. Mean and variance for sum of densities	59
F. Summary of the NAFE'06 soil moisture observations	60
G. Derivation of soil moisture distribution	61
Summary	63
Samenvatting	65
Bibliography	67
Curriculum Vitae	75
List of publications	76

List of Figures

1.1. Schematic representation of the hydrological cycle.	3
1.2. Ranges of spatial and temporal scales of common hydrological processes.	3
1.3. Scaling triplet.	4
2.1. Map of Illinois and location of the WARM sites.	6
2.2. Climatology of Illinois for the years 1989–2004.	7
2.3. Simulated soil moisture distribution.	9
2.4. Effect of active soil depth on the soil moisture distribution.	10
2.5. Simulated and ERA40 soil moisture distribution.	10
3.1. Root water uptake in an experimental field in Louvain-la-Neuve.	12
3.2. Relative impact of uptake strategy on evaporative flux and soil moisture.	15
3.3. Scaled relations between root water uptake and average soil moisture.	15
3.4. Analytical and simulated relations between root water uptake and soil moisture.	16
4.1. Location of the study sites.	18
4.2. Daily evapotranspiration for different sites under rainless conditions.	22
4.3. Distribution of evapotranspiration decay time for the GSWP-2 models.	22
5.1. Location of the study areas and observation sites.	25
5.2. Normal probability plot of the normalized soil moisture fields.	30
5.3. Relative standard error as a function of the number of observations.	30
5.4. Rank stability plots for the three datasets.	31
5.5. Land surface characteristics versus versus mean soil moisture difference.	32
5.6. Differences between local soil moisture and the spatial mean for Louvain-la-Neuve.	34
6.1. Location of observation sites.	36
6.2. Distribution of wetness index.	37
6.3. Observed and simulated soil moisture variability versus mean soil moisture content.	39
6.4. Vegetation, soil, and landscape contributions to change in spatial variance.	39
7.1. Map of the Yanco region.	42
7.2. Precipitation and soil moisture during NAFE'06.	44
7.3. Relation between spatial mean and variability of surface soil moisture.	44
7.4. Steady-state distribution of field-scale mean surface soil moisture.	46
8.1. Location of the field and experimental setup.	48
8.2. Observed and simulated soil moisture variability.	50
8.3. Vegetation and soil contributions to variance budget.	50
8.4. Relation between mean and variability for the years 1989 and 2002.	51
8.5. Location of the field and experimental setup.	52
G.1. Definition of the model.	61

List of Tables

4.1. Summary of the datasets and results of the regression analysis.	20
5.1. Sampling strategies and corresponding uncertainties.	28
6.1. Parameter values used to simulate soil moisture variability.	38
7.1. Parameters and their values.	45
D.1. Regression results for GSWP-2 simulations.	58
F.1. Summary of the NAFE'06 soil moisture observations.	60

1. Prologue

1.1. About the cover

The cover picture was taken by the author on 13 November 2006, during the National Airborne Field Experiment (NAFE'06, see Chap. 7) in New South Wales, Australia. The field is located in the Coleambally Irrigation Area (CIA). The CIA is one of the largest irrigated land settlement schemes in Australia and was established during the 1960's. From 2001 onwards, the region suffered from serious drought conditions. In large parts of New South Wales and the Murray Darling basin, the multi-year rainfall deficiencies were among the highest ever recorded. For the Murray Darling basin, 2006 was the third driest year on record, and New South Wales experienced its fifth warmest year on record for statewide averaged mean temperatures. As a result, farmers were confronted with severe water restrictions being imposed, resulting in significant harvest reduction. While summer droughts are an inherent part of natural climate variability, it is expected that both their frequency and intensity will increase under global warming. This can have profound physical, ecological, social, and economic consequences. The cover picture illustrates the central role of soil moisture in the human perception of droughts: dry, crusted soils, covered with wilted, yellowish crops.

1.2. Problem outline

The hydrological or water cycle (Fig. 1.1) forms a key part of the global climate system. Water has several unique properties that are of importance to climate, especially its high latent heat of fusion ($3.34 \cdot 10^5 \text{ J kg}^{-1}$) and latent heat of vaporization ($2.50 \cdot 10^6 \text{ J kg}^{-1}$). Since vaporization involves the breakage of hydrogen bonds, its latent heat is much larger than the latent heat of fusion. The large latent heat of vaporization consumes much of the incoming solar radiation at the Earth's surface wherever water is present. As a result, temperature cycles are generally more pronounced in waterless regions (deserts) than in humid regions.

The hydrological cycle is most intense over the oceans. Despite the net water vapor flux from the oceans to the continents, most of the continental precipitation originates from terrestrial evapotranspiration. Most of this evapotranspiration takes place through plants' stomata (Fig. 1.1), although evaporation from interception can be significant (*Dolman and Gregory, 1992; Savenije, 2004*). Plant roots play a key role in the climate by their ability to extract soil moisture from the whole soil profile. In this way, they prevent percolation of precipitation to the groundwater. In fact, most (59%) of the precipitation that falls over the continents is returned to the atmosphere through evapotranspiration. Despite its central place in the hydrological cycle, the soil moisture storage constitutes only a very small part of the total water reserves on Earth (Fig. 1.1).

Plants rely on the availability of water for photosynthesis, and they adjust their stomatal resistance to water transfer according to the availability of soil moisture. Since plants have evolved over millions of years, their stomata are optimized to local climate (see *Hetherington and Woodward, 2003*, for a review). The adaptation of vegetation to climate is most noticeable in ecosystems where water is a limiting resource. For instance, the woody cover in savannas and species distribution in tropical forests are known to be governed by water availability (*Sankaran et al., 2005; Engelbrecht et al., 2007*). In the Amazon, evergreen forests have developed deep roots to maintain green canopy and high evapotranspiration rates during the dry season (*Nepstad et al., 1994*). In the Mojave desert, vegetation is adapted to interannual climate variability and rapidly adjusts its productivity to the available rainfall (*Scanlon et al., 2005*). *Huxman et al. (2004)* report that different biomes tend towards a constant rain use efficiency that is determined by the minimum yearly rainfall. This shows that there exists a close link between soil moisture, transpiration, vegetation, and climate. Models should reproduce this link correctly.

The development of numerical models of the global climate system (so-called Global Circulation Models, GCMs), have enabled scientists to study the impact of land surface conditions and soil moisture on the global climate. For example, it is known that rooting depth is one of the critical parameters in the climate system

PROLOGUE

(Zeng *et al.*, 1998). A small increase in rooting depth can potentially compensate increased temperatures due to increased atmospheric CO₂ levels (Milly, 1997). Soil moisture is not only directly affected by atmospheric conditions (most directly through precipitation), it can in turn also affect these atmospheric conditions through its control on the surface energy balance. The resulting positive feedback (i.e., lower rainfall leads to lower soil moisture and evaporation, and lower evaporation to lower precipitation) can increase the duration and intensity of climate extremes at sub-continental scales. Experiments with GCMs have successfully isolated the effect of this feedback on droughts (e.g., Hong and Kalnay, 2000; Schubert *et al.*, 2004), heatwaves (e.g., Seneviratne *et al.*, 2006a), and floods (e.g., Pal and Eltahir, 2002). The strength of the feedback is most noteworthy in mid-continental regions with transitional climate (Koster *et al.*, 2004). The presence of groundwater might amplify wet and dry anomalies at longer (interannual) timescales (Bierkens and van den Hurk, 2007).

Since soil moisture directly controls fluxes of water and energy at the land surface, it is an important variable in most environmental (land surface) models (LSMs) such as those used for weather and climate prediction, groundwater flow, rainfall-runoff, and crop growth. In order to simulate soil moisture, models need atmospheric forcing, initial conditions, and parameter values at every spatial grid point. For forecasting, near-realtime soil moisture fields are required as initial condition. Three problems associated with soil moisture modeling have received considerable attention in the recent literature: the problem of parameter identification, spatial representativeness, and initialization.

Firstly, models need calibration in order to make realistic predictions. For instance, calibrated soil parameters can significantly improve evapotranspiration estimates with respect to soil parameters derived from soil maps by pedotransfer functions (Soet and Stricker, 2003; Gutmann and Small, 2007). As a result, the predictive skill of uncalibrated LSMs is poor, and different LSMs can produce (very) different results (Soet *et al.*, 2000). Reduction of predictive uncertainty has been recognized as a key research challenge in the IAHS Prediction in Ungauged Basins (PUB) initiative. One way of reducing this uncertainty is by developing robust parameterizations (i.e., having little sensitivity to parameter values). A more pragmatic solution is to use different models in an ensemble mode, and assume that the ensemble mean is more realistic than any of the ensemble members (e.g., Dirmeyer *et al.*, 2006b). While the key water- and energy fluxes at a particular site are related to only very few climate variables (Abramowitz, 2005), the number of (uncertain) parameters in LSMs has increased dramatically over the past decades. In such underdetermined systems, different parameters sets can produce similar results: a principle known in hydrology as equifinality (e.g., Schulz and Beven, 2003).

The second issue is that of spatial representativeness. Parameterizations are generally validated at the point-scale, while LSMs are applied at grid sizes up to the regional scale. In this case, LSMs need to account for the effects of small-scale heterogeneities affecting non-linear processes within their parameterizations, in order to maintain correct grid-average fluxes by upscaling or so-called closure schemes (Kim and Stricker, 1996; Kim *et al.*, 1997; Giorgi and Avissar, 1997). For example, LSMs applied at the catchment scale need closure schemes for highly variable and nonlinear processes that occur at smaller scales such as interception, infiltration and root water uptake (see Fig. 1.2). The development of such closure schemes is complex (Regianni *et al.*, 1999; Montaldo and Albertson, 2003), and requires a thorough understanding of the small-scale heterogeneities (Western *et al.*, 2002).

A third problem is the current lack of soil moisture observations required for initialization. Soil moisture observations can either be made in situ or by remote sensing (for reviews of methods see Schmugge *et al.*, 1980; Njoku and Entekhabi, 1996; Walker *et al.*, 2004; Kerr, 2007). Each technique has its own spatial support and uncertainty (noise), and is generally applied with different spatial extent and spacing. This so-called scale triplet is illustrated in Fig. 1.3. Remote sensing techniques have the major advantage of their areal coverage, but the penetration depth is limited and validation problematic. The upcoming Soil Moisture and Ocean Salinity mission (SMOS, see Kerr *et al.*, 2001) will deliver global soil moisture with a regional-scale support, but with a sensing depth of only a few cm. In situ techniques can be applied to the whole profile, but their spatial support is limited. Currently, there is no dedicated soil moisture satellite mission, and in situ soil moisture networks exist only in few regions (e.g., Hollinger and Isard, 1994; Schneider *et al.*, 2003). As an alternative to direct soil moisture observations, soil moisture can be estimated indirectly from screen level observations of temperature and/or humidity (Mahfouf, 1991; Calvet *et al.*, 1998).

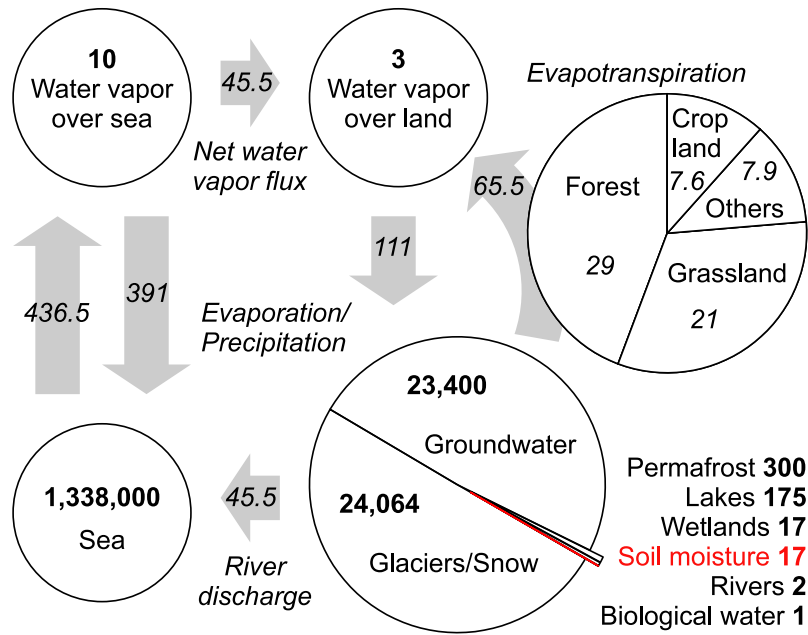


Figure 1.1. Schematic representation of the global hydrological cycle (excluding Antarctica) with the size of the different stores (**bold**, in km³) and fluxes (*italic*, in km³ y⁻¹). Numbers from *Oki and Kanae (2006)*.

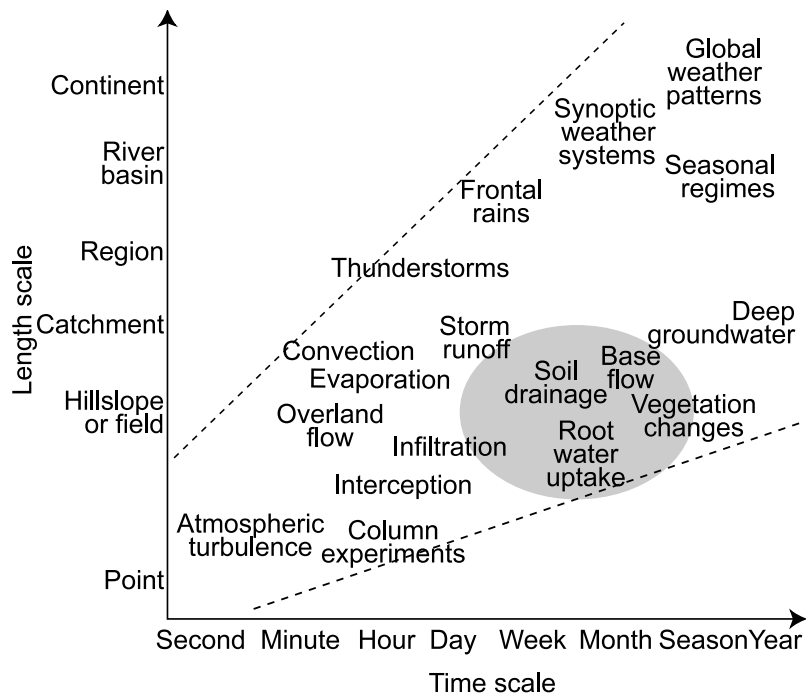


Figure 1.2. Ranges of spatial and temporal scales of some common processes in the terrestrial water cycle. The grey area indicates the focus of this thesis. After *Brutsaert (2005)*.

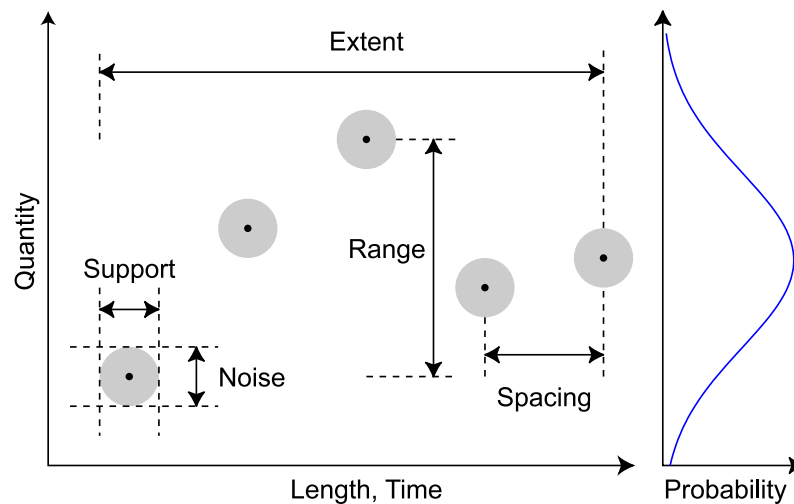


Figure 1.3. Scaling triplet. Modified after *Western and Blöschl (1999)*.

1.3. This thesis

This thesis aims at linking spatial and temporal variations in soil moisture to evapotranspiration and climate. It focusses at the first two of the problems mentioned in Section 1.2. Figure 1.2 indicates the position of the principal processes in this thesis and their associated temporal and spatial scales relative to other processes in the hydrological cycle. The spatial scales range from the point to the regional scale, and the temporal scales from days to months. Figure 1.3 illustrates the key problem in this thesis: if a certain combination of processes results in a set of soil moisture states, what can we tell about the resulting probability distribution? Or, alternatively, if only changes in the distribution are known, what do these changes tell us about the underlying processes? Throughout the thesis there are two central principles. The first principle is that of conservation of mass. Although this may seem trivial, there are many studies on land surface hydrology where this principle is simply not considered or even violated. In this thesis the water balance will be applied throughout. A second principle that is used throughout this thesis is that of Occam's razor. This principle (or philosophy) can be expressed as follows: "all things being equal, the simplest solution tends to be the best one". Occam's razor is applied by adapting the model complexity to the research question. In addition to applying these two principles, the thesis focusses on the dry soil moisture range, in which evapotranspiration fluxes are strongly controlled by the soil moisture state.

The first part of this thesis, namely **Chapters 2–4**, deals with *temporal dynamics* of soil moisture at the point- to field-scale. Here, spatial variability is not considered explicitly, although vertical distribution of soil moisture is considered in **Chapter 3**. All three chapters deal with wet-dry transitions in climates that have a strong seasonality in their rainfall. In **Chapter 2** the impact of non-linearities in the relation between soil moisture and water fluxes at the land surface on the temporal distribution of soil moisture is investigated by means of stochastic simulation. Some theoretical aspects of how plant roots control evapotranspiration is further investigated analytically in **Chapter 3**. In contrast to the more qualitative approach in **Chapter 3**, **Chapter 4** investigates the strength of the relation between soil moisture and evapotranspiration from evapotranspiration observations.

The second part of the thesis, namely **Chapters 5–8**, deals with *spatial variability* (and its dynamics) of point-scale soil moisture at the field- or catchment-scale. The dynamics of spatial soil moisture fields are investigated by means of statistical analysis (**Chapter 5**), stochastic simulation (**Chapters 6 and 8**), and low-dimensional analytical models (**Chapter 7**). **Chapter 5** deals with the representativeness of point-scale soil moisture observations to the spatial mean soil moisture. **Chapters 6 and 8** both focus on the relation between spatial mean root zone soil moisture and its variability. While **Chapter 6** investigates why this relation is different for three different datasets, **Chapter 8** explores the impact of climate variability on this relation for a single site. In **Chapter 7**, the focus is on surface rather than root zone soil moisture. Here, the dynamics of and the relation between spatial mean soil moisture at the field scale and its variability are investigated, as well as the sensitivity of the temporal soil moisture distribution to changes in precipitation characteristics.

2. On bimodality in warm season soil moisture observations*

It has recently been suggested that the bimodality in warm season soil moisture observations in Illinois provides evidence for a soil moisture-precipitation feedback. Other studies however provide little evidence for a strong feedback in this region. Here we show that seasonality in the meteorological conditions in combination with the non-linearity of the soil moisture response alone can induce this bimodality. The existence of preferred wet and dry soil moisture states may have implications for the understanding and modeling of soil moisture dynamics in mid-latitude regions.

2.1. Introduction

In continental climates, a significant but varying fraction of warm season precipitation can originate from recycled local evaporation (e.g., *Brubaker et al.*, 1993; *Savenije*, 1995). It has been argued that anomalous soil moisture conditions, through their effects on evapotranspiration and subsequent precipitation, might sustain themselves causing periods of enhanced floods and droughts. Although rainfall formation is a complex process and the effect of soil moisture is not necessarily positive at all spatial scales (e.g., *Giorgi et al.*, 1996; *Ek and Holtslag*, 2004; *Taylor and Ellis*, 2006), positive feedbacks have indeed been reported in several Atmospheric General Circulation Model (AGCM) studies (*Shukla and Mintz*, 1982; *Oglesby and Erickson*, 1989; *Beljaars et al.*, 1996; *Bosilovich and Sun*, 1999; *Hong and Kalnay*, 2000; *Koster et al.*, 2004).

Since Illinois (Fig. 2.1) is one of the few continental regions where long-term soil moisture as well as precipitation records are available, many studies focus on this region. Although there is consensus about the significance of the soil moisture-precipitation feedback over the Great Plains region (*Findell and Eltahir*, 2003; *Koster et al.*, 2003, 2004), there is an ongoing debate about whether the feedback controls soil moisture and precipitation dynamics in Illinois (e.g., *Findell and Eltahir*, 1997; *Salvucci et al.*, 2002; *D’Odorico and Porporato*, 2004). *Findell and Eltahir* (2003) showed that soil moisture can indeed influence the triggering of deep convection in this region, but *Salvucci et al.* (2002) were unable to detect a causal relation between soil moisture and subsequent precipitation in observations.

Rodríguez-Iturbe et al. (1991) showed that precipitation recycling over large continental regions can lead to two modes in the steady-state soil moisture probability density function (pdf). Recently, *Kochendorfer and Ramírez* (2005) concluded that this bimodality does not occur when conditions typical to the central United States (including Illinois) are considered. *D’Odorico and Porporato* (2004) showed that bimodality in the steady-state pdf can occur in Illinois when causality between observed soil moisture and subsequent precipitation is assumed. Moreover they showed that a majority of the soil moisture stations in Illinois show bimodality in their warm season (May–September) soil moisture pdf, which they argued was experimental evidence of the existence of such a feedback. Here we investigate the origin of the bimodality in the Illinois soil moisture observations. We argue that the bimodality is not indicative for a strong soil moisture-precipitation feedback, but can be explained by the existence of soil moisture states that show little sensitivity to changes in forcing.

2.2. Effects of seasonality

D’Odorico and Porporato (2004, pp. 8850) used “the fact that in this region the late growing season can be considered to be practically under statistically steady conditions” to support their explanation for the observed

*This chapter is an edited version of: Teuling, A. J., R. Uijlenhoet, and P. A. Troch (2005), On bimodality in warm season soil moisture observations, *Geophys. Res. Lett.*, 32(5), L05404, doi:10.1029/2005GL023223. Copyright 2005 American Geophysical Union.

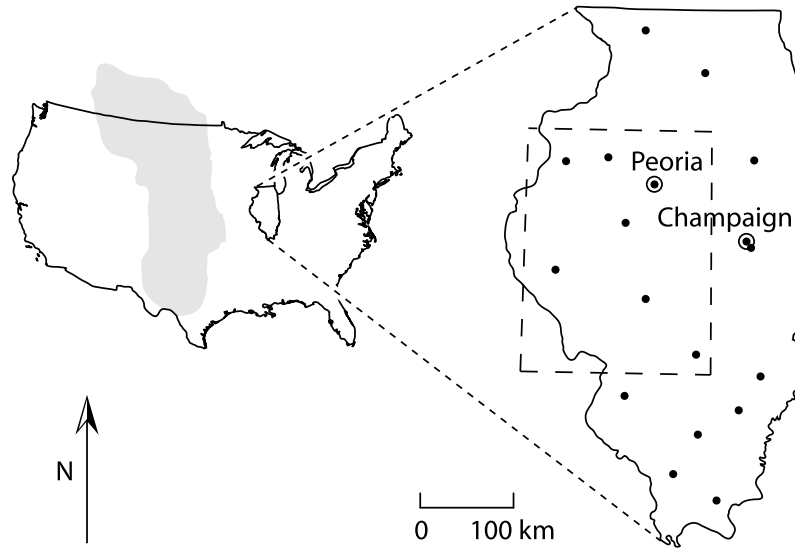


Figure 2.1. Map of Illinois (USA) showing the location of the relevant WARM sites and the selected ERA40 grid cell. The Great Plains, which have been reported to exhibit the strongest potential for soil moisture-precipitation feedback (*Koster et al.*, 2003, 2004), are shown in grey.

bimodality. While the assumption of stationary soil moisture conditions might be valid at a daily timescale, as in *Salvucci* (2001), it loses its validity at longer (sub)seasonal time scales. Figures 2.2A–C show the results of an analysis of meteorological data from the Illinois State Water Survey Water and Atmospheric Resources Monitoring Program (WARM, data available from www.sws.uiuc.edu/warm), averaged over the different stations. Precipitation (through storm frequency λ and depth α) as well as potential evapotranspiration (E_p) show a clear seasonal trend extending to well beyond the warm season. Moreover, as will be discussed later on, this results in a transition from a net precipitation surplus in May to a deficit in August.

Both leaf area index (ξ) and soil moisture (θ) respond to the seasonality in meteorological forcing. Leaf area index typically shows a strong seasonal cycle on the North American continent (e.g., *van den Hurk et al.*, 2003), with a peak in August. As an illustration, Fig. 2.2C shows measurements made on a grassland site in Kansas in 2001 and 2002 (*Gower*, 2000–2004). Illinois soil moisture data are described by *Hollinger and Isard* (1994), and are available through the Global Soil Moisture Data Bank (*Robock et al.*, 2000). Figure 2.2D reveals that the assumption of stationarity is not valid for soil moisture on seasonal timescales: the persistent dry-down during summer covers nearly the full mean soil moisture range (see also *Findell and Eltahir*, 1997, their Fig. 2).

We study the effect of seasonality on the warm season soil moisture pdf by applying a modified version of the model used by *Laio et al.* (2001) and *D’Odorico and Porporato* (2004). The stochastic model solves the water balance at a daily time scale:

$$\frac{d\theta}{dt} = \frac{1}{L} [\varphi(\theta, t) - \chi(\theta)], \quad (2.1)$$

where θ is the volumetric soil moisture content of the active soil depth L , φ the infiltration, and χ is the loss function. Infiltration equals precipitation P that is not intercepted, or the remaining storage capacity $L(\theta_s - \theta)$, whichever is smaller. θ_s is the porosity of the soil. The size of the interception reservoir is taken proportional to ξ , with a proportionality constant of 0.2 mm per unit of ξ . Daily rainfall occurrence is modeled as a Bernoulli process with occurrence probability $\lambda(t)dt$ ($dt = 1$ d), and depth drawn from an exponential distribution with mean $\alpha(t)$. A key difference with previous work is that we allow for seasonality in λ and α , assuming θ to be driven by meteorological forcing rather than θ to be the main driver of this forcing (as is explicitly assumed in *D’Odorico and Porporato*, 2004).

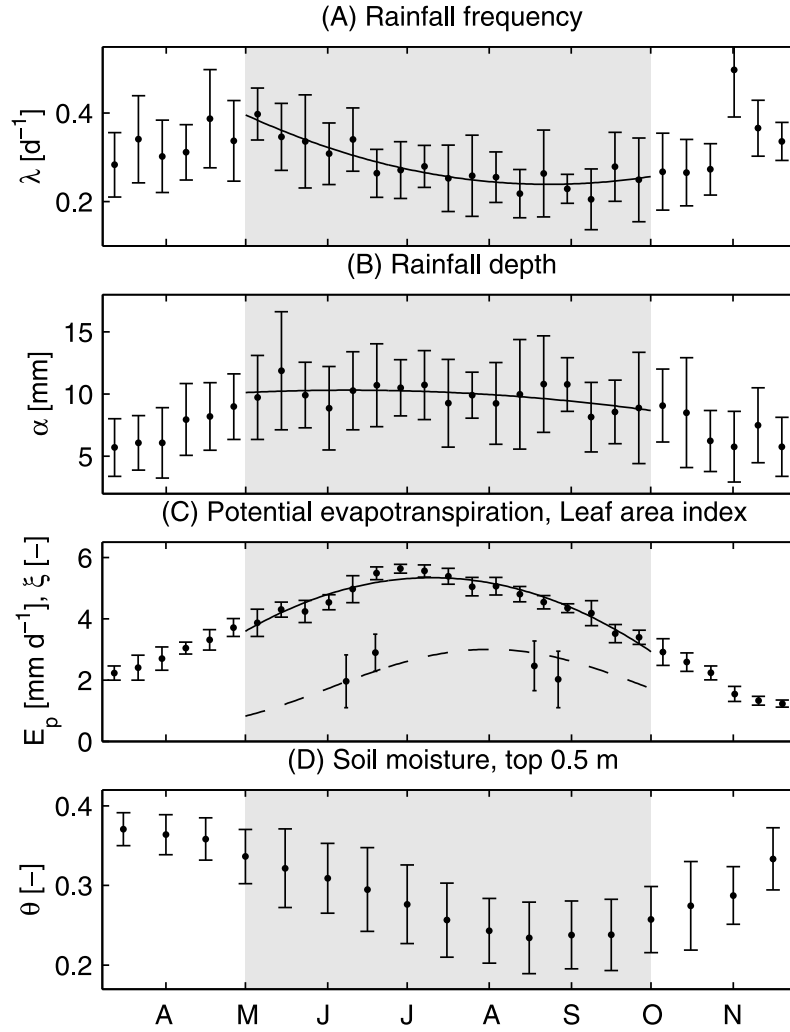


Figure 2.2. Climatology of Illinois. Error bars denote interannual variability (standard deviation) for the years 1989–2004 (A–C) or 1981–2004 (D). Forcing was binned into 17 nine-day periods spanning the period May–September. Solid lines are second-order polynomial regressions for the warm season, and the dashed line is the sine curve for ξ .

The loss function $\chi(\theta)$ combines daily losses due to drainage and evapotranspiration (App. A):

$$\chi(\theta) = \begin{cases} E_w \frac{\theta - \theta_h}{\theta_w - \theta_h}, & \theta_h < \theta \leq \theta_w \\ E_w + (E_{max} - E_w) \frac{\theta - \theta_w}{\theta_c - \theta_w}, & \theta_w < \theta \leq \theta_c \\ E_{max} + k_s \left(\frac{\theta}{\theta_s}\right)^{2b+3}, & \theta_c < \theta \leq \theta_s, \end{cases} \quad (2.2)$$

where E_w is the residual evaporation at wilting point θ_w , θ_h the hygroscopic point, θ_c the critical moisture content marking the transition between soil- and atmosphere-controlled evapotranspiration, E_{max} the maximum evapotranspiration rate of the vegetation, k_s the saturated hydraulic conductivity, and b is a pore size distribution parameter. We differ from *Laio et al.* (2001) by incorporating the effect of varying ξ and E_p on E_{max} as (e.g., *Al-Kaisi et al.*, 1989):

$$E_{max} = \left(1 - e^{-c\xi}\right) E_p, \quad (2.3)$$

where c is an extinction coefficient for global radiation (0.4 for grass). Other parameters are adopted from *Laio et al.* (2001) and *D'Odorico and Porporato* (2004): $k_s = 20 \text{ mm d}^{-1}$, $\theta_h = 0.06$, $\theta_w = 0.08$, $\theta_c = 0.24$, $\theta_s = 0.45$, $b = 5.39$, $L = 0.5 \text{ m}$, and $E_w = 0.2 \text{ mm d}^{-1}$. A comparison of (2.2) with independent estimates of $\chi(\theta)$ for Illinois confirms the non-linear shape of the loss function (Fig. 2.3A). Field capacity θ_f in Fig. 2.3 is defined as the point where drainage losses are 10% of E_{max} (*Laio et al.*, 2001).

In order to allow for direct comparison with observations, we evaluate (2.1)–(2.3) over the period May–September using the regressions in Figs. 2.2A–D. As initial condition we assume stationary conditions on 1 May. Since an analytical solution of this problem is not easy to obtain, Fig. 2.3A shows the soil moisture pdf $p(\theta)$ based on Monte Carlo simulations of the model (50,000 seasonal realizations). The pdf shows a distinct bimodality. This bimodality is also apparent, although less pronounced, in the shorter period June–August (not shown). The pdf compares well to observations from Peoria, which according to *D’Odorico and Porporato* (2004) have the strongest bimodal tendency. In the following, we argue that the origin of this bimodality differs from their interpretation.

2.3. Characterizing wet and dry modes

A visual comparison between Figs. 2.3A and B reveals that the bimodal pdf for the period May–September is a near-perfect mixture between the steady-state solutions of $p(\theta)$ for wet (May) and dry (August) regimes. This is confirmed by the observations from Peoria for the individual wet and dry months. These show no bimodality (Fig. 2.3B), but follow the skewness predicted by the steady-state solutions without feedback. This conflicts with the view of *D’Odorico and Porporato* (2004, pp. 8850) that “*summer soil moisture dynamics evolve toward either a dry or a wet state in which the system may remain locked for the rest of the warm season*”. Instead, soil moisture is in a wet state at the beginning of the warm season, and switches to a dry state whenever actual evaporation starts to exceed the precipitation. This switch generally takes place in the period June–July.

This can be explained as follows. Since, in climatic average terms, $P \neq E_{max}$, no steady-state pdf exists with a mode between θ_c and θ_f (since $d\chi(\theta)/d\theta \approx 0$). In this region, θ is always in transition. Outside this region, the inequality between P and E_{max} can be balanced by either increased drainage caused by the strong non-linear dependence of the hydraulic conductivity on θ (in case $P > E_{max}$) or soil moisture limitation on transpiration ($P < E_{max}$). Hence these regions will act as “attractors” in the soil moisture probability density space. The wet “attractor” is often referred to as field capacity.

The transition between wet and dry modes can occur very rapidly. In the absence of rainfall, the time span of this transition is the time needed for the soil to dry from θ_f to θ_c . With the parameters of Fig. 2.3A, this yields a value of ~ 20 d. The occurrence of bimodality is controlled by the ratio (Ψ) between the climatological average maximum precipitation deficit in the course of the warm season D_P (relative to E_{max}) and the amount of water between θ_f and θ_c that is accessible for transpiration (through L):

$$\Psi = \frac{D_P}{L(\theta_f - \theta_c)}. \quad (2.4)$$

In climates with precipitation surplus in winter, no bimodality occurs if $\Psi < 1$. Figure 2.4 shows the effect of varying Ψ on $p(\theta)$, obtained by increasing L . The resulting pdf’s have a shape similar to observations from Champaign, one of the stations that does not show bimodal behavior. This confirms that local variations in Ψ through either climate, soil, or vegetation properties control the variations in soil moisture dynamics in Illinois. Since the shape of $\chi(\theta)$ in Fig. 2.3A is not unique for Illinois (nor is the climate), similar dynamics are likely to occur in other mid-latitude regions. A rapid transition between wet and dry states has also been observed in studies of spatial soil moisture patterns in a small Australian catchment (*Grayson et al.*, 1997).

To investigate if coupled land-atmosphere models are capable of reproducing the observed soil moisture dynamics, we study the ERA40 reanalysis soil moisture data (obtained from the ECMWF data server) for the warm seasons of the years 1981–2002 (Fig. 2.1). Whereas observations tend to be bimodally distributed, the ERA40 data show one distinct peak and less dynamical range (Fig. 2.5). Since we concluded that the bimodality is related to the shape of $\chi(\theta)$, we investigate to what extent this shape controls the soil moisture pdf by repeating our model runs with soil parameters and the simplified loss function of the ERA40 land surface scheme (Fig. 2.5). This (daily average) function was derived from the model equations (see *van den Hurk et al.*, 2000) under assumptions of instantaneous vertical soil moisture redistribution, full vegetation cover, stomatal conductance only reduced by soil moisture, and equal aerodynamic and minimum surface resistance. The results, although showing a slightly higher variability, show similar dynamics as the ERA40 data and no bimodality. Although other factors contribute to the damped soil moisture dynamics in ERA40 (e.g., *Seneviratne et al.*, 2004), this shows that the simulated soil moisture dynamics are strongly controlled by the parameterization of the soil moisture losses.

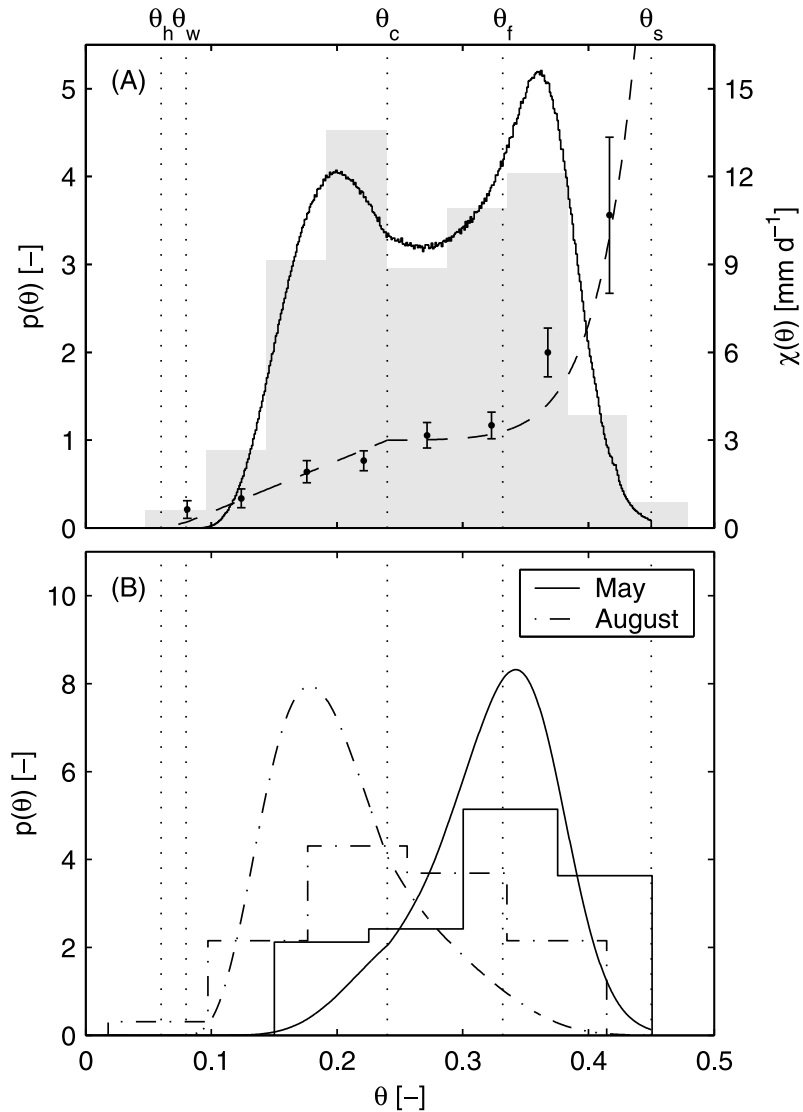


Figure 2.3. (A) Simulated soil moisture pdf (solid line) and observations (top 0.5 m) from Peoria (1981–2004, grey), both for the period May–September. The dashed line is $\chi(\theta)$, with $E_{max} = 3 \text{ mm d}^{-1}$, with estimates of $\chi(\theta)$ by Salvucci (2001) for the period June–August. (B) Steady-state pdf's from Laio *et al.* (2001) with parameters taken from Fig. 2.2 on 31 May ($P > E_{max}$) and 31 August ($P < E_{max}$), and observations (top 0.5 m) from Peoria for May and August. Histogram bin widths are adjusted to the number of observations (Scott, 1979).

2.4. Discussion and Conclusions

In this chapter we show that soil moisture bimodality cannot be considered as conclusive evidence for the existence of a soil moisture-precipitation feedback, since no feedback is necessary to explain the existence of the wet and dry modes. However, our results do not exclude the possibility that such a feedback exists in Illinois. Recent work suggests that feedback-induced bimodality might exist in other regions (Lee and Hornberger, 2006). Although many processes (including soil moisture-precipitation feedback) can lead to bimodal soil moisture distributions, we think the process described here dominates possible other processes in their effect on soil moisture dynamics in Illinois. The conditions that generate the bimodality are not limited to Illinois nor to regions where a land-atmosphere feedback may exist. Not surprisingly, similar bimodal soil moisture dynamics have been reported for other regions (Miller *et al.*, 2007). Understanding these dynamics can aid the development, parameterization, and validation of land surface models.

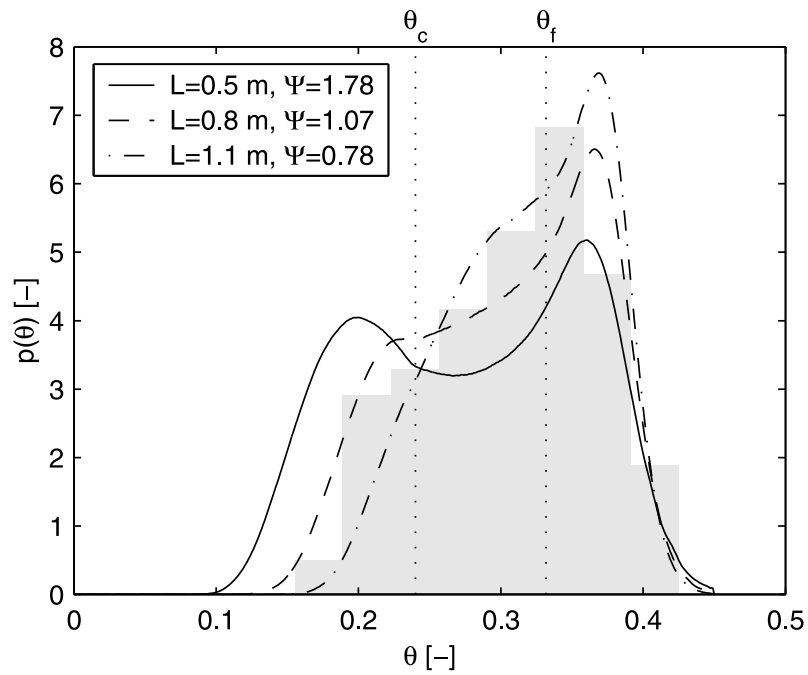


Figure 2.4. Effect of active soil depth on the (smoothed) soil moisture pdf for the period May–September, and observations (top 0.5 m) from Champaign for the same period in the years 1984–2004 (grey).

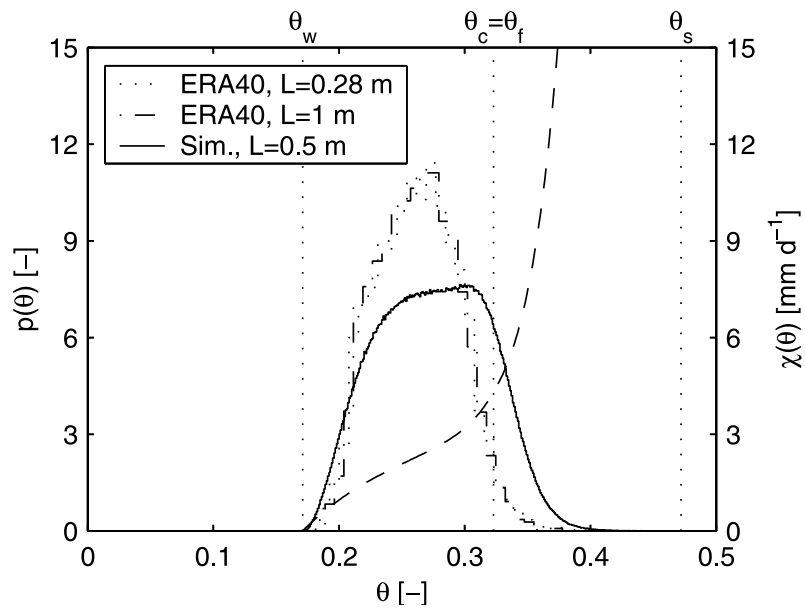


Figure 2.5. Simulated and ERA40 soil moisture pdf for the period May–September, and simplified $\chi(\theta)$ (dashed line) with $E_{max} = 3 \text{ mm d}^{-1}$.

3. Impact of plant water uptake strategy on soil moisture and evapotranspiration dynamics during drydown*

Experiments have shown that plants can compensate for water stress in the upper, more densely rooted, soil layers by increasing the water uptake from deeper layers. By adapting root water uptake to water availability, plants are able to extend the period of unstressed transpiration. This strategy conflicts with the approach in many land surface schemes, where plant water uptake is treated as a static process. Here we derive expressions for the typical drydown trajectories of evapotranspiration and soil moisture for both strategies. We show that the maximum difference in evapotranspiration between the two strategies during drydown can exceed 50%. This in turn leads to a difference in root zone soil moisture of up to 25%. The results stress the importance of incorporating realistic root water uptake concepts in land surface schemes.

3.1. Introduction

Climate model simulations are sensitive to root water uptake parameters in their land surface schemes (*Desborough, 1997; Milly, 1997; Kleidon and Heimann, 1998; Zeng et al., 1998*). A correct parameterization of the root water uptake (hereafter RWU) process is essential to predict the long-term (multiple day to monthly) evolution of energy flux partitioning at the land surface. At seasonal timescales, perennial vegetation is known to adapt its root pattern to the availability of soil moisture (*Nepstad et al., 1994; Wan et al., 2002*). At much shorter timescales (multiple days to weeks), there is also evidence that (non-drought adapted) annual vegetation has strategies to cope with water shortage in (the upper) part of the soil. This often results in water extraction from deeper layers at rates much higher than would be expected on the basis of the root density (*Sharp and Davies, 1985; Green and Clothier, 1995*). By doing so, plants are able to delay loss of turgor, prevent stomatal closure, and maintain a high rate of photosynthesis. Rather than by a complete adjustment of the root density profile, plants adapt to drought by rapidly developing fine roots (*Coelho and Or, 1999*), or by increasing the activity and efficiency of deep roots (*Sharp and Davies, 1985*). Deep roots can be responsible for the bulk of the water uptake (*Lai and Katul, 2000*). Hydraulic lift of water via roots to drier parts of the soil may also affect local extraction rates (*Jackson et al., 2000*).

Several algorithms have been developed that can compensate for water stress in part of the root zone by allowing increased uptake from other parts (*Hoogland et al., 1981; Jarvis, 1989; Adiku et al., 2000; Li et al., 2001*). These algorithms allow for a longer period of unstressed transpiration, without altering the rooting depth or the available soil moisture. Here we distinguish two possible RWU strategies:

- A Static strategy (hereafter referred to as S). Here, local RWU is driven by atmospheric demand and local soil moisture conditions only.
- An Adaptive strategy (hereafter referred to as A). Here, local RWU also depends on root zone average soil moisture conditions.

Next, we investigate the potential impact of the RWU strategy on the coupled dynamics of soil moisture and evaporation during drydown for the simplified case where root water uptake dominates other flow mechanisms.

*This chapter is an edited version of: Teuling, A. J., R. Uijlenhoet, F. Hupet, and P. A. Troch (2006), Impact of plant water uptake strategy on soil moisture and evapotranspiration dynamics during drydown, *Geophys. Res. Lett.*, 33(3), L03401, doi:10.1029/2005GL025019. Copyright 2006 American Geophysical Union.

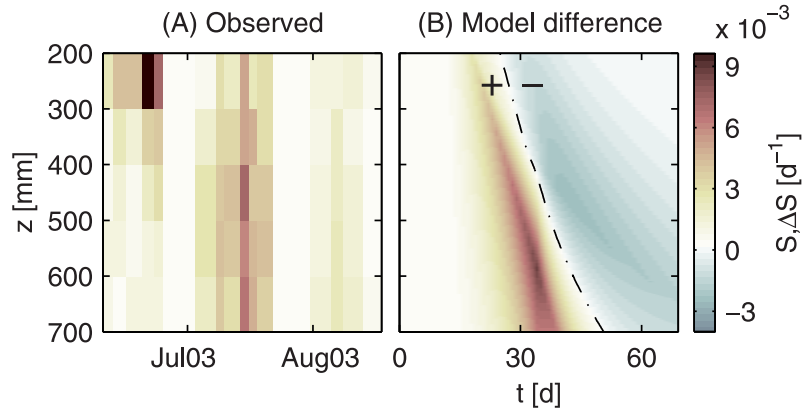


Figure 3.1. Root water uptake (S) in an experimental field in Louvain-la-Neuve, Belgium. (A) Observed. (B) Model difference ΔS between the algorithm of *Jarvis* (1989) and $S = E_m \beta(\theta) p_r^*(z)$, using $E_m = 4 \text{ mm d}^{-1}$, $\lambda = 3 \text{ m}^{-1}$, $\theta_w = 0.16$, $\theta_c = 0.22$, $\theta_0 = 0.35$, and a critical value of the weighted stress index of 0.2.

3.2. A field example

Figure 3.1A shows the RWU as derived from successive soil moisture measurements during periods without significant rainfall made in a field cropped with maize (*Zea mays* L.) in Louvain-la-Neuve (Belgium) during the 2003 European heat wave (*Hupet and Vanclooster, 2005*). During the initial stage of drying (June), the higher RWU in the upper part of the profile mimics the exponential root density profile. During the second stage (mid July), the bulk of the RWU shifted downwards due to drying of the topsoil. Moreover, the rate of water uptake at these depths was fourfold that of the previous period, indicating a transition of RWU from root distribution-controlled towards water availability-controlled (*Green and Clothier, 1995*). In August the uptake at all measured depths was low.

To illustrate the effect of RWU parameterization on the simulation of similar events, Fig. 3.1B shows the difference in RWU between a numerical evaluation of the *Jarvis* (1989) algorithm with stress compensation (strategy A) and without compensation (strategy S). The parameters were chosen to match the conditions at the site and vertical flow was neglected. Initially, both models give identical results. However, large differences occur for $t > 25 \text{ d}$ when reduced uptake in the upper part of the soil for strategy S is compensated by higher uptake rates at larger depths for strategy A. Interestingly, both the depth and timing of these differences are similar to the increased uptake in Fig. 3.1A. Later, the differences switch sign, but are of smaller magnitude. This example shows that models based on strategy S might fail to capture the actual RWU dynamics. The timescales where the differences are large are highly relevant to drought forecasting.

3.3. Modeling root water uptake

The water budget in the root zone is described by:

$$\frac{\partial \theta}{\partial t} = -\frac{\partial q}{\partial z} - S \quad (3.1)$$

where θ is the volumetric soil moisture content, z a vertical coordinate (positive downwards), q the vertical moisture flux, and S a sink term representing RWU. Land surface modelers often adopt strategy S and assume that RWU is proportional to a maximum (unstressed) evapotranspiration rate E_m , the root density distribution p_r , and a water stress factor β (*Feddes et al., 2001*). For many plants, root density is highest near the land surface and decays exponentially with depth (*Gerwitz and Page, 1974*). For practical reasons we use the apparent root density distribution $p_r^*(z)$ defined over the effective rooting depth L :

$$p_r^*(z) = \lambda' e^{-\lambda z}, \quad 0 \leq z \leq L \quad (3.2)$$

where λ is the inverse of the e -folding depth of the root density, and $\lambda' = \lambda/(1 - e^{-\lambda L})$ such that $\int_0^L p_r^*(z) dz = 1$. We assume the e -folding depth of the root density and the effective rooting depth to be related, i.e., $L = c/\lambda$. If L is taken as the depth in (3.2) above which 95% of the roots are found (e.g., *Schenk and Jackson, 2002*), then $c \approx 3$. Water stress can be modeled as a piecewise linear function of θ :

$$\beta = \beta(\theta) = \begin{cases} 0, & \theta \leq \theta_w \\ \frac{\theta - \theta_w}{\theta_c - \theta_w}, & \theta_w < \theta \leq \theta_c \\ 1, & \theta_c < \theta \leq \theta_s \end{cases} \quad (3.3)$$

where θ_s is the moisture content at saturation, θ_c the critical moisture level, and θ_w the wilting point. When $\partial q/\partial z \ll S$ (as is typical under dry conditions), the local soil moisture decay can be obtained by solving $\partial \theta(z, t)/\partial t = -E_m \beta(\theta) p_r^*(z)$. Starting from a (uniform) initial soil moisture content θ_0 at $t = 0$ with $\theta_0 > \theta_c$, this yields the following expression for $\theta(z, t)$ at a daily timescale:

$$\theta'(z, t) = \begin{cases} \theta'_0 - \lambda' e^{-\lambda z} E_m t, & 0 \leq t < t_c(z) \\ \theta'_c \exp\left(\frac{\theta'_0 - \theta'_c}{\theta'_c} - \frac{\lambda' \exp(-\lambda z) E_m t}{\theta'_c}\right), & t \geq t_c(z) \end{cases} \quad (3.4)$$

where $t_c(z)$ relates the time t_c and corresponding depth z_c of the first reduction of S ($\theta'(z, t) = \theta_c$):

$$t_c(z) = \frac{\theta'_0 - \theta'_c}{E_m \lambda' \exp(-\lambda z)} \Leftrightarrow z_c(t) = \frac{1}{\lambda} \ln\left(\frac{E_m \lambda' t}{\theta'_0 - \theta'_c}\right) \quad (3.5)$$

and θ' denotes the transformed variable $\theta' = \theta - \theta_w$.

For strategy A algorithms, an expression for $\theta'(z, t)$ will also depend on the co-evolution of the root zone averaged soil moisture $\bar{\theta}(t)$ (*Jarvis, 1989*). Since our interest is in the total (depth integrated) RWU rather than $\theta'(z, t)$, we assume that the total RWU response for strategy A algorithms is similar to (3.3) evaluated directly with $\bar{\theta}$, i.e., with stress $\beta(\bar{\theta})$. The validity of this assumption increases with the plants ability to compensate for stress (e.g., *Guswa et al., 2002*). Since the onset of reduced RWU occurs at $\min[t_c(z)]$ or at $\max[p_r^*(z)]$, it can be seen from (3.5) that strategy A (single reservoir with effective uniform p_r) tends to maximize t_c . In this way, the onset of water stress is postponed, but at the risk of more severe stress at a later stage.

3.4. Evapotranspiration decay

The total RWU for strategy S is obtained by integrating $S(z, t)$ over the profile (denoted by \widehat{S}), while accounting for vertical differences in soil moisture reduction:

$$\widehat{S}(t) = \begin{cases} \lambda' E_m \int_0^L e^{-\lambda z} dz = E_m, & 0 \leq t < t_c(0) \\ \lambda' E_m \int_0^{z_c} \frac{\theta'(z, t)}{\theta'_c} e^{-\lambda z} dz + \lambda' E_m \int_{z_c}^L e^{-\lambda z} dz, & t_c(0) \leq t < t_c(L) \\ \lambda' E_m \int_0^L \frac{\theta'(z, t)}{\theta'_c} e^{-\lambda z} dz, & t \geq t_c(L) \end{cases} \quad (3.6)$$

where $z_c(t)$ is given by (3.5). Integration of (3.6) with substitution of $z_c(t)$ and (3.4), and rearranging of the different terms yields (App. B):

$$\sigma_S(\tau) = \begin{cases} 1, & 0 \leq \tau < \frac{1-f}{b} \\ \frac{1}{\tau} - \frac{f}{\tau} \exp\left(\frac{1-f}{f} - \frac{b\tau}{f}\right) - b e^{-c}, & \frac{1-f}{b} \leq \tau < \frac{1-f}{b e^{-c}} \\ \frac{f}{\tau} \exp\left(\frac{1-f}{f}\right) \left[\exp\left(-\frac{b\tau}{f} e^{-c}\right) - \exp\left(-\frac{b\tau}{f}\right) \right], & \tau \geq \frac{1-f}{b e^{-c}} \end{cases} \quad (3.7)$$

where the dimensionless variables $\sigma = \widehat{S}/E_m$, $f = \theta'_c/\theta'_0$, $b = \lambda'/\lambda$, and $\tau = \lambda E_m t/\theta'_0$ have been introduced for convenience. If $\theta_0 \leq \theta_c$ (or $f \geq 1$), the solution reduces to:

$$\sigma_S(\tau) = \frac{1}{\tau} \left[\exp\left(-\frac{b\tau}{f} e^{-c}\right) - \exp\left(-\frac{b\tau}{f}\right) \right]. \quad (3.8)$$

PLANT WATER UPTAKE

For strategy A, the time to first reduction on RWU becomes: $t_c = L(\theta'_0 - \theta'_c)/E_m$, or $\tau_c = c - cf$. By using $\bar{\theta}$ rather than θ in (3.3), the time evolution of σ_A can be written as:

$$\sigma_A(\tau) = \begin{cases} 1, & 0 \leq \tau < c - cf \\ \exp\left(\frac{1-f}{f} - \frac{\tau}{cf}\right), & \tau \geq c - cf. \end{cases} \quad (3.9)$$

We define the relative difference $\Delta\sigma$ at time $\tau = \tau^*$ between strategy A and S as:

$$\Delta\sigma|_{\tau=\tau^*} = \sigma_A(\tau^*) - \sigma_S(\tau^*). \quad (3.10)$$

The maximum difference $\max(|\Delta\sigma|)$ occurs at the onset of reduced uptake for A. With the values used in Fig. 3.1B, this corresponds to $t \approx 33$ d. The difference $\Delta\sigma|_{\tau=c-cf}$ can be evaluated by using $\sigma_A = 1$ and inserting $\tau = c - cf$ in (3.7). For Fig. 3.1B this yields $\max(|\Delta\sigma|) \approx 46\%$.

Values for f depend on soil, climate, vegetation, and/or initial conditions, but are typically in the range of 0.3–0.6. In Fig. 3.2A, $\Delta\sigma(\tau)$ is evaluated for different f . Strategy A initially leads to considerably higher evaporation rates than strategy S, with a maximum difference of over 50% for low f . During later stages of drydown the difference is opposite but much smaller in magnitude (see also Fig. 3.2B). The maximum difference is strongly dependent on f . For $f \geq 1$, this difference ($\Delta\sigma|_{\tau=c-cf}$) reduces to less than 10%.

3.5. Soil moisture decay

The evolution of soil moisture averaged over a layer of thickness L and scaled by θ'_0 , i.e., $\omega = \bar{\theta}/\theta'_0$, can be derived from (3.4) by separating between non-, partly-, and fully reduced RWU trajectories similar to (3.6). For strategy S this yields (App. C):

$$\omega_S(\tau) = \begin{cases} 1 - \frac{\tau}{c}, & 0 \leq \tau < \frac{1-f}{b} \\ 1 + \frac{b\tau}{c}e^{-c} + \frac{1}{c} \ln\left(\frac{1-f}{b\tau}\right) + \frac{f-1}{c} + \frac{f}{c} \exp\left(\frac{1-f}{f}\right) \left[E_1\left(\frac{1-f}{f}\right) - E_1\left(\frac{b\tau}{f}\right) \right], & \frac{1-f}{b} \leq \tau < \frac{1-f}{be^{-c}} \\ \frac{f}{c} \exp\left(\frac{1-f}{f}\right) \left[E_1\left(\frac{b\tau}{f}e^{-c}\right) - E_1\left(\frac{b\tau}{f}\right) \right], & \tau \geq \frac{1-f}{be^{-c}} \end{cases} \quad (3.11)$$

where E_1 is related to the exponential integral $Ei(x)$: $E_1(x) = -Ei(-x)$ (App. C). For $\theta_0 \leq \theta_c$ the solution reduces to:

$$\omega_S(\tau) = \frac{1}{c} \left[E_1\left(\frac{b\tau}{f}e^{-c}\right) - E_1\left(\frac{b\tau}{f}\right) \right]. \quad (3.12)$$

Similarly, the normalized soil moisture evolution for strategy A for $\theta_0 > \theta_c$ is given by:

$$\omega_A(\tau) = \begin{cases} 1 - \frac{\tau}{c}, & 0 \leq \tau < c - cf \\ f \exp\left(\frac{1-f}{f} - \frac{\tau}{cf}\right), & \tau \geq c - cf \end{cases} \quad (3.13)$$

which is similar to (3.4). We define $\Delta\omega$ as the difference in transformed and normalized soil moisture between strategy A and S:

$$\Delta\omega|_{\tau=\tau^*} = \omega_A(\tau^*) - \omega_S(\tau^*). \quad (3.14)$$

Evaluation of $\Delta\omega(\tau)$ in Fig. 3.2B shows that strategy A systematically leads to lower values of the available root zone soil moisture during drydown when compared to strategy S. This is caused by a rapid reduction of \hat{S}_S and associated lower $d\bar{\theta}_S/dt$. The maximum difference for low values of f is in the order of 25%. Since soil moisture reflects the effect of preceding RWU, the maximum difference in $\Delta\omega$ lags behind the maximum difference in $\Delta\sigma$. With the values used in Fig. 3.1B, the maximum $\Delta\omega$ occurs at $t \approx 53$ d. These timescales are especially relevant in the context of seasonal forecasting. Since for both strategies soil moisture is integrated over the same layer, $\Delta\omega = 0$ for $\tau \rightarrow \infty$. Although the maximum of $\Delta\sigma|_{\tau=\tau^*}$ is strongly reduced for large f , this reduction is less pronounced in the integrated effect on $\Delta\omega|_{\tau=\tau^*}$. Here the maximum absolute difference only shows a slight reduction for high f .

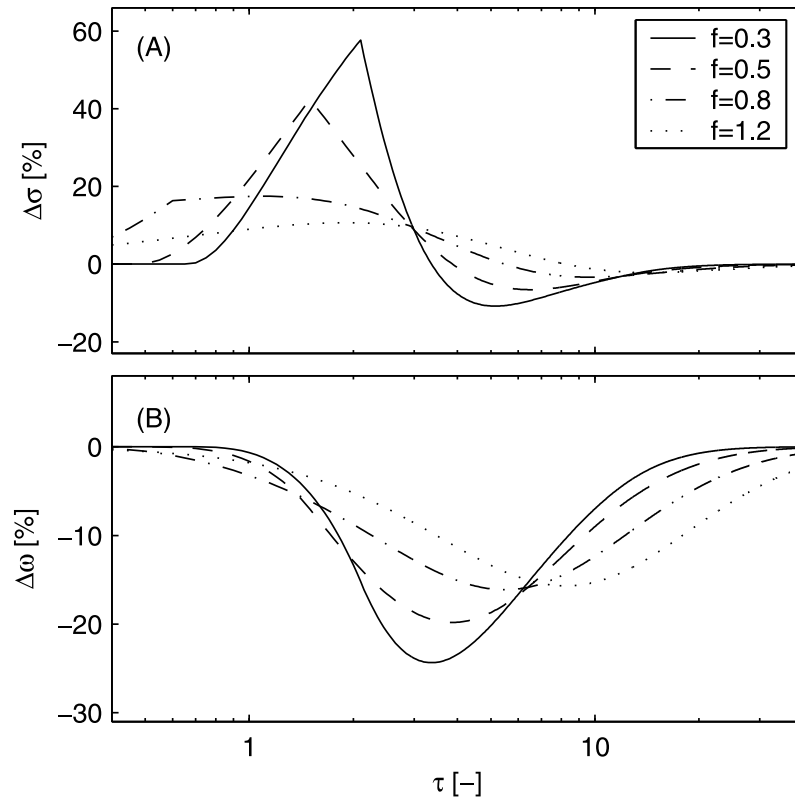


Figure 3.2. Relative impact of uptake strategy on (A) evaporative flux σ and (B) soil moisture ω as a function of normalized time $\tau = \lambda E_m t / \theta'_0$, for different f .

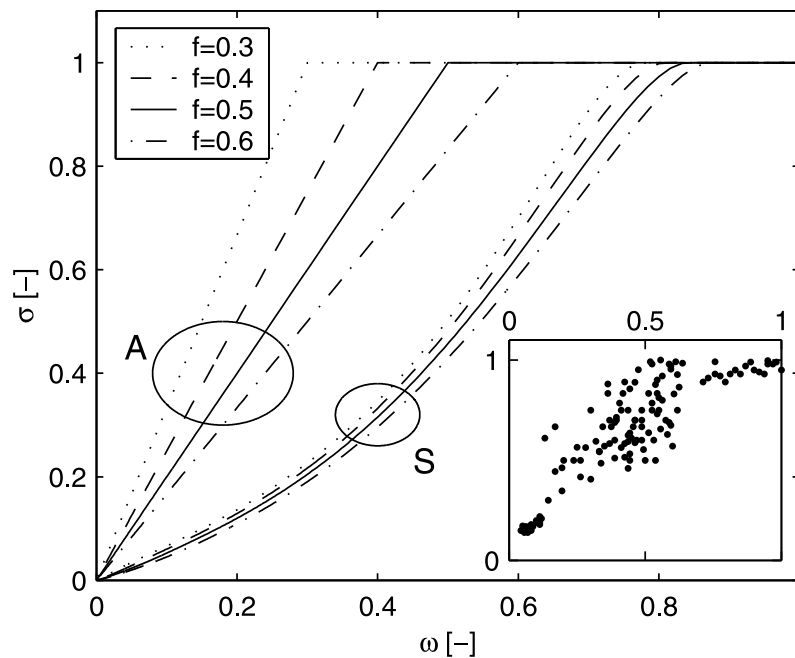


Figure 3.3. Scaled relations between root water uptake and root zone average soil moisture for static (S) and adaptive (A) RWU and different values of f during drydown. Inset: lysimeter observations made by Homae et al. (2002) on alfalfa (*Medicago Sativa* L.) with $L = 0.6$ m.

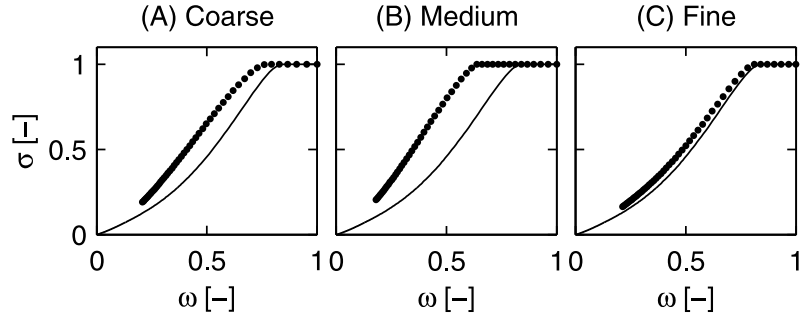


Figure 3.4. Relation between daily σ and ω for strategy S ($f = 0.5$) for a Richards' equation-based model (dots, $E_m = 4 \text{ mm d}^{-1}$, $\lambda = 3 \text{ m}^{-1}$), and equations (3.7) and (3.11) without vertical flow (curves). (A) Coarse, (B) Medium, and (C) Fine soil.

3.6. Root zone aggregation

The uptake strategy also determines the relation between soil moisture and evaporation aggregated over the root zone. Figure 3.3 shows the drydown trajectories plotted in the ω, σ -domain for different f (0.3–0.6). The curves for strategy S reveal little sensitivity to f . For small f , the difference in evaporative flux between the two strategies at a given value of ω , $\Delta\sigma|_{\omega=\omega^*}$, can exceed $\Delta\sigma|_{\tau=\tau^*}$. The difference is largest for $\bar{\theta} = \theta_c$ ($\omega = f$). $\Delta\sigma|_{\omega=f}$ easily exceeds 50% for low f . Figure 3.3 shows that even when reliable estimates of root zone soil moisture are available, estimates of actual evapotranspiration can be highly uncertain due to a wrong RWU conceptualization, and vice versa. Some theoretical aspects of the aggregated ω, σ -relation are discussed by *Guswa et al. (2002)* and *Metselaar and de Jong van Lier (2007)*. The inset in Fig. 3.3 shows an example of the observed relation between ω and σ (*Homae et al., 2002*). The piecewise linear behavior ($f \approx 0.5$) is typical for many other similar experiments. Since the curves serve as an upper envelope for the measurements, they are best characterized by strategy A (see also Fig. 3.1). Only few points fall below the curves for strategy S.

To test whether our results are dependent on the assumption of no vertical moisture transport, we performed drydown simulations with a Richards' equation based model with RWU according to strategy S (by definition, the results for strategy A are trivial). θ_0 was set as the average soil moisture after 3 days of free drainage starting from saturation. Figure 3.4 shows that for typical coarse and fine soils the results closely match the curve without vertical flow. For medium textured soils, redistribution has a compensating effect on vertical differences in RWU, so that maximum RWU can be sustained at lower $\bar{\theta}$. The results will converge towards our analytical model for lower θ_0 (through its strong nonlinear effect on conductivity) or λ (through smaller gradients). Also the occurrence of rainfall events will influence our results for strategy S by their influence on the vertical soil moisture distribution. The associated hysteresis effects that arise from partial rewetting of the soil profile are discussed by *Guswa (2005)*.

3.7. Discussion and Conclusions

In this paper we show that different RWU strategies can lead to large differences in the temporal evolution of evapotranspiration and soil moisture during drydown, even when the available soil moisture is left unaltered. We find that, in absence of vertical flow, these differences can be as high as 50% for evaporation and 25% for soil moisture. The compensating effect of vertical flow in the soil profile depends on several factors, but is likely to be minor for most realistic conditions. We find that even for a relatively high initial soil moisture content, the assumption of no vertical flow is reasonable for coarse and fine soils. Our results suggest that land surface schemes with a realistic (static) root distribution but no stress compensation underestimate the actual RWU in water-limited conditions. The timescales at which the largest differences occur (multiple weeks) are highly relevant for drought forecasting.

4. Observed timescales of evapotranspiration response to soil moisture*

The sensitivity of evapotranspiration (ET) to soil moisture storage plays an important role in the land-atmosphere system. Yet little is known about its magnitude, or its dependence on vegetation, soil, and/or climate characteristics. Here we relate the sensitivity to the timescale of ET decay in absence of rainfall, and show that it can thus be derived from time series of ET alone. We analyze ET observations from 15 vegetated sites covering a range of climate conditions, yielding timescales of 15–35 days. Longer timescales (weaker ET sensitivity) are found in regions with seasonal droughts, or at sites with woody vegetation. We compare observed values with output of different land surface models (LSMs) from the Second Global Soil Wetness Project, revealing large inter-model differences and significant differences with observations. Our methodology can lead to improved representation of soil moisture effects on ET in LSMs.

4.1. Introduction

Plants play a central role in the global water and energy cycles by regulating the partitioning of energy fluxes at the land surface in response to the soil moisture availability in the root zone and atmospheric conditions. Soil water dynamics in the root zone is dominated by rapid infiltration and subsequent vertical redistribution following rainfall, in contrast to slow drydown due to water uptake by roots for evapotranspiration (ET) during interstorm periods. Parameterization of the latter process is complicated by the adaptive behavior of plant water uptake (see Chap. 3). Key parameters and states (i.e., root distribution, soil moisture) are difficult to measure at the appropriate scale, and they can show large spatial and temporal variability.

The sensitivity of ET to soil moisture is a central parameter within the coupled land-atmosphere system. Several studies with Global and Regional Climate Models (GCMs, RCMs) suggest that it might influence low frequency atmospheric variability in precipitation and temperature (e.g., *Koster et al.*, 2004, 2006; *Seneviratne et al.*, 2006a). Moreover, it is also relevant for the timescales of soil moisture autocorrelation (e.g., *Koster and Suarez*, 2001; *Seneviratne et al.*, 2006b). While many studies have investigated simulated evapotranspiration sensitivities (*Scott et al.*, 1997; *Lohmann and Wood*, 2003; *Wang et al.*, 2006), little is known about the actual magnitude of this parameter, or on its dependence on vegetation, soil, and/or climate characteristics. This is mainly due to the lack of simultaneous observations of ET and soil moisture at similar spatial scales. New ways to analyze data from existing networks are needed. *Salvucci* (2001) for instance present a method to estimate the storage-dependency of losses (including ET) in data-limited environments from sparse soil moisture observations and daily rainfall.

Here we propose a method to derive this parameter from ET decay during wet-dry transitions in absence of rainfall. We analyze data from different sites with contrasting soil, vegetation, and climate characteristics. For two sites, the derived sensitivity parameters/decay timescales are compared to simulations with different Land Surface Models (LSMs) participating in the Second Global Soil Wetness Project (GSWP-2, *Dirmeyer et al.*, 2006a). Since no calibration has been performed for these sites, the (dis)agreement both among the different LSMs and with the observations is likely to be indicative for the current uncertainty in parameterization of ET sensitivity to soil moisture. A larger sample of comparison sites would be desirable for a more comprehensive analysis, but this is limited by the lack of ET observations in the GSWP-2 time period (1987–1996).

*This chapter is an edited version of: Teuling, A. J., S. I. Seneviratne, C. Williams, and P. A. Troch (2006), Observed timescales of evapotranspiration response to soil moisture, *Geophys. Res. Lett.*, 33(23), L23403, doi:10.1029/2006GL028178. Copyright 2006 American Geophysical Union.

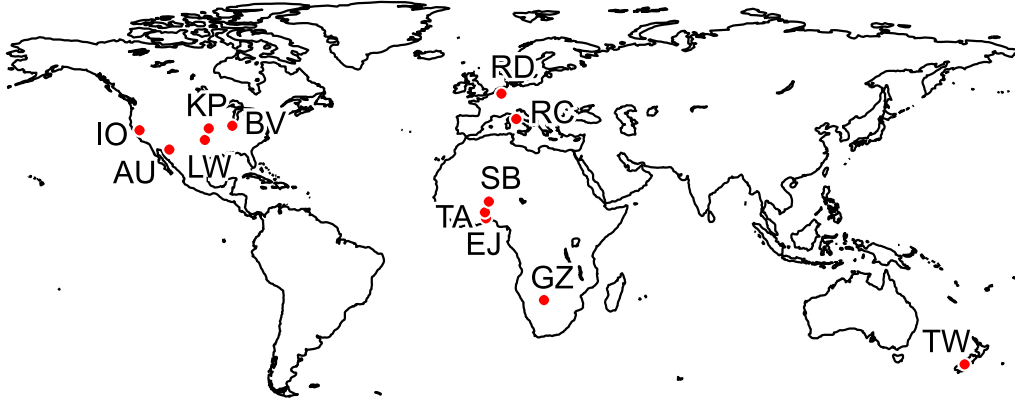


Figure 4.1. Location of the sites mentioned in this study. See Table 4.1 for abbreviations.

4.2. Data

Daily time series of ET are analyzed for 15 vegetated sites, covering a wide range of geographical, climate, and land cover conditions (see Fig. 4.1 and Table 4.1). Several sites (AU, BV, LW, IO, RC) are part of FLUXNET. For details see the project website (www.fluxnet.ornl.gov). For BV and LW, the data are extracted from the daily gap-filled Marconi Collection (Falge *et al.*, 2005). At other sites the observations were part of shorter campaigns, e.g., FIFE (KP), SEBEX (SB), or GLOWA-Volta (EJ and TA). Most datasets have already been described in the literature (Table 4.1). In most cases, ET fluxes are derived from eddy covariance measurements. In some cases, they are derived by energy balance closure (SB, EJ, TA). All fluxes were measured above the canopy. At RD, ET was calculated from the daily change in lysimeter weight, corrected for drainage. All the data are converted to daily values and appropriate units. Occasional missing (half-)hourly ET values are linearly interpolated either from the daily course on the preceding and antecedent days (if not missing) or hours. Days with either too many missing values or minor rainfall are excluded from the analysis. In addition, we utilize daily average observations of global and net radiation.

Model data come from GSWP-2 (grads.iges.org/gswp2). In this project different LSMs produced a Multi-Model land surface analysis on a 1° global grid using the same forcing and boundary conditions (Dirmeyer *et al.*, 2006a). Here we use the baseline integrations (B0) for RD (51°N , 6°E) and SB (13°N , 2°E) both for the individual LSMs and the Multi-Model analysis. For details on GSWP-2 and the individual models we refer to the project website. Additionally, we also analyzed GSWP-2 simulations with the ERA40 LSM.

4.3. Theory

Here we consider a vegetated land surface with deep groundwater (i.e., little capillary rise). Since vegetation water storage is much smaller than soil moisture storage in the root zone (order of mm), we neglect its changes during drydown. Under conditions where availability of soil moisture in the root zone limits root water uptake by vegetation for ET , we assume a proportionality between ET and the available soil moisture storage S :

$$ET(t) = cS(t), \quad (4.1)$$

where the proportionality constant c is the sensitivity of ET for S . For convenience, we will consider the inverse of c , i.e., $\lambda = c^{-1}$, which has the dimension of time. The (simplified) terrestrial water balance is:

$$\frac{dS(t)}{dt} = P(t) - q(t) - ET(t), \quad (4.2)$$

where P is rainfall and q is drainage. In absence of rainfall ($P = 0$), the soil rapidly drains to field capacity below which water is held against gravity ($q = 0$). In this case, (4.2) reduces to:

$$\frac{dS(t)}{dt} = -ET(t). \quad (4.3)$$

By combining (1) and (3) it follows that under rainless conditions:

$$ET(t) = ET_0 \exp\left(-\frac{t'}{\lambda}\right), \quad (4.4)$$

where ET_0 is ET at $t = t_0$ and $t' = t - t_0$. Exponential decay of ET in water-limited conditions has been reported previously from observations (Williams and Albertson, 2004; Dardanelli *et al.*, 2004) and has been widely applied in probabilistic soil moisture analysis (e.g., Rodríguez-Iturbe and Porporato, 2004). The e -folding time λ (or c^{-1}) is the key parameter controlling the temporal evolution of ET . From (4.4) it follows that λ can be estimated from observations of ET alone by (linear) regression of $\ln(ET)$ on t' .

In practice, the relation between S and ET (or t' and $\ln(ET)$) is not perfectly linear. We use R^2 resulting from the regression between t and $\ln(ET)$ to indicate the goodness of fit between S and ET . Obviously, the hydrological significance of λ not only depends on R^2 but rather on the range in observed ET (and thus soil moisture). In order to link λ (or c) to LSM soil physical and root parameters, it is useful to estimate the size of the storage volume S_0 that would be depleted during full drydown ($t \rightarrow \infty$) after the last rainfall event (at t_0):

$$S_0 = \int_{t_0}^{\infty} ET(t) dt = \lambda ET_0, \quad (4.5)$$

where ET_0 is estimated from the regression.

4.4. Results

4.4.1. Observations

The results of the linear regression between $\ln(ET)$ and t' are shown in Fig. 4.3 and are summarized in Table 4.1. At all sites, there is a strong relation between $\ln(ET)$ and t' . High R^2 values (often > 0.9) at many sites suggest the existence of a tight linear relation between S and ET . For three sites, namely BV, RD, and LW (Fig. 2C, 2D, and 2F), we have data for multiple years. This allows us to test the hypothesis that c is different for every drydown. Interestingly, even with different ET_0 , the interannual differences in λ are non-significant at the 95% level. This means the hypothesis cannot be rejected based on the observational evidence we present. This suggests that the assumption of constant (though site-specific) sensitivity of ET for S is reasonable.

At GZ (Fig. 4.2B), two sites only 2 km apart but with different land cover show similar drydown. At IO (Fig. 4.2E), Vaira and Tonzi Ranch are also less than 2 km apart but show a distinct difference in drydown, with the woodland being more persistent. Note that in both cases, both sites would likely be assigned very similar root parameters. Schenk and Jackson (2002) report 50% and 95% rooting depths for temperate savanna of 23 and 140 cm, respectively, and for semi-desert shrubland 28 and 130 cm, respectively. AU (Fig. 4.2G) has a low ET_0 , likely due to low vegetation cover. Through its multiplicative effect on ET , the fraction of vegetation cover affects ET_0 rather than λ .

There appears to be a stronger relation between λ and vegetation cover than between λ and soil type or depth. Small λ (< 20 d) are found at grassland sites (KP, IO-V, TW), while larger λ (> 30 d) are found at sites with tree cover (RC, IO-T) and/or sites that experience seasonal droughts (SB, AU, EJ). Dardanelli *et al.* (2004) report c to be 0.096 d^{-1} for several agricultural crops (corresponding to $\lambda = 10.4$ d). This is smaller than any of the values in Table 4.1, even for the cropland site BV. At the Sahelian sites SB and EJ, the large λ suggests that the perennial vegetation has adapted to the seasonal droughts by developing deep roots that prevent a rapid decay of ET during the dry season. The role of deep roots in maintaining high ET rates during the dry season is well-documented for the Amazon (Nepstad *et al.*, 1994; Bruno *et al.*, 2006; Hasler and Avissar, 2007). Interestingly, the large λ are in contrast with the very shallow soils (< 0.5 m) that were reported for the SB sites (Verhoef *et al.*, 1999). This suggests that the depth to which roots penetrate is not constrained to the shallow soil layer.

To test whether the decay in ET is a soil moisture and not a radiation effect, we normalize ET both by daily average global and net radiation (R_g and R_n , respectively). R_g can be considered as the main external driving force of ET , since it does not depend directly on conditions at the land surface. In general, e -folding times of ET/R_g are close to those obtained by analysis of ET alone, with comparable R^2 (Table 4.1). Considerably larger e -folding times are found for ET/R_n , indicating a dependence of the denominator on ET (associated with a surface temperature and albedo increase during drydown). The RD lysimeter data enables us to check

Table 4.1. Summary of the datasets and results of the regression analysis. The entries are sorted alphabetically. ET indicates regression of daily ET with time, ET/R_g and ET/R_n regression of daily ET normalized by global and net radiation, respectively. References to the datasets are given as footnotes.

Site	Abbreviation	Latitude	Longitude	Vegetation/Land use	Year	ET		ET/R_g		ET/R_n		S_0 [mm]
						λ [d]	R^2	λ [d]	R^2	λ [d]	R^2	
Audubon	AU	31.59°N	110.51°W	Desert grassland	2004	34.7	0.93	32.9	0.94	34.7	0.89	53.7
Bondville	BV	40.01°N	88.29°W	Cropland	1998	18.0	0.68	18.8	0.56	22.5	0.73	81.7
					1999	13.4	0.92	15.5	0.85	18.9	0.86	61.5
Ejura ^a	EJ	7.33°N	1.27°E	Transitional savanna	2002	117.	0.59	116.	0.50	-228.	0.22	175.
Ghanzi ^b	GZ-g	21.51°S	21.74°E	Grassland	2002	14.2	0.97	13.8	0.92	20.1	0.91	43.9
Ghanzi ^b	GZ-m	21.50°S	21.75°E	Mixed (shrub/trees)	2002	16.2	0.96	16.7	0.95	21.3	0.92	52.3
Ione (Tonzi Ranch) ^c	IO-T	38.43°N	120.97°W	Oak savanna	2001	36.8	0.86	35.0	0.79	-	-	146.
Ione (Vaira Ranch) ^c	IO-V	38.41°N	120.95°W	Annual grassland	2001	14.1	0.94	13.4	0.94	15.1	0.94	49.8
Konza Prairie ^d	KP	39.08°N	96.56°W	Tallgrass prairie	1987	12.4	0.89	15.8	0.85	22.3	0.80	31.5
Little Washita ^e	LW	34.96°N	97.98°W	Grassland	1997	23.7	0.76	26.0	0.78	37.2	0.70	68.1
					1998	32.3	0.96	29.7	0.97	39.9	0.93	110.
Rheindahlen ^f	RD	51.18°N	6.43°E	Grassland	1990	21.0	0.63	36.9	0.63	37.9	0.58	64.8
					1991	19.1	0.84	26.5	0.80	33.8	0.61	109.
					1995	20.3	0.80	25.3	0.82	29.8	0.77	38.4
Roccarespampani	RC	42.39°N	11.92°E	Deciduous broadleaf forest	2003	36.0	0.91	36.8	0.92	35.2	0.91	164.
SEBEX ^g	SB-s	13.25°N	2.28°E	Fallow savanna	1989	47.2	0.69	50.7	0.64	78.3	0.46	141.
SEBEX ^g	SB-t	13.25°N	2.28°E	Tiger-bush	1989	118.	0.26	136.	0.21	758.	0.01	274.
Tamale ^a	TA	9.48°N	0.91°E	Guinea savanna	2002	19.0	0.88	20.8	0.96	25.7	0.87	51.3
Twizel ^h	TW	44.23°S	170.15°E	Tussock grassland	1998	16.6	0.80	15.3	0.82	16.7	0.74	28.1

^a Schittenmeyer et al. (2006).

^b Williams and Albertson (2004).

^c Baldocchi et al. (2004).

^d Brutsaert and Chen (1995).

^e Meyers (2001).

^f Xu and Chen (2005).

^g Verhoef et al. (1999).

^h Hunt et al. (2002).

the validity of the zero drainage assumption. Indeed, drainage only accounted for a negligible 1.03% (1990), 0.02% (1991), and 0.29% (1995) of the total water loss. Not surprisingly, we find very similar estimates of λ when ET is regressed directly against the lysimeter storage S : 20.0, 19.3, and 21.5 d, for the years 1990, 1991, and 1995, respectively.

Table 4.1 also lists estimates of S_0 made by means of (4.5). These range from as little as 30 mm for shallow rooting grass vegetation to over 150 mm for sites with deep rooting trees. Note that S_0 should not be interpreted as the total storage in the root zone. Ideally, it is only the part in which storage limits ET . In most cases however, soil moisture might already have been limiting ET before the last rainfall. For TW, *Hunt et al.* (2002) report that 53% of the available storage was utilized before ET was reduced.

4.4.2. GSWP-2 simulations

Figure 4.3A shows λ derived from regressions between $\ln(ET)$ and t' for all models for the 1995 drought at RD. The results for 1990 and 1991 are similar (App. D). For most of the models, λ compares well to the observations. This is also true for the Multi-Model analysis. Some models have low λ , even below the lowest value in Table 4.1. In contrast, some other models hardly show an effect of soil moisture depletion on ET . Since all models have the same forcing, inter-model differences in λ are likely (although not necessarily) caused by differences in soil moisture parameterization. Most R^2 values are smaller than those in the observations, suggesting that most models have a less strong coupling between S and ET . The *Dardanelli et al.* model significantly underestimates the observations at RD and is among the models with smallest λ .

At SB, the situation is different (Fig. 4.3B). Although most LSMs simulate a near-perfect exponential decay of ET (see R^2 in App. D), the variability in λ between the models is large. Some models reduce ET by 63% (e^{-1}) in several days, while in other models this takes months. Although most models (and the Multi-Model analysis) exhibit larger λ for SB than for RD, there seems to be a structural underestimation of the observed λ for both the savanna (SB-s) and tiger-bush (SB-t) site. This structural difference can be explained by the fact that most models do not account for water uptake by deep roots.

The inter-model variability is comparable to that found in previous LSM intercomparison studies. *Lohmann and Wood* (2003) reported composite e -folding times for ET/R_n for LSMs participating in the PILPS phase 2(c) Red-Arkansas River experiment. From their results, e -folding times can be derived ranging from 4.3 to 42.0 d with an inter-model coefficient of variation (CV) of 0.75. Even when only the significant regressions in our analysis are considered, the CV among the models is comparable: 0.59 and 0.72 for RD (1995) and SB, respectively. Although we test the GSWP-2 results only for 2 sites, the problems of some current generation LSMs under conditions where soil moisture limits ET are likely to be typical for many other regions.

4.5. Discussion and Conclusions

The use of ET observations to determine the sensitivity c of ET to soil moisture storage has important advantages. Firstly, the estimates are constrained by the water balance (4.3). Secondly, no soil moisture observations and root parameters are required. Thirdly, ET observed at a flux tower will reflect soil moisture dynamics at the scale of a footprint. Although both the size and the location of the footprint vary with atmospheric boundary layer conditions, the derived c will represent a much larger area than a point-scale soil moisture observation. A disadvantage of the method is that wet-dry transitions without significant rainfall might not occur frequently. Minor incidental rainfall (<1 mm) will be intercepted and readily evaporated, and will not influence the results as long as these days are excluded from the regression. More research is needed to test the robustness of our results against factors such as vegetation dynamics, seasonality, and landscape complexity.

The timescales in Table 4.1 can serve as important benchmarks for LSM performance. The confrontation of state-of-the-art GSWP-2 LSM simulations with observations for two sites suggests that the representation of soil moisture effects on ET can still be improved in many LSMs. For many regions, estimates of the parameter c from Table 4.1 might be used directly to diagnose c in LSMs. For regions such as the Sahel, it might prove necessary to include a parameterization that captures the effect of deep roots on ET . Calibration/validation of LSMs under more extreme conditions (like the wet-dry transitions studied in this paper) can lead to improved model-dependent parameters or states (e.g., “effective” rooting depth, leaf area index). This, in turn, might lead to more robust simulations of land surface hydrology under a range of (changing) climatic conditions.

SOIL MOISTURE TIMESCALES

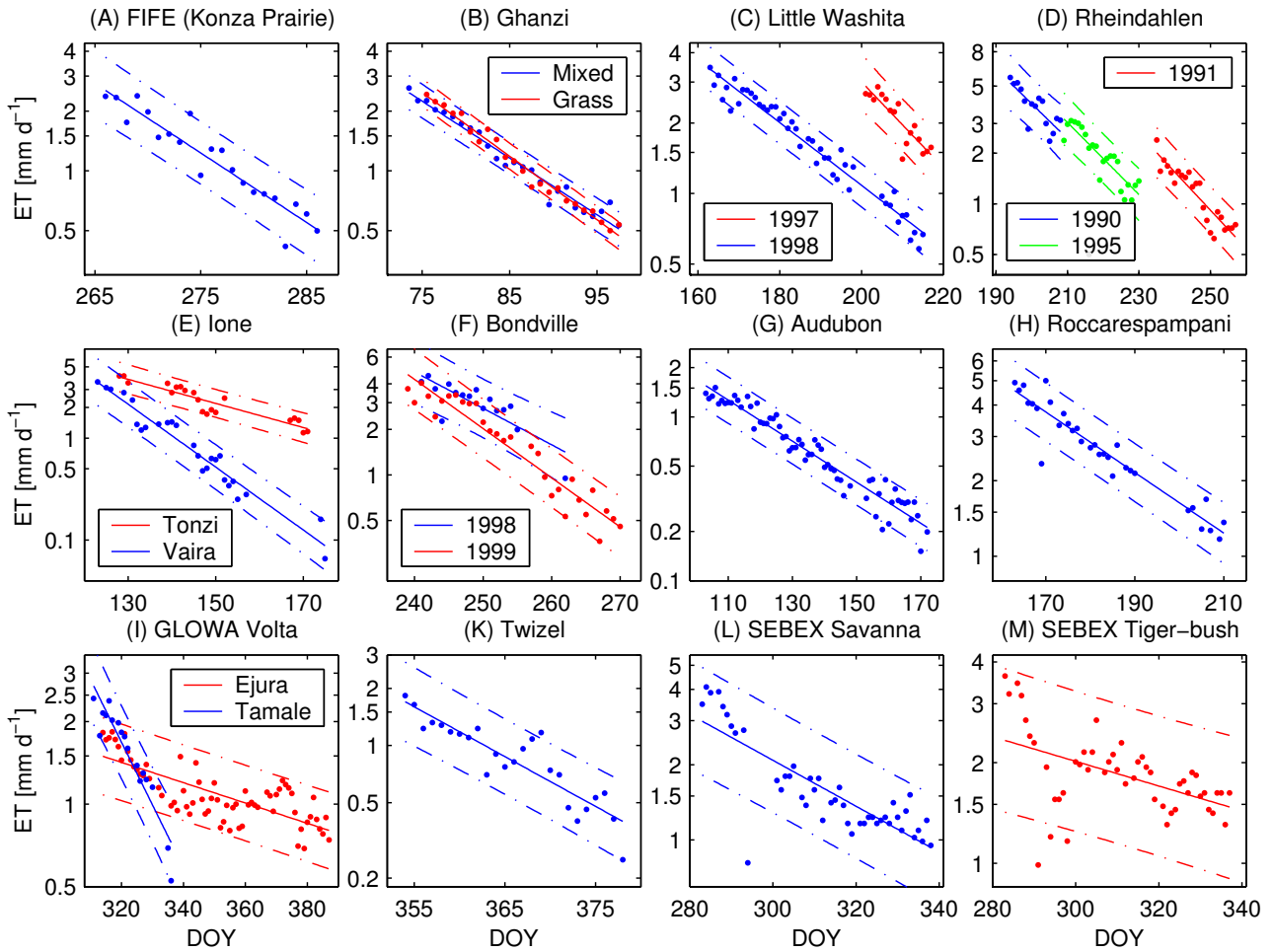


Figure 4.2. Daily ET versus day of year (DOY) for different sites under rainless conditions. Dashed lines correspond to the 95% prediction intervals.

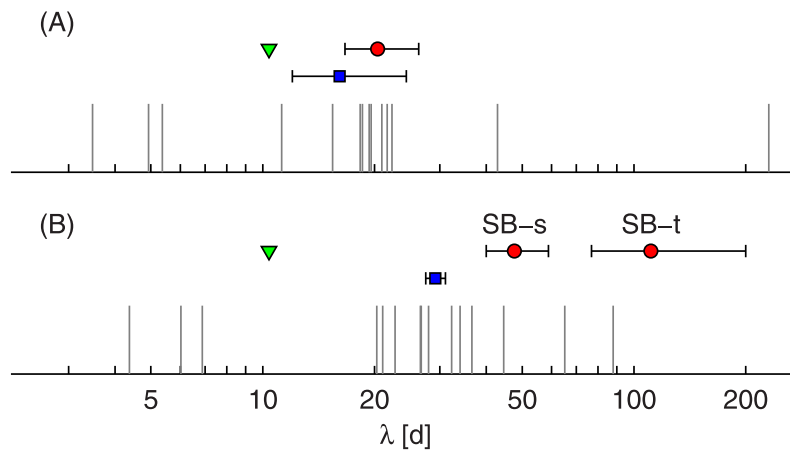


Figure 4.3. Distribution of λ for the GSWP-2 LSMs at (A) Rheindahlen (1995), and (B) SEBEX. Observations (circle) and GSWP-2 Multi-Model analysis (square) are plotted with 95% confidence limits. Triangle indicates the *Dardanelli et al.* (2004) model.

5. Estimating spatial mean root-zone soil moisture from point-scale observations*

Root zone soil moisture is a key variable in many land surface hydrology models. Often, however, there is a mismatch between the spatial scales at which models simulate soil moisture and at which soil moisture is observed. This complicates model validation. The increased availability of detailed datasets on space-time variability of root-zone soil moisture allows for an a posteriori analysis of the uncertainties in the relation between point-scale observations and the spatial mean. Here we analyze three comprehensive datasets from three different regions, and identify different strategies to select observation sites. For each strategy, we present methods to quantify the associated uncertainty. In general there is a large correspondence between the different datasets with respect to the relative uncertainties for the different strategies. The uncertainty can be strongly reduced if some information is available that relates soil moisture content at that site to the spatial mean. Selection of the site closest to the spatial mean on a single date only leads to minor reduction of the uncertainty over seasonal timescales. The correlation with leaf area index or a wetness coefficient alone is insufficient to predict if a site is representative for the spatial mean soil moisture content.

5.1. Introduction

Soil moisture controls several processes at or near the land surface. Accurate soil moisture observations are needed to predict these processes. However soil moisture observations are often available at the point-scale, while most models utilize effective parameters representative for the average soil and vegetation. Similar problems arise when point scale soil moisture observations are combined with flux measurements. Vertical fluxes of water and/or energy at several meters above the surface might be affected by spatial average soil moisture conditions at the scale of the flux footprint. At many stations, for instance in the FLUXNET network (*Baldocchi et al.*, 2001), root zone soil moisture is monitored at a scale several orders of magnitude smaller than the corresponding flux footprint. When validating model simulations with point-scale soil moisture observations, or when assimilating these observations in models, attention should be paid to the uncertainty that results from upscaling the point-scale observations to areal average soil moisture.

One of the first reports of soil moisture variability was made by *Reynolds* (1970). Other early reports on extensive studies of soil moisture variability were made by *Bell et al.* (1980) and *Hawley et al.* (1983). Several authors have noted that, despite the large spatial variability, the soil moisture patterns themselves remain relatively stable over time (e.g., *Vachaud et al.*, 1985; *Mohanty and Skaggs*, 2001). This temporal persistence in the spatial pattern of soil moisture was used by *Vachaud et al.* (1985) to show that some sites maintain a similar rank throughout the year, i.e., that some sites are more representative of the spatial mean than others. *Vachaud et al.* (1985) called these sites “time stable”. Here we use the term “rank” stability rather than “temporal” stability, following the arguments of *Chen* (2006). Rank stability has been used in many other studies to investigate space-time dynamics of soil moisture fields and the potential of using a limited number of sites to observe the mean response (e.g., *Kachanoski and de Jong*, 1988; *Comegna and Basile*, 1994; *Grayson and Western*, 1998; *Gómez-Plaza et al.*, 2000; *Mohanty and Skaggs*, 2001; *Grant et al.*, 2004; *Jacobs et al.*, 2004; *Petrone et al.*, 2004; *Martínez-Fernández and Ceballos*, 2005; *Starks et al.*, 2006). *Pachepsky et al.* (2005) reported rank stability to exist also in the vertical soil moisture distribution.

*This chapter is an edited version of: Teuling, A. J., R. Uijlenhoet, F. Hupet, E. E. van Loon, and P. A. Troch (2006), Estimating spatial mean root-zone soil moisture from point-scale observations, *Hydrol. Earth Syst. Sci.*, 10(5), 755–767.

MEAN SOIL MOISTURE ESTIMATION

Several authors have reported that soil moisture patterns reflect patterns in vegetation (e.g., *Hupet and Van-clooster*, 2002; *Schume et al.*, 2003; *Cantón et al.*, 2004; *Hupet and Van-clooster*, 2005), soil texture (e.g., *Price and Bauer*, 1984; *Vachaud et al.*, 1985; *Seyfried*, 1998; *Grant et al.*, 2004) and/or landscape characteristics (e.g., *Anderson and Kneale*, 1980; *Nyberg*, 1996; *Crave and Gascuel-Odoux*, 1997; *Bárdossy and Lehmann*, 1998; *Famiglietti et al.*, 1998; *Qiu et al.*, 2001). It is also known from field observations that soil moisture patterns can reflect patterns in landscape and/or soil characteristics in a wet state, while reflecting vegetation and/or soil characteristics in a dry state (*Grayson et al.*, 1997; *Fitzjohn et al.*, 1998; *Gómez-Plaza et al.*, 2000). Recent advances in the theoretical understanding of these empirical findings have been made by *Albertson and Montaldo* (2003). They showed that the temporal evolution of soil moisture variability is driven by the sum of the covariances between soil moisture and different fluxes. The temporal dynamics of these different covariance terms can be used to explain the different relations between mean soil moisture and its spatial variability (Chaps. 6 and 8). The fact that different controls operate on the spatial soil moisture pattern depending on the mean moisture content (e.g., *Wilson et al.*, 2005, Chap. 8) has important implications for soil moisture sampling and the applicability of the rank stability concept. For instance, *Martínez-Fernández and Ceballos* (2005) concluded that it might take a year of sampling (a complete seasonal cycle) to correctly identify the most rank stable site.

Spatial soil moisture fields are known to exhibit a correlation structure. *Western et al.* (1998) provide an comprehensive table listing different geostatistical analyses of soil moisture fields. In general, correlation lengths for soil moisture are small, with values of only 10–25 m being common (*Loague*, 1992). Even in experiments with a relatively dense network, spatial correlation is often non-existent (*Comegna and Basile*, 1994; *Hupet and Van-clooster*, 2002). When terrain has a significant impact on the soil moisture pattern, the larger correlation lengths can mainly be attributed to terrain indexes (*Western et al.*, 1998). In Tarrawarra, the spatial structure of the soil moisture field is known to be governed by topographic features in the wet state, while there is little spatial correlation in the dry state (*Western et al.*, 1999). *Manfreda and Rodríguez-Iturbe* (2006) used the concept of correlation lengths in land surface properties to study the space-time sampling of artificial soil moisture fields.

Here we investigate the relation between the dynamics of individual soil moisture observations and those of the spatial mean at the field- or small catchment scale. We perform this exercise for three different datasets, each having its own typical geographic and climatic conditions. By doing so, (dis)similarities between the datasets can be identified. Different sampling strategies are identified and methods are presented to quantify the corresponding uncertainties.

5.2. Data

The datasets were selected based on three criteria: a) observations on multiple depths so that a root-zone average soil moisture content can be estimated, b) a sufficient number of sites that allows for accurate estimation of the spatial mean root zone soil moisture content, and c) sufficient temporal dynamics so that the temporal variability over a complete seasonal cycle is well represented. For the depth of the root zone we used the upper ~70 cm of the soil, which represents most (if not all) of the temporal dynamics of the soil moisture that is available for root water uptake. Typically, 50% of the roots are already located in the upper decimeters of soil (*Schenk and Jackson*, 2002). The depth is partly constrained by the observations, since we choose to include the observations made at 60 cm depth (see below). Furthermore we choose a constant depth for all datasets, so that the results can be compared directly. It should be noted that the temporal dynamics of soil moisture strongly decrease with depth, so that our results are not very sensitive to the exact depth over which soil moisture is averaged.

The 10.5 ha Tarrawarra catchment is located in southeastern Australia (Fig. 5.1A). The catchment has been subject to several intensive monitoring campaigns that aimed at investigating the soil moisture spatial pattern at the small catchment scale. The soil texture in the catchment varies from silty-loam to clay, and the topography is undulating with a maximum relief of 27 m. The climate is temperate. Land use is perennial pastures used for grazing. At 59 dates between 20 September 1995 and 10 June 1997, soil moisture was monitored at 20 locations by means of a Neutron Moisture Meter (NMM). Observations were made at depths of 15, 30, 45, 60, 90, 120, and 150 cm, or to the depth of the access tube. Root zone soil moisture is taken as the average value of the observations at 15, 30, 45, and 60 cm depth. Site 20 was excluded from the analysis since this data is suspected to be erroneous (*Grayson and Western*, 1998). Furthermore days with missing observations for one

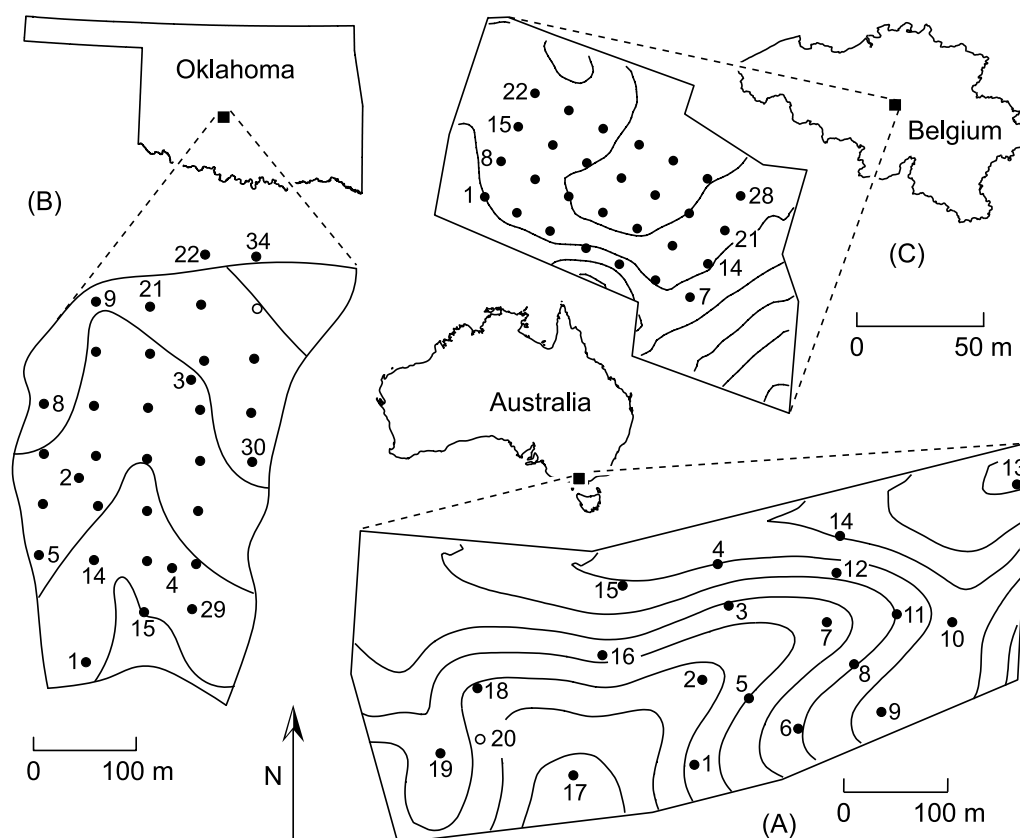


Figure 5.1. Location of the study areas and observation sites. (A) Tarrawarra (2 m interval contour lines), (B) R-5 (~3 m interval contour lines), (C) Louvain-la-Neuve (0.5 m interval contour lines). In (B) and (C) the numbering of sites is continuous along rows. Open circles indicate sites that were omitted in the analysis.

or more sites were excluded, leaving observations at 54 days at 19 sites. The NMM data, along with a detailed 5×5 m Digital Elevation Model, was extracted from the Tarrawarra database (*Western and Grayson, 1998*).

The R-5 experimental catchment is located northeast of Chickasha, Oklahoma (USA). The USDA Agricultural Research Service intensively monitored R-5 from 1966 to 1978. The 10 ha catchment is a native grassland pasture used for grazing. The surface is gently sloping with an average slope of 3% (Fig. 5.1B). At 84 dates between 21 January 1971 and 24 June 1974, NMM observations of soil moisture were made at 34 sites and at 8 different depths. Here we use the average value of the observations made at 15, 30, 45, and 60 cm depth. One site (21) was excluded from the analysis since soil moisture at this site exhibited a suspicious drift, leaving observations at 84 days and 33 sites. The R-5 dataset is described in detail by *Loague (1992)*.

Soil moisture variability was measured in an 0.65 ha agricultural field in Louvain-la-Neuve (Belgium) as part of a campaign that aimed at investigating the within-field spatial variability of evapotranspiration. Observations were made on 45 days between 30 May 1999 and 13 September 1999. The observations were made on a regular 4×7 grid (see Fig. 5.1C) at different depths. Here we use the average value of the Time Domain Reflectometry (TDR) observations (0–20 cm), and the NMM observations at depths of 25 and 50 cm. The soil in the field is classified as well-drained silty-loam and there is little relief. During the campaign the field was cropped with maize. The climate is moderate humid. We also employ the Leaf Area Index (LAI) measurements that were taken at each site on 12 July 1999. The dataset is described in detail by *Hupet and Vanclooster (2002)*.

5.3. Method

5.3.1. Notation

We study the volumetric soil moisture field $\theta(x, t)$. Observations of this field are available at discrete intervals in space and time, namely $x = \{x_1, x_2, \dots, x_n\}$ and $t = \{t_1, t_2, \dots, t_k\}$ where n and k refer to the number of observation sites respectively dates. The indexes i and j refer to selected locations in space and/or time. The number m refers to the number of observations used in calculations when not all available observations are used ($m < n$). We will analyse different strategies to estimate average soil moisture from point scale observations. Two main classes of strategies can be distinguished: those where the interest is in the soil moisture content itself (strategies I–V, see Sect. 5.3.3), and those where the interest is only in observing the dynamics of the spatial mean (strategies VI–IX, see Sect. 5.3.4). An overview of these strategies is given in Table 5.1.

5.3.2. Soil moisture distribution

We focus on the question if a set of soil moisture observations in space can, on average, be expected to follow a normal distribution. From other field experiments it is known that, while most sets are approximately normally distributed, individual sets of observations can show significant skewness and/or kurtosis (*Famiglietti et al.*, 1998). Although there is no fundamental reason why soil moisture should follow a normal distribution, the use of this distribution has obvious advantages. Since soil moisture is bounded between residual moisture content and saturation, bounded distributions might be more appropriate for some applications (*Wood*, 1997; *Ryu and Famiglietti*, 2005). We perform a visual test for normality. For all k observation dates, the individual samples $\theta(x, t_j)$ are normalized by subtracting the observed spatial mean $\bar{\theta}_j$ and dividing by the observed standard deviation $s(\theta_j)$. These are estimated by:

$$\hat{E}[\theta(t_j)] = \bar{\theta}_j = \frac{1}{n} \sum_{i=1}^n \theta(x_i, t_j) \quad (5.1)$$

and

$$\widehat{\text{Var}}[\theta(t_j)] = s(\theta_j)^2 = \frac{1}{n-1} \sum_{i=1}^n [\theta(x_i, t_j) - \bar{\theta}_j]^2. \quad (5.2)$$

These normalized values are ranked from dry to wet and plotted with their corresponding cumulative probability level. The probability axis is transformed such that a normal distribution yields a straight line.

5.3.3. Mean soil moisture estimation

In practice, the spatial average soil moisture content is often assumed to equal that at a single observation site (strategy I). For this strategy, the uncertainty of this estimate is controlled by the spatial variability. This spatial variability might depend on the mean moisture content, which is generally unknown (since this is to be estimated). Therefore we define the “expected” spatial variability for each dataset, i.e., the variance that can be expected at a given moment in time without prior knowledge of $\bar{\theta}_j$ (App. E):

$$\hat{E}[\text{Var}(\theta)] = \frac{1}{k} \sum_{j=1}^k \text{Var}[\theta(t_j)]. \quad (5.3)$$

With the a priori knowledge that soil moisture patterns are persistent, some sites are more representative of the spatial mean than others. Following *Vachaud et al.* (1985), we define the spatial difference $\delta(x, t_j)$ between the soil moisture content $\theta(x, t_j)$ and the spatial mean water content $\bar{\theta}_j$ as:

$$\delta(x, t_j) = \theta(x, t_j) - \bar{\theta}_j \quad (5.4)$$

In contrast to previous studies on rank stability where δ was normalized by $\bar{\theta}_j$, we express δ in the same units as θ . Note that since δ is corrected for the spatial mean soil moisture at all t_j , it reflects the persistence in the spatial pattern of θ rather than in its actual magnitude. The temporal mean difference for every site $\bar{\delta}_i$ is estimated as:

$$\hat{E}[\delta(x_i)] = \bar{\delta}_i = \frac{1}{k} \sum_{j=1}^k \delta(x_i, t_j), \quad (5.5)$$

and the temporal variability of δ at site i , $\widehat{\text{Var}}[\delta(x_i)]$, as:

$$\widehat{\text{Var}}[\delta(x_i)] = s(\delta_i)^2 = \frac{1}{k-1} \sum_{j=1}^k (\delta(x_i, t_j) - \bar{\delta}_i)^2. \quad (5.6)$$

Although various definitions can be found in the literature for the most rank stable site Φ , the most straightforward definition is the site having the smallest absolute mean difference so that this site can be used directly to estimate the mean soil moisture content (e.g., *Grayson and Western, 1998*):

$$\Phi = \{i \mid |\bar{\delta}_i| < |\bar{\delta}_m| \quad \forall \quad m \neq i\}. \quad (5.7)$$

Through this definition, the most rank stable site can only be selected if the spatial and temporal dynamics of the soil moisture field are known. This applies to cases where an area was first subjected to an intensive monitoring campaign, and where monitoring is continued only at the site which, on average, is closest to the spatial mean (strategy II). For strategy II we will assume $E(\bar{\delta}_\Phi) = 0$.

If the space-time variability of a soil moisture field is known from a preceding campaign, the spatial mean might also be predicted from a regression between soil moisture at an individual site and the spatial mean. Since the soil moisture differences at individual locations might be a function of $\bar{\theta}_j$, this strategy can be expected to yield more accurate estimates of $\bar{\theta}_j$ than strategy II. Since in general the best site will be chosen, we quantify the uncertainty associated with this approach as the minimum of the variances around the regressions for the individual sites (strategy III).

A serious drawback for application of strategy II is that a priori knowledge on the space-time dynamics of the soil moisture field is required. This requires intensive sampling. As was suggested in previous studies (e.g., *Vachaud et al., 1985; Comegna and Basile, 1994*), a more practical method would be to select the most rank stable site from one initial field survey at time t_j . With this strategy (strategy IV), the most rank stable site Φ_j is the one that is closest to $\bar{\theta}_j$. We therefore determine Φ_j for all k spatial soil moisture fields. The effective uncertainty associated with the approach of taking Φ_j to represent $\bar{\theta}_j$ is influenced both by $\bar{\delta}_i$ and $\text{Var}[\delta(x_i)]$. The expression for this ‘‘overall’’ variance is derived in App. E.

If the mean soil moisture can be estimated from multiple measurements located randomly (strategy V), the uncertainty of the mean will decrease with the number of observations m . Whereas in previous studies the focus was mainly on the relative accuracy of the mean estimated from multiple observations (or the numbers of observations needed to achieve a required level of relative accuracy), we focus here on the absolute uncertainty since this is a more relevant parameter for many modeling purposes. In the idealized case where the observations are completely independent, the standard error of the mean s_m is given by:

$$s_m = \frac{s}{\sqrt{m}}, \quad (5.8)$$

where s is the standard deviation of the individual observations. Since the soil moisture field exhibits spatial correlation, the actual dependence of s_m on the number of observations will differ from (5.8). To investigate whether the actual dependence differs from (5.8), we derived this dependence from the observations. For all observation dates and for $1 \leq m \leq n/2$, the spatial mean was estimated for all independent sets of observations of size m . These sets of observations were selected randomly, but every site was only allowed to occur once, yielding a maximum number of n/m sets. The standard error of the mean was then calculated as the standard deviation of the estimated means. This procedure was repeated 20 times to reduce sampling effects, and the results were averaged.

5.3.4. Mean soil moisture time series estimation

One might argue that for a particular site i the bias with respect to the spatial mean ($\bar{\delta}_i$) is of little importance as long as the dynamics of the spatial mean are well represented. In this case the goal of soil moisture monitoring might be to estimate the spatial mean soil moisture dynamics rather than its actual value. The variability of the difference between a time series at one site and the time series of the spatial mean is expressed by $\text{Var}[\delta(x_i)]$. This quantity expresses the temporal variability of a site with respect to the spatial mean, similar to $\text{Var}[\theta(t_j)]$

Table 5.1. Sampling strategies and corresponding uncertainties. Values are expressed as one standard deviation (volumetric moisture content). In the “Goal” column, “Abs” refers to absolute value of the spatial average volumetric soil moisture content, and “Dyn” refers to the dynamics of the spatial average.

Strategy	Goal	No. of sites	Location of site(s)	Tarrawarra	R-5	Louvain-la-Neuve
			Climate	0.0639	0.0726	0.0471
I	Abs	1	Random	0.0274	0.0263	0.0167
II	Abs	1	On average closest to spatial mean	0.0079	0.0122	0.0067
III	Abs	1	Best regression with spatial mean	0.0014	0.0055	0.0025
IV	Abs	1	At single date closest to spatial mean	0.0166	0.0187	0.0150
V	Abs	2	Random	0.0128	0.0128	0.0083
		3		0.0072	0.0078	0.0048
VI	Dyn	1	Random	0.0162	0.0163	0.0115
VII	Dyn	1	Smallest variability in difference to mean	0.0076	0.0088	0.0042
VIII	Dyn	1	Smallest RMSE	0.0079	0.0099	0.0067
IX	Dyn	2	Random	0.0075	0.0077	0.0054
		3		0.0042	0.0045	0.0031

for the spatial mean. If a site is randomly selected (strategy VI), the “expected” temporal variance with respect to the spatial mean is (App. E):

$$E\{\text{Var}[\delta(x_i) - \bar{\delta}_i]\} = \frac{1}{m} \sum_{j=1}^m \text{Var}[\delta(x_i, t_j)]. \quad (5.9)$$

If the goal is to capture the temporal dynamics of the spatial mean from a single observation site, a different definition of rank stability might be more appropriate. In this case (strategy VII) one would prefer the site with the smallest temporal variance of δ :

$$\Phi = \{i \mid s(\delta_i)^2 < s(\delta_m)^2 \quad \forall \quad m \neq i\}. \quad (5.10)$$

Note that through this definition, the most rank stable site can only be identified if the complete space-time dynamics are known. This is different from strategy IV, where only one spatial field is needed to identify the site closest to the mean. Other definitions for the most rank stable site can also be found. For instance, *Jacobs et al.* (2004) account for both the bias and variance of the soil moisture difference time series in the definition of the most rank stable site by minimizing the root mean square error:

$$\text{RMSE}_i = \{\bar{\delta}_i^2 + \text{Var}[\delta(x_i, t)]\}^{\frac{1}{2}} = E\{[\delta(x_i)]^2\}^{\frac{1}{2}}. \quad (5.11)$$

This case (strategy VIII) will be analyzed in addition to the other definitions of rank stable sites. As was already mentioned in the preceding paragraph, the soil moisture differences might depend on θ_j . This means that a better estimate of the mean response can be obtained by regression of soil moisture at an individual site to the spatial mean. Since uncertainty around a regression is not affected by bias, this is the same as strategy III. The uncertainty in the soil moisture time series at a single site with respect to the spatial mean time series might be reduced by taking the time series of soil moisture averaged over different randomly located sites (strategy IX). To quantify this reduction, we used an approach similar to that for strategy V. For all observation dates and for $1 \leq m \leq n/2$, the spatial mean was estimated for all independent sets of observations of size m . The uncertainty was then calculated as the variability in the difference between the time series of these estimates and the time series of the “true” spatial mean.

5.3.5. A priori site selection

The location of the sites that best represent the mean conditions might be identified a priori; i.e., based on land surface properties that are known to influence soil moisture dynamics (soil texture, vegetation). For instance, *Vachaud et al.* (1985) already discussed the relation between rank stability and soil texture. They stated that “there is a high probability that if a location is the most wet at a given time, it will remain the most wet at other times because it has the highest clay content”. For more hilly areas, *Grayson and Western* (1998, pp. 79) argued that these sites “are in areas that are neither strongly convergent nor divergent, tend to be near the mid-slopes and are in areas that have topographic aspect close to average for the catchment”. Different wetness indices can be found in the literature that predict zones of below/above average wetness based on topography (see *Western et al.*, 1999, for their application to Tarrawarra). In this study we employ a wetness index developed by *Svetlitchnyi et al.* (2003). The relative wetness coefficient at any point (η_i) is defined as the ratio of expected soil moisture at that point (as influenced by topography alone) and the expected soil moisture for a flat surface (without effects of topography). The (semi-)empirical model accounts for the effects of slope profile shape, slope aspect, distance from the divide, and slope gradient on the soil moisture distribution in the top 0.5 m of the soil (*Svetlitchnyi et al.*, 2003, see also Chap. 6). In this way both effects of subsurface flow and exposure are accounted for. Details of the model can be found in *Svetlitchnyi et al.* (2003). Here we investigate the correlation between the wetness coefficient and the mean soil moisture difference $\bar{\delta}_i$ for Tarrawarra.

Leaf area index is known to positively influence evapotranspiration rates (e.g., *Al-Kaisi et al.*, 1989; *Hupet and Vanclooster*, 2004). This means that sites with higher than average LAI will have evaporated more in the preceding period. At this site, one should expect a below-average soil moisture. In this way, a site with average LAI might be associated with average evapotranspiration rates, and average soil moisture. Here we investigate the correlation between LAI and the mean soil moisture difference $\bar{\delta}_i$ for Louvain-la-Neuve.

5.4. Results

5.4.1. Soil moisture distribution

Figure 5.2 shows the normalized soil moisture versus the cumulative probability. The straight line indicates the standard normal distribution. In this plot, any structural deviation from a normal distribution will result in a deviation from the straight line. From the scatter in the points (indicated by error bars) it can be seen that individual distributions can deviate significantly from normal. However on average the points tend to cluster around the normal line. This shows that, if no a priori information on the spatial soil moisture distribution is available, the assumption of normality is reasonable. R-5 shows the least temporal variability in the shape of the soil moisture distribution. These findings are in agreement with previous studies (*Cosh et al.*, 2004).

To illustrate that the clustering around the straight line is not the result of sampling or the Central Limit Theorem, we performed the same analysis on randomly generated spatial fields drawn from a lognormal distribution. The inset in Fig. 5.2 shows that sampling has a minor impact on the results. The randomly generated data from a non-normal distribution clearly deviates from a straight line.

5.4.2. Mean soil moisture estimation

With only one observation site located randomly (strategy I), the uncertainty associated with estimates of the mean soil moisture is controlled by the spatial variability. Effective variability values are listed in Table 5.1. Tarrawarra and R-5 have comparable standard deviations of 0.027 and 0.026, while Louvain-la-Neuve has a somewhat smaller value of 0.017. This is likely due to the smaller size of the area (more than an order of magnitude), the little variation in topography and/or soils as compared to the other sites. Since the spatial distribution of soil moisture is approximately normal, 95% confidence intervals can be constructed with a width of twice the expected spatial standard deviation. It is interesting to compare these values to variability in the climate signal itself, that is the temporal variability of the spatial mean $\bar{\theta}_j$. Since this is the signal that one actually wants to observe, a comparison with the uncertainty (or noise) provides something that can be interpreted as a signal-to-noise ratio. The variability of the climate signal is also listed in Table 5.1.

The sites that are on average closest to the spatial mean (strategy II) are indicated in Fig. 5.4 by the downward triangles. With this strategy the uncertainty reduces to the temporal variability of the difference between soil

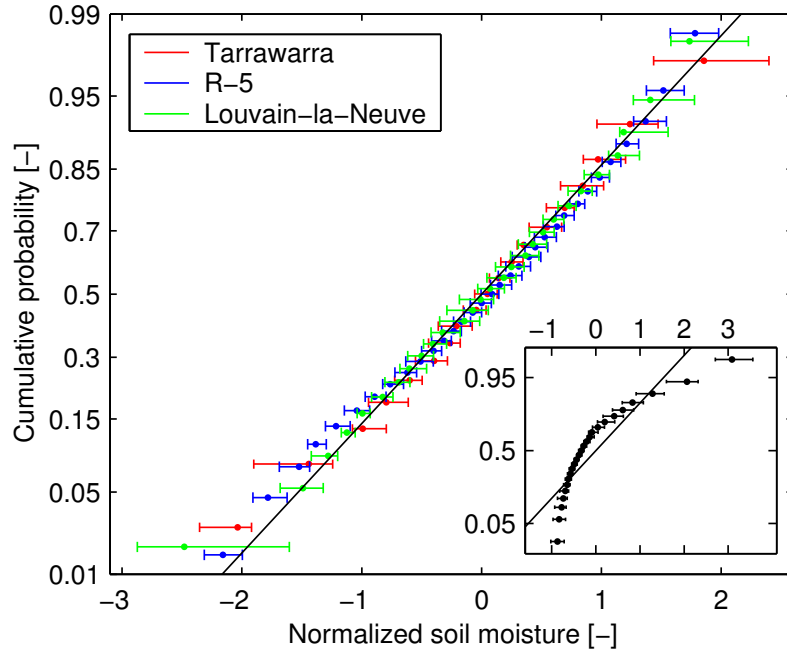


Figure 5.2. Normal probability plot of the normalized spatial soil moisture fields. Dots indicate the median value, error bars indicate 25% and 75% percentiles of time variability. The inset shows the same procedure applied to randomly generated fields from a lognormal distribution, with $n = 25$ and $k = 60$.

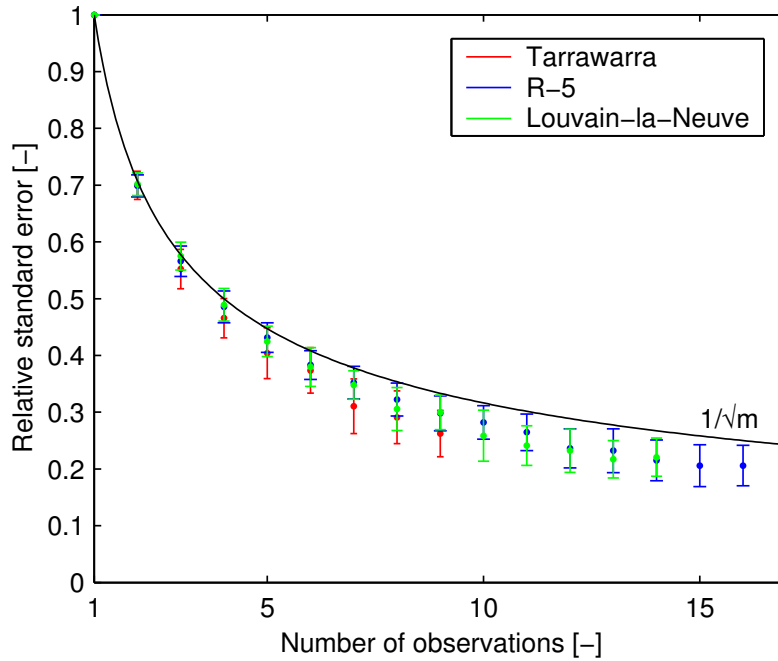


Figure 5.3. Relative standard error as a function of the number of observations that is used to estimate the spatial mean. The black line is the theoretical curve for independent observations.

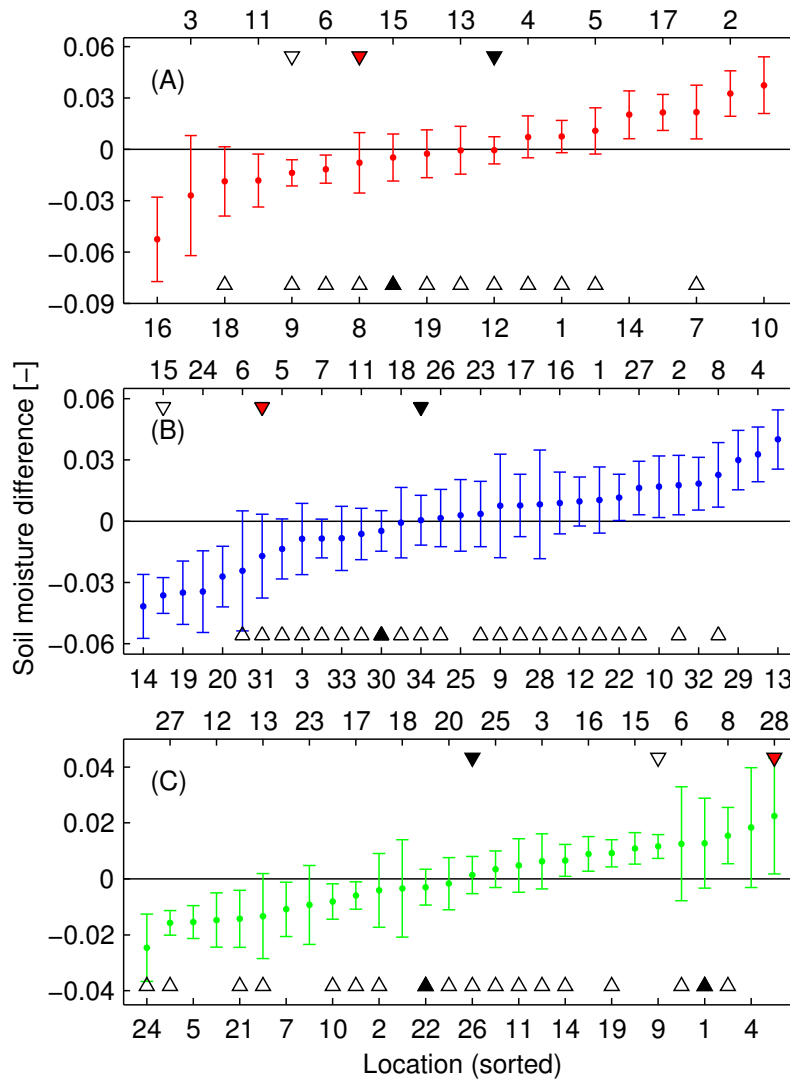


Figure 5.4. Rank stability plots for the three datasets. The sites are ranked according to $\bar{\delta}_i$. The error bars indicate temporal variability (standard deviation). The numbers refer to sites in Fig. 5.1. (A) Tarrawarra, (B) R-5, (C) Louvain-la-Neuve. Downward triangles at the top indicate the most rank stable site (filled for strategy II, open for strategy VII, red for strategy III, green for strategy VIII), upward triangles at the bottom indicate most rank stable sites for strategy III with the most probable one(s) filled.

moisture at this site and the spatial mean. These values vary between 0.007 and 0.012 (see Table 5.1). Even more precise estimates of the mean soil moisture from a single site are obtained with strategy III. Table 5.1 lists the minimum values of this observation strategy. The corresponding sites are identified in Fig. 5.4. For all three datasets, these sites differ from the sites that are on average closest to the mean. These sites also have a large time variability, indicating that the corresponding regression not only has an offset, but also that the slope differs from 1. The low uncertainty (0.0014 to 0.0055) indicates that accurate soil moisture estimation from a single site is possible over a range of wetness conditions; but only if the space-time dynamics of the soil moisture field are known from a preceding campaign.

As noted before, the site closest to the mean might in practice be identified from a single spatial survey (strategy IV). If there would exist perfect rank stability, this would give the same result as strategy II. However careful analysis reveals that the site that is on average closest to the mean has a low probability of being identified at a given moment in time. These probabilities are only 7% (4/54), 10% (8/84), and 4% (2/45) for Tarrawarra, R-5, and Louvain-la-Neuve, respectively. On individual dates, between 60 to 70% of all the sites would be identified as being closest to the spatial mean. These sites are identified in Fig. 5.4 by the upward

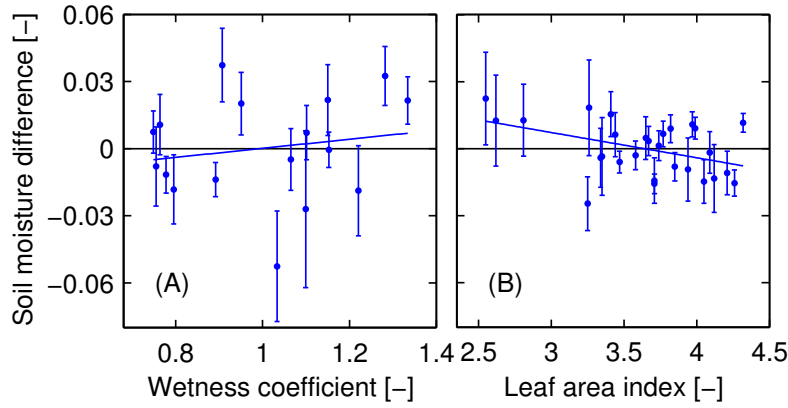


Figure 5.5. Land surface characteristics versus mean soil moisture difference. (A) Wetness coefficient η at Tarrawarra ($R^2 = 0.03$), (B) Leaf area index at Louvain-la-Neuve ($R^2 = 0.18$). Error bars indicate the temporal variability in soil moisture difference for each site, similar to Fig. 5.4.

triangles. The site(s) that is (are) most likely to be identified as being closest to the mean on individual dates (indicated by filled upward triangles) differ in all three cases from the site that is on average closest to the mean. For Tarrawarra, R-5, and Louvain-la-Neuve these sites are 15, 30, and 1(22), with probabilities of 19% (10/54), 14% (12/84), and 11% (5/45), respectively. The large variation in sites being closest to the mean on individual dates adds considerable uncertainty to strategy II. For Louvain-la-Neuve, this uncertainty is almost equal to the spatial variability (0.0150 vs. 0.0167). This is caused by the selection of some sites with a large temporal variability of the soil moisture difference. For the other two datasets, the uncertainty for strategy IV is still 61% (Tarrawarra) and 71% (R-5) of the effective spatial standard deviation.

Figure 5.3 shows how the relative (to the spatial variability) uncertainty decreases with the number of randomly located observation sites. In spite of any possible spatial correlation, the empirical relations for the different datasets are close to the theoretical relation for fully independent samples ($1/\sqrt{m}$). For all datasets, this relation slightly overestimates the actual uncertainty. When the mean of 4 independent samples is used to estimate the “true” spatial mean, the uncertainty reduces to approximately 50% of the spatial variability. For 9 sites, this reduction is 70 to 75%. For independent samples, this reduction should be 50% for four samples, and 66.7% for nine samples.

5.4.3. Mean soil moisture time series estimation

One might expect the uncertainty associated with the estimation of the temporal dynamics of the spatial mean from a single site to be much less than that associated with the estimation of the mean itself. The effective values of the uncertainty associated with the time series range between 0.0115 and 0.0163 (see Table 5.1). It is interesting to compare the values in Table 5.1 for strategies I and VI. Strategy I represents the effective (for all sampling dates) uncertainty caused by spatial heterogeneity, while strategy VI represents the effective (for all sampling sites) uncertainty due to temporal or process heterogeneity. The ratios of the temporal and spatial standard deviation around the spatial mean range between 0.59 and 0.68.

There are large differences in the temporal variability between the different sites. For some sites, the temporal variability exceeds the spatial variability, while other sites show little temporal variability in their difference to the spatial mean. The sites with minimum temporal variability are indicated in Fig. 5.4. In all the three datasets, these sites do not correspond to the optimal sites for the other strategies. In two datasets (R-5 and Louvain-la-Neuve), these sites even differ from all the sites that are closest to the spatial mean at individual dates. The uncertainty for these sites is small: between 0.0042 and 0.0088. However even for the “best” site, the standard deviation is still 10% of the climate signal.

The site with the lowest RMSE is indicated in Fig. 5.4. In two datasets (Tarrawarra and Louvain-la-Neuve) the site with the lowest RMSE is on average also closest to the spatial mean, showing that in practice there might be little difference between the definitions. The uncertainties for strategy VIII (0.0053–0.0080) are comparable

to the values for strategies II and VII. If the time series of the spatial mean is estimated from the time series of the mean of several randomly located sites (strategy IX), then the relative uncertainty (with respect to the “expected” temporal variability) decreases with the number of sites in a similar fashion to Fig. 5.3 (not shown). Table 5.1 lists the uncertainties in the case that four or nine sites are used to estimate the spatial mean. These values are roughly 45% or 25 to 30%, respectively, of the variability in the individual time series (strategy VI), which again is only slightly less than would follow from (5.8).

5.4.4. A priori site selection

Figure 5.5A shows the relation between the mean soil moisture difference $\bar{\delta}_i$ and the wetness coefficient for the Tarrawarra catchment. This coefficient is indicative for the distribution of soil moisture in the upper 0.5 m of the soil (Svetlitchnyi *et al.*, 2003). The distribution of the wetness coefficient closely resembles the observed detailed soil moisture patterns at Tarrawarra (e.g., *Western and Grayson*, 1998). Above average wetness is encountered along the drainage lines, and below average wetness on the exposed north-facing slope. If point-scale soil moisture is only distributed according to topography, one might expect a clear relation with the wetness coefficient. Ideally, the sites that are closest to the spatial mean would have a wetness coefficient near unity. However the actual correlation between the mean soil moisture difference and the wetness coefficient is close to zero. The low correlation is illustrated by the fact that the site which has a wetness coefficient closest to unity is on average the driest! This result is both surprising and contradicting: while the pattern of the wetness coefficient seems very similar to detailed observed soil moisture patterns at Tarrawarra, there is hardly any correlation between the individual NMM sites and the wetness coefficient. This is in line with the findings by *Wilson et al.* (2004), who showed that even in catchments with significant topographic variability, the topographic component might not be the largest contributor to the overall spatial variance.

For Louvain-la-Neuve, vegetation rather than topography can be expected to have the largest impact on the spatial soil moisture pattern. Figure 5.5B shows the relation between LAI and the mean soil moisture difference $\bar{\delta}_i$ for each site. Although the correlation is higher than for the wetness coefficient at Tarrawarra, it is still low ($R^2 = 0.18$). This might be due to the fact that LAI was observed only once under relatively wet soil moisture conditions early in the growing season. The soil moisture pattern under these conditions might reflect the pattern of soil texture rather than vegetation (LAI). However the correlation with the yield, which was measured at the end of the growing season (*Hupet and Vanclooster*, 2002), is even lower ($R^2 = 0.16$). These correlations are too weak to predict the location of rank stable sites from LAI alone.

5.5. Discussion and Conclusions

So far, the local soil moisture differences δ_i to the spatial mean have only been discussed in terms of their expected distribution. It is also interesting to look at their temporal correlation. Figure 5.6 shows the space-time distribution of $\delta(x,t)$ for Louvain-la-Neuve sorted by the temporal mean difference for every site and the spatial mean soil moisture for every date. This reveals an interesting property of the soil moisture field. For a large part of the mean soil moisture range (indicated by “wet”), the local soil moisture differences remain nearly constant, indicating a similar spatial pattern. Similarly, another (different!) spatial pattern exists in the “dry” domain, with a less defined transition in between. These patterns likely reflect properties of the soil in the “wet” domain, and vegetation in the “dry” domain. The apparent switch between two preferred spatial patterns is similar to the one observed in Tarrawarra (*Grayson et al.*, 1997). It should be noted that the LAI observations were made in the “wet” domain, while the impact on the soil moisture pattern might be more pronounced in the “dry” domain. This might partly explain the low correlation in Fig. 5.5A.

So far, we have not discussed the uncertainty introduced by measurement error. From a geostatistical analysis of Tarrawarra TDR soil moisture, *Western et al.* (1998) report nugget values ranging from 0.020 to 0.024 (standard deviation) including both effects of small scale heterogeneity and measurement error. *Western and Grayson* (1998) report the NMM observations to have an error standard deviation of 2.5 volumetric moisture percent, i.e., 0.025. These values seem to overestimate the actual random error. Table 5.1 shows that the scatter around the regression between soil moisture at individual sites and the spatial mean (strategy III) can be as low as 0.0014. This is probably a better estimate of the true random error. For Louvain-la-Neuve, *Hupet et al.* (2004) report total measurement uncertainties for the NMM and TDR of 0.0091 to 0.0095 resp. 0.0158

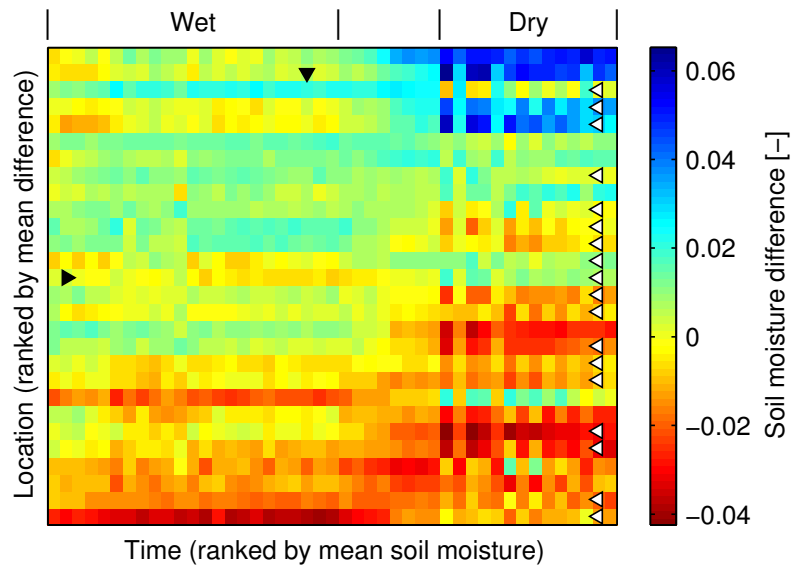


Figure 5.6. Differences ($\delta(x,t)$) between local soil moisture and the spatial mean for Louvain-la-Neuve. The sites have been ranked as in Fig. 5.4, and the dates according to their mean soil moisture content. Three domains can be distinguished: a wet domain in which soil moisture variability reflects soil properties, a transition domain, and a dry domain in which the variability reflects vegetation properties. The leftward triangle indicate the site that is on average closest to the mean (strategy II), rightward triangles the sites that on single dates are closest to the mean, and the downward triangle the date of LAI observations.

to 0.0176 (standard deviation of the volumetric moisture content). The contribution of the instrument alone is estimated as 0.005801 resp. 0.0021 to 0.0028. This is very close to the value for strategy III in Table 5.1 (0.0025). This suggests that it is possible to monitor spatial average soil moisture with approximately the same accuracy as point-scale soil moisture, provided that the regression between the two is known.

On average, the spatial distribution of soil moisture is well approximated by a normal distribution. The temporal dynamics of the spatial mean soil moisture can be estimated more accurately from a randomly located site than the mean soil moisture itself. However the standard deviation of the uncertainty on these temporal dynamics is still $\sim 66\%$ of the effective spatial variability. Rank stable sites exist for all three datasets. The uncertainty on the estimated spatial mean is reduced considerably (to $\sim 40\%$ of the effective spatial variability) if one of these sites is used to monitor soil moisture. However identification of these sites requires intensive sampling. If such a site is selected from a single spatial survey, the overall uncertainty is still $\sim 75\%$ of the effective spatial variability.

For many sites, the temporal correlation in the soil moisture differences to the spatial mean results in an accurate linear regression between soil moisture at that site and the spatial mean. The accuracy of this regression is close to the random observation error for a single soil moisture observation. To first order, the relative (to the spatial variability) standard error of the spatial mean soil moisture reduces with the inverse of the square root of the number of randomly located sites used to estimate the mean. This means that the uncertainty can be reduced by $\sim 50\%$ if the mean is estimated from four sites rather than from a single site.

Although the spatial soil moisture pattern is known to be related to a combination of soil, vegetation, and landscape characteristics, neither a wetness coefficient derived from a DEM or the LAI showed a high correlation with the temporal mean soil moisture differences to the spatial mean for the different sites. It should therefore not be expected that a particular site with an average wetness coefficient or average LAI has a close to average soil moisture. The results presented in this paper are based on analysis of three datasets only. The large consistency in the relative uncertainties between the different observation strategies (Table 5.1) suggest they might be indicative for other areas as well.

6. Improved understanding of soil moisture variability dynamics*

Different trends of soil moisture variability with mean moisture content have been reported from field observations. Here we explain these trends for three different data sets by showing how vegetation, soil and topography controls interact to either create or destroy spatial variance. Improved understanding of these processes is needed for the transformation of point-scale measurements and parameterizations to scales required for climate studies, operational weather forecasting, and large scale hydrological modeling.

6.1. Introduction

Although the quantitative contribution of soil moisture to the global water budget is negligible, it plays a central role in the global water cycle by controlling the partitioning of water and energy fluxes at the earth's surface, and may control the continental water distribution through land-surface atmosphere feedback mechanisms (*Koster et al.*, 2003). The ability of coupled models to reproduce these processes will strongly depend on the parameterization of soil moisture state-flux relations at the regional scale. The lack of accurate observations of land surface states and fluxes at this scale, combined with the variability of soil moisture and the high non-linearity of land-surface processes at the small scale, requires aggregation of small scale processes to larger scales in order to prevent systematic biases in modeled water- and energy fluxes (*Crow and Wood*, 2002). For successful aggregation, knowledge on soil moisture variability controls is indispensable.

Several scientists have reported soil moisture variability to increase with decreasing mean moisture content (e.g., *Famiglietti et al.*, 1999; *Hupet and Vanclooster*, 2002). Other scientists reported opposite trends (e.g., *Western and Grayson*, 1998; *Famiglietti et al.*, 1998), were unable to detect a trend (e.g., *Hawley et al.*, 1983; *Charpentier and Groffman*, 1992), or found the trend to depend on the mean soil moisture state (e.g., *Owe et al.*, 1982; *Albertson and Montaldo*, 2003). Although many scientists have speculated about the origin of soil moisture variability, there have been only few quantitative studies looking at how different processes act to either increase or decrease the spatial variability of soil moisture. By using the similar media concept, *Salvucci* (1998) showed how variability in soil texture leads to different soil moisture variability states in different limiting cases. *Albertson and Montaldo* (2003) showed how covariances between soil moisture and fluxes, originating from variability in soil moisture, forcing and/or land surface properties, can lead to either an increase or decrease in soil moisture variability.

Here we develop a simple model that is able to reproduce the different observed soil moisture variability trends for the three different data sets that were used in this study (see Figs. 6.1 and 6.3, upper panels). We also show that the apparent contradictory observations can be explained by the temporal dynamics of the interaction between soil, vegetation, and topography controls.

6.2. Data

Soil moisture (0–20 cm) variability was measured at an agricultural field in Louvain-la-Neuve (Belgium) on 60 days between 30 May 1999 and 13 September 1999 as part of a campaign with the objective to investigate the within-field spatial variability of transpiration (*Hupet and Vanclooster*, 2002). The soils in the field are classified as well-drained silty-loam and there is little relief. During the campaign the field was cropped with

*This chapter is an edited version of: Teuling, A. J., and P. A. Troch (2005), Improved understanding of soil moisture variability dynamics, *Geophys. Res. Lett.*, 32(5), L05404, doi:10.1029/2004GL021935. Copyright 2005 American Geophysical Union.

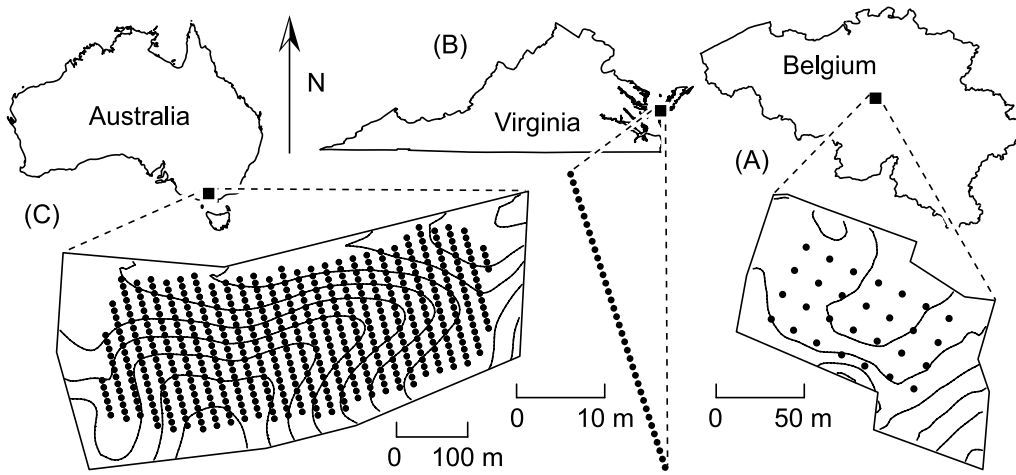


Figure 6.1. Location of the soil moisture observation sites. (A) Louvain-la-Neuve, with 0.5 m contour lines, (B) VCR-LTER site, (C) Tarrawarra, with 2 m contour lines.

maize. The climate is temperate humid. Meteorological observations are available from 1 January 1999 until 31 December 1999.

From 24 June 1998 to 26 January 1999, soil moisture (0–30 cm) was measured with 36 TDR sensors (spacing 1 m) at a gently sloping field transect at the Virginia Coastal Reserve Long Term Ecological Research (VCR-LTER) site on the eastern shore of Virginia, USA (*Albertson and Montaldo, 2003*). The sandy loam soils were covered by Johnson grass. Meteorological observations are available for the period 30 June 1998 until 27 September 1998.

The Australian Tarrawarra dataset results from an experiment that aimed at investigating the spatial pattern of soil moisture at the small catchment scale. Between 27 September 1995 and 29 November 1996 a total of 13 soil moisture (0–30 cm) patterns were measured (*Western and Grayson, 1998*). Additional measurements are summarized in *Western et al. (2004)*. The soils in the catchment are silty-loam to clay, and the topography is undulating with a maximum relief of 27 m. The climate is temperate. Land use is perennial pastures used for grazing. Meteorological observations are available for the period 10 August 1995 until 25 October 1997.

6.3. Modeling variability

6.3.1. Point-scale soil moisture dynamics

Under most conditions, lateral flow in the upper part of the soil can be neglected, and the vertically integrated soil moisture balance over a depth L can be written as:

$$\frac{d\theta}{dt} = \frac{1}{L} (T - R - q - S) \quad (6.1)$$

where θ is the volumetric soil moisture content averaged over a depth L , T the throughfall, R the saturation excess runoff, q the deep drainage, and S the root water uptake. Here $L = 0.5$ m. Throughfall is the rainfall P that is not intercepted by vegetation. The size of the interception reservoir is taken proportional to the leaf area index ξ , with a proportionality constant of 0.2 mm, and the reservoir is assumed to evaporate every day. Since $0 \leq \theta \leq \theta_s$, where θ_s is the porosity, R equals T for $\theta = \theta_s$ and is 0 for $\theta < \theta_s$. We assume bare soil evaporation to be small in comparison to the root uptake over the entire profile. Drainage is calculated using Darcy's law with the unit-gradient assumption. Using the *Campbell (1974)* parameterization yields:

$$q = k(\theta) = k_s \left(\frac{\theta}{\theta_s} \right)^{2b+3} \quad (6.2)$$

where k_s is the saturated hydraulic conductivity, and b a pore size distribution parameter. We write the vertically integrated root water uptake S as:

$$S = f_r \beta \left(1 - e^{-c\xi} \right) E_p \quad (6.3)$$

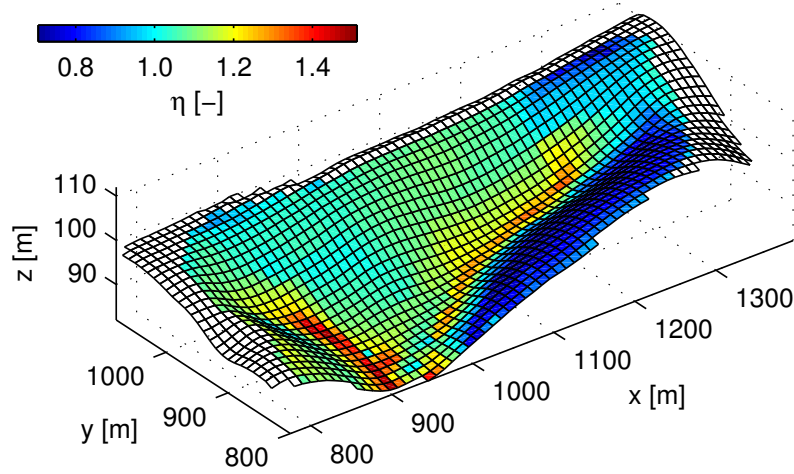


Figure 6.2. Distribution of the wetness index η in the Tarrawarra catchment.

where f_r is the root fraction in the layer of depth L , β a soil moisture stress function, c a light use efficiency parameter, and E_p the potential evapotranspiration. The factor $1 - \exp(-c\xi)$ allows for spatially variable response of unstressed transpiration to atmospheric boundary layer conditions (*Al-Kaisi et al.*, 1989). For Louvain-la-Neuve, the positive relation between ξ and S was confirmed by *Hupet and Vanclooster* (2004). Soil moisture stress is modeled as:

$$\beta = \beta(\theta) = \begin{cases} 0, & \theta \leq \theta_w \\ \frac{\theta - \theta_w}{\theta_c - \theta_w}, & \theta_w < \theta \leq \theta_c \\ 1, & \theta_c < \theta \leq \theta_s \end{cases} \quad (6.4)$$

where the critical moisture content θ_c defines the transition between unstressed and stressed transpiration, and the wilting point θ_w the point below which plants are no longer able to extract water from the soil matrix. Land cover (or ξ) is modeled with a spatial and temporal component:

$$\xi = \xi_{max} \left[c_1 - (1 - c_1) \sin \left(2\pi \frac{\text{DOY} - c_2}{c_3} + \frac{\pi}{2} \right) \right] \quad (6.5)$$

where ξ_{max} is the local maximum of ξ , and c_i specify the seasonal development of ξ .

The model defined by (6.1)–(6.5) sufficiently captures the non-linearities and dynamics of the soil moisture loss processes, and similar models have proven successful in reproducing point scale soil moisture dynamics (e.g., *Albertson and Kiely*, 2001; *Laio et al.*, 2001). Here we choose a simple model since adding more complexity to the model as presented would result in an increasing number of (generally unknown) covariances between the parameters. In order to match the observed forcing, the model was integrated to yield daily values (App. A).

6.3.2. Spatial closure

We reproduce the first and second order spatial moments of θ ($\bar{\theta}$ and σ_m^2) by running a large ensemble of the model defined by (6.1)–(6.5) with variable parameters. Initial conditions of θ are set by adjusting θ to a spatially uniform q of 1 mm d^{-1} . We assume both $\ln(k_s)$ and ξ_{max} to follow a normal distribution with parameters $\mu_{k,\xi}$ and $\sigma_{k,\xi}$. Since θ_s and b are generally correlated with k_s , we related these to k_s by linear regression with $\ln(k_s)$, fitted to the data provided by *Clapp and Hornberger* (1978). This yields $\theta_s = -0.0147 \ln(k_s) + 0.545$ and $b = -1.24 \ln(k_s) + 15.3$. Due to the positive effect of high k_s on canopy growth through better aeration, soil temperature and water transport to roots, we assume a (perfect) positive linear correlation between $\ln(k_s)$ and ξ_{max} . Other vegetation parameters are taken as constants. Atmospheric forcing (P and E_p) was calculated from available observations and assumed to be constant in space.

Table 6.1. Parameter values used in the simulation of σ_s .

Parameter	Louvain-la-Neuve	VCR-LTER	Tarrawarra
$\mu_k, \sigma_k \ln[\text{mm d}^{-1}]$	5.6,0.63 ^a	6.5,1.0	5.2,0.96 ^a
$\theta_w, \theta_c [-]$	0.15 θ_s ,0.44 θ_s	0.22 θ_s^b ,0.50 θ_s^b	0.35 θ_s ,0.67 θ_s
$\mu_\xi, \sigma_\xi [-]$	3.6,0.50 ^a	3.6,0.50	6.0,1.0 ^c
$c [-]$	0.55 ^d	0.40	0.40
$f_r [-]$	0.90	0.80	1
$c_1, c_2, c_3 [-, \text{d}, \text{d}]$	0.5,114,260 ^e	1,-,-	0.5,139,365 ^c
$\sigma_\eta [-]$	N/A	N/A	0.1530 ^f
$\varepsilon [-]$	0.005	0.005	0.013 ^g

^a Fitted from observations.

^b Adapted from *Albertson and Kiely (2001)*.

^c From biomass observations using a specific leaf area of $0.02 \text{ m}^2 \text{ g}^{-1}$.

^d From *Al-Kaisi et al. (1989)*.

^e For $114 \leq \text{DOY} \leq 283$, else 0.

^f Derived from a $5 \times 5 \text{ m}$ digital elevation model.

^g From *Western and Grayson (1998)*.

6.3.3. Total simulated variability

In order to account for spatial differences in the water balance caused by differences in exposure due to sloping of the landscape, we follow *Svetlitchnyi et al. (2003)* and write the non-local effect of topography (subscript T) on the distribution of available soil moisture $\theta^* = \theta - \theta_w$ in the top 0.5 m of the soil in terms of a wetness coefficient η :

$$\theta_T^* = \eta \bar{\theta}^*, \quad (6.6)$$

where $\bar{\theta}^*$ is the expected value of θ^* for a flat surface. In (6.6), local values of η depend on slope profile shape, slope aspect, distance from the divide, and slope gradient (Fig. 6.2), and can be derived from a digital elevation model. We refer to *Svetlitchnyi et al. (2003)* for more details. As a first order approach, we add the variance caused by (6.6) to σ_m^2 , assuming $\bar{\eta} = 1$. To allow direct comparison with observations, we also account for apparent variability due to a (bias-free and stationary) measurement error ε . The total simulated soil moisture variance σ_s^2 can now be written as:

$$\sigma_s^2(t) = \sigma_m^2(t) + \sigma_\eta^2 \bar{\theta}^{*2}(t) + \varepsilon^2. \quad (6.7)$$

6.4. Analysis and Results

Figure 6.3 shows the results of the simulations with the parameters listed in Table 6.1. The range of $\bar{\theta}$ as well as the magnitude, trend, and hysteresis of σ_s for the different data sets compare well to the observations. In order to distinguish the contribution of different controls on the time evolution of σ_s , we derive an expression for $d\sigma_s^2/dt$ quantifying their effect. Subtracting the spatial average equivalent of (6.1) from itself yields:

$$\frac{d\theta'}{dt} = \frac{1}{L}(T' - R' - q' - S') \quad (6.8)$$

where $'$ denotes a deviation from the spatial average. Multiplying (6.8) by $2\theta'$, performing a chain rule operation to the left hand side, and averaging the result yields:

$$\frac{d\bar{\theta}'^2}{dt} = \frac{d\sigma_m^2}{dt} = \frac{2}{L}(\bar{\theta}'T' - \bar{\theta}'R' - \bar{\theta}'q' - \bar{\theta}'S') \quad (6.9)$$

which is the expression for the time evolution of the spatial soil moisture variance derived by *Albertson and Montaldo (2003)* but applied to our balance equation (6.1). Since the right-hand side of (6.9) consists of

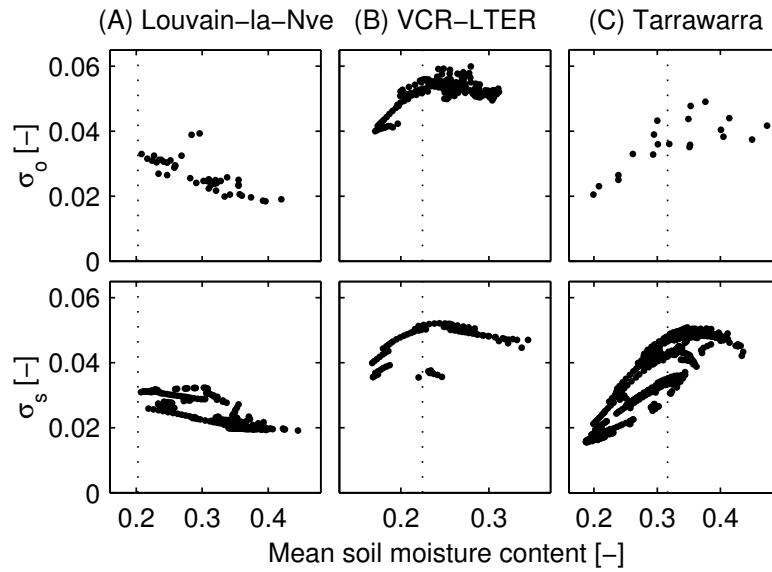


Figure 6.3. Observed (σ_o) and simulated (σ_s) soil moisture variability versus mean soil moisture content ($\bar{\theta}$). Dotted lines indicate the spatial mean critical moisture content $\bar{\theta}_c$.

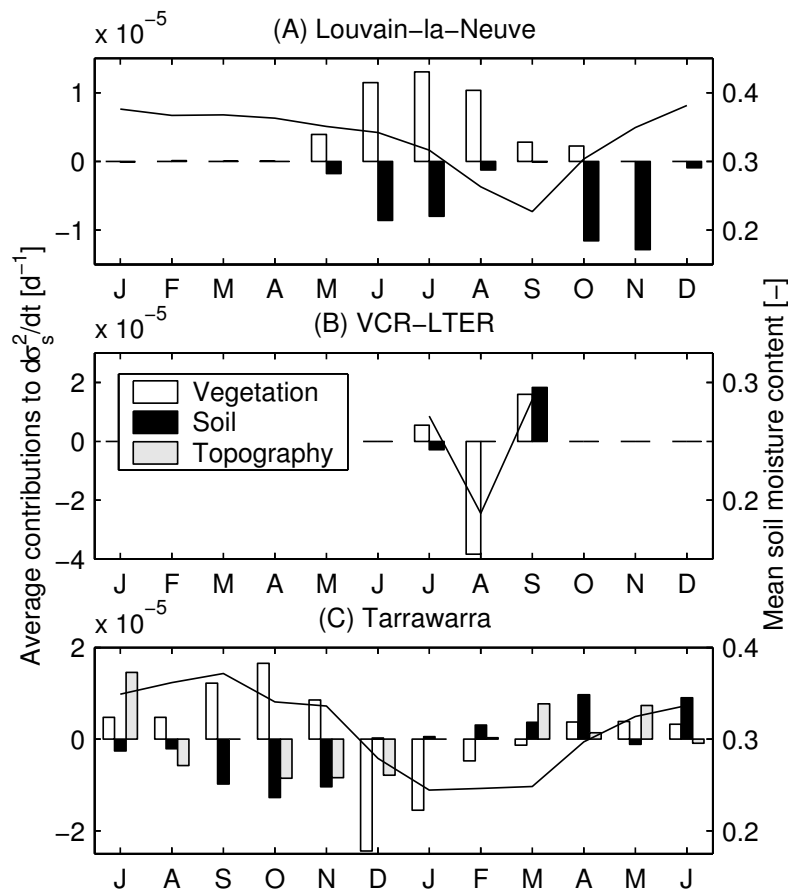


Figure 6.4. Monthly average vegetation, soil, and landscape contributions to $d\sigma_s^2/dt$, as in (6.10), and mean soil moisture content ($\bar{\theta}$).

covariance terms, their contribution depends on the magnitude of soil moisture and flux anomalies as well as on their mutual correlation. The sign of the correlation controls whether the different processes act to create or destroy spatial soil moisture variance (see *Albertson and Montaldo*, 2003, for synthetic examples). Combining (6.9) with the time derivative of (6.7) yields:

$$\frac{d\sigma_s^2}{dt} = \underbrace{\frac{2}{L} (\overline{\theta'T'} - \overline{\theta'S'})}_{\text{Vegetation}} - \underbrace{\frac{2}{L} (\overline{\theta'R'} + \overline{\theta'q'})}_{\text{Soil}} + \underbrace{\sigma_\eta^2 \frac{d\bar{\theta}^2}{dt}}_{\text{Landscape}}. \quad (6.10)$$

In stead of evaluating all terms separately, we group the correlated terms as (local) vegetation and soil controls, and non-local landscape control. Figure 6.4 explains the different trends in Fig. 6.3 by evaluating the contribution of the different groups in (6.10). For clarity the terms have been converted to monthly averages. Since drainage is generally a fast process compared to evapotranspiration (*Albertson and Kiely*, 2001), much of the soil contributions in Fig. 6.4 take place within days following major precipitation events. Daily values of the vegetation contribution are of lower magnitude, but show less spread.

In the Louvain-la-Neuve dataset, soil moisture variability increases during the growing season. During winter and spring (December–April), precipitation surplus causes soil moisture to remain near field capacity, and the variance is fully adjusted to the soil footprint (Fig. 6.4A). Here the soil footprint is the soil moisture variance under constant q . Until July, increases in variance due to heterogeneous transpiration are effectively (although not entirely) canceled out by drainage. When drainage becomes negligible (August–September), spatially variable water uptake by vegetation acts to create additional variance. This increase is only destroyed during the first rainfall events in the late growing season (October–November), when the variance is “reset” to that of the soil footprint ($\overline{\theta'q'} > 0$). It should be noted that even during summer root water uptake is not limited by the availability of soil moisture ($\theta > \theta_c$). Since high S will ultimately lead to low θ , $\overline{\theta'S'} < 0$.

For the VCR-LTER data, this behavior is almost opposite (Fig. 6.4B). The (small) initial increase in σ_s during July (Figs. 6.3 and 6.4), is due to heterogeneous but unstressed transpiration ($\overline{\theta'S'} < 0$). However, the coarse grained soils in combination with high E_p lead to rapid soil moisture limitation on S . This causes a sharp decrease in variance ($\overline{\theta'S'} > 0$) during August. Similar to the Louvain-la-Neuve case, rainfall events in September force σ_s to re-adjust to the soil footprint, causing $\overline{\theta'q'} < 0$. Here a spatially variable q causes an increase rather than a decrease in spatial variance of θ .

Tarrawarra shows a more complex pattern (Fig. 6.4C). In southern hemisphere spring (September–November), vegetation controls act to create variance ($\overline{\theta'S'} < 0$). This variance is initially destroyed by drainage of rainfall. In this period, drying of the soil ($d\bar{\theta}^2/dt < 0$) causes a transition from non-local to local controls on σ_s (*Grayson et al.*, 1997). This can be seen by the negative landscape contributions. Later during summer (December–February), soil and landscape controls become effectively zero due to advanced drying. The strong soil controlled root water uptake ($\theta < \theta_c$) causes a transition of the sign of the correlation between S and θ ($\overline{\theta'S'} > 0$) resulting in a strong decrease in σ_s^2 . The re-adjustment to the winter soil moisture state is accompanied by an increase in σ_s^2 caused by both soil and (non-local) landscape controls.

6.5. Discussion and Conclusions

Our simulations show that both soil and vegetation controls can act to either create or destroy spatial variance. The main discriminating factor between both behaviors is whether or not the soil dries below θ_c . This depends on the soil texture as well as on the maximum precipitation deficit, which can show considerable interannual variability in many regions. Including the effects of interannual variability in meteorological forcing on soil moisture variability might be subject of future research. The fact that much of the observed soil moisture variability is actually created by vegetation anomalies (and thus $\rho(\theta, \xi) \neq 0$) calls for new approaches to the soil moisture aggregation problem. This suggests that future field campaigns can further contribute to our understanding of the soil-vegetation-atmosphere system not only by looking at soil moisture variability, but also at how this variability is related to anomalies in soil and vegetation characteristics.

7. Dry-end surface soil moisture variability during the National Airborne Field Experiment 2006*

Characterization of the space-time variability of soil moisture is important for land surface and climate studies. Here we develop an analytical model to investigate how, at the dry-end of the soil moisture range, the main characteristics of the soil moisture field (spatial mean and variability, steady state distribution) depend on the intermittent character of low intensity rain storms. Our model is in good agreement with data from the recent National Airborne Field Experiment (NAFE'06) held in the semiarid Australian Murrumbidgee catchment. We find a positive linear relationship between mean soil moisture and its associated variability, and a strong dependency of the temporal soil moisture distribution to the amount and structure of precipitation.

7.1. Introduction

The central role of soil moisture in the climate system is nowadays widely recognized. Soil moisture directly controls the water- and energy budgets at the land surface, and may also affect the persistence of anomalous atmospheric conditions. Global soil moisture monitoring, however, is complicated due to large spatial and temporal variability of soil moisture. Passive microwave remote sensing is among the most promising techniques, but its applicability is complicated by its shallow sensing depth (few cm) and the coarse spatial resolution (tens of km) of space-borne sensors (such as ESA's upcoming Soil Moisture and Ocean Salinity mission, SMOS). Methods to quantify the space-time dynamics of the surface soil moisture field can lead to improved sampling, retrieval, validation, and downscaling.

Previous field experiments have shown that the spatial variability of surface soil moisture may depend, among other factors, on the spatial mean soil moisture state. *Reynolds* (1970) has already hypothesized that due to the effect of soil heterogeneity, spatial variability increases during infiltration, and is minimum after drydown. Based on detailed observations along a hillslope transect, *Famiglietti et al.* (1998) found that the spatial mean and variance have identical behavior. Both peaked after rainfall events, and decreased rapidly during drydown. While both studies reported a decrease in variability with decreasing spatial mean soil moisture, opposite or more complex relations have also been reported (see Chaps. 6 and 8, and discussion in *Famiglietti et al.*, 1998). A theoretical framework to analyze the changes in spatial variability of root-zone soil moisture was presented by *Albertson and Montaldo* (2003). Here we apply this framework to study surface layer soil moisture in the dry-end of the soil moisture range. The model is a limited case of the more comprehensive models utilized by *Albertson and Montaldo* (2003) and in Chap. 6, and allows for full analytical characterization of the spatial and temporal soil moisture variability. The model is subsequently tested on a unique, recently collected data set.

7.2. Data

The 3-week long National Airborne Field Experiment 2006 (NAFE'06) was undertaken in the Australian Murrumbidgee catchment (Fig. 7.1A) during October–November 2006. The region experienced severe drought conditions from 2001 onwards, and had no rainfall in the five weeks preceding the campaign. In the Murray Darling basin, 2006 was the third driest year on record. Fortunately, during NAFE'06 there were several minor rainfall events totaling ~20 mm (Fig. 7.2A). The objective of NAFE'06 was to provide data for SMOS

*This chapter is an edited version of: Teuling, A. J., R. Uijlenhoet, R. Hurkmans, O. Merlin, R. Panciera, J. P. Walker, and P. A. Troch (2007), Dry-end surface soil moisture variability during NAFE'06, *Geophys. Res. Lett.*, 34(17), L17402, doi:10.1029/2007GL031001. Copyright 2007 American Geophysical Union.

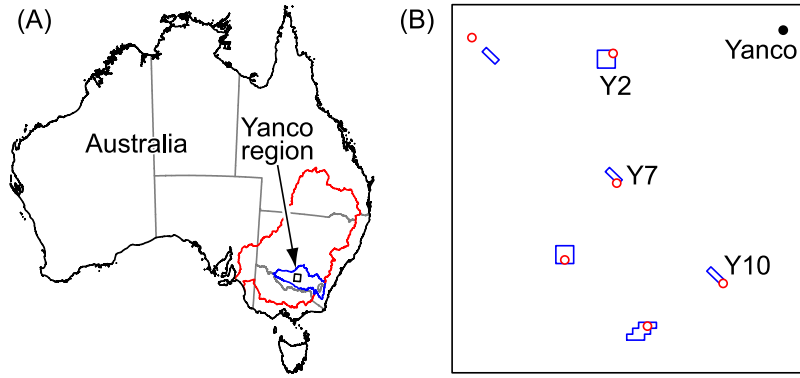


Figure 7.1. Map of the Yanco region. (A) Location within the Murray Darling basin (red) and the Murrumbidgee catchment (blue). (B) Location of the NAFE'06 field sites and rainfall stations (\circ).

soil moisture retrieval, downscaling, and data assimilation (see <http://www.nafe.unimelb.edu.au>). Ground observations of surface soil moisture were made at 6 field sites in the 60×60 km Yanco region (35°S , 146°E , Fig. 7.1B). At each field, point soil moisture and precipitation were recorded at 20 min resolution. Here we analyse soil moisture variability in the non-irrigated fields Y2, Y7, and Y10, which are all dry pastures used for grazing. The predominant soil type is clay.

Soil moisture observations were made by means of the Hydraprobe Data Acquisition System (HDAS, *Panciera et al.*, 2006), which integrates a GPS and the Vitel Hydra Probe (*Seyfried and Murdock*, 2004) in a GIS environment. (The mention of product names does not constitute an endorsement of this product.) HDAS made it possible to rapidly monitor surface (0–5 cm) soil moisture on a predefined grid within large field sites. During NAFE'06, the different teams took a total of 16,937 HDAS readings. A maximum number of 3 separate readings were taken at each sampling location in order to get a representative point-scale value. HDAS observations were calibrated against gravimetric measurements (taken throughout the campaign at different locations) by means of a third-order polynomial regression. Some field-scale statistics are summarized in App. F.

7.3. Temporal dynamics

In developing our model, we consider the volumetric soil moisture θ in a shallow surface layer of depth L . In dry conditions, this layer is effectively “decoupled” from the deeper soil moisture (*Capehart and Carlson*, 1997). For convenience, we only model the dynamics of the transformed soil moisture ϑ :

$$\vartheta = \theta - \xi, \quad (7.1)$$

where ξ is the residual soil moisture content. In the following, we denote the field-scale mean of any quantity x by \bar{x} , and its standard deviation by σ_x . With little vegetation and low intensity rainfall, the water balance is dominated by infiltration of precipitation (P) and evaporation. Both processes occur in an alternating fashion, with the latter process being much slower.

During storms ($P > 0$), point-scale variability in land surface properties (e.g., texture, vegetation, microtopography, macropores) causes variable infiltration (e.g., *Reynolds*, 1970). Without explicitly modeling these processes, we assume that at any point a fixed fraction (α) of P contributes to the antecedent soil moisture. During interstorm periods ($P = 0$), daily evaporation is proportional to the available surface moisture ϑ (*Kurc and Small*, 2004). The resulting point-scale water balance is:

$$\frac{d\vartheta}{dt} = \begin{cases} \alpha P/L, & P > 0 \\ -\vartheta/\tau, & P = 0, \end{cases} \quad (7.2)$$

where τ is the time scale of surface evaporation. In practice, τ will also be subject to spatial variability. In the model however, a spatial variability in τ introduces a complicating time-dependent covariance between

α and ϑ , which would also destroy rank stability (see below). Since drydown is a dissipative process, this simplification has little impact on the results. The horizontal average of (7.2) at the field-scale ($\sim 1 \text{ km}^2$) is obtained by replacing ϑ and α by their field-scale means $\bar{\vartheta}$ and $\bar{\alpha}$, respectively:

$$\frac{d\bar{\vartheta}}{dt} = \begin{cases} \bar{\alpha}P/L, & P > 0 \\ -\bar{\vartheta}/\tau, & P = 0, \end{cases} \quad (7.3)$$

where spatial variability of P at the field-scale is neglected. Integrating (7.3) over different periods with constant P , each starting at subsequent t_0 and of duration Δt , yields:

$$\bar{\vartheta}(t_0 + \Delta t) = \begin{cases} \bar{\vartheta}(t_0) + \bar{\alpha} \frac{P}{L} \Delta t, & P > 0 \\ \bar{\vartheta}(t_0) e^{-\Delta t/\tau}, & P = 0. \end{cases} \quad (7.4)$$

The simplified water balance can also be written in terms of its deviations (ϑ') from the spatial mean (i.e., $\vartheta' = \vartheta - \bar{\vartheta}$). Multiplying the resulting equation by $2\vartheta'$, applying the chain rule ($2\vartheta' d\vartheta'/dt = d\vartheta'^2/dt$), and spatially averaging the result yields the spatial variance budget (Albertson and Montaldo, 2003):

$$\frac{d\overline{\vartheta'^2}}{dt} = \frac{d\sigma_{\vartheta}^2}{dt} = \begin{cases} \frac{2P}{L} \overline{\alpha' \vartheta'}, & P > 0 \\ -\frac{2}{\tau} \sigma_{\vartheta}^2, & P = 0, \end{cases} \quad (7.5)$$

where $\overline{\alpha' \vartheta'}$ is the covariance between α and ϑ . By using:

$$\overline{\alpha' \vartheta'} = \sigma_{\alpha} \sigma_{\vartheta} \rho_{\alpha, \vartheta}, \quad (7.6)$$

where $\rho_{\alpha, \vartheta}$ is the correlation coefficient between α and ϑ , and the chain rule ($d\sigma_{\vartheta}^2/dt = 2\sigma_{\vartheta} d\sigma_{\vartheta}/dt$), (7.5) can be further simplified. In this case, ϑ' is linearly (and only) related to α' , so $\rho_{\alpha, \vartheta} = 1$. Time integration yields:

$$\sigma_{\vartheta}(t_0 + \Delta t) = \begin{cases} \sigma_{\vartheta}(t_0) + \sigma_{\alpha} \frac{P}{L} \Delta t, & P > 0 \\ \sigma_{\vartheta}(t_0) e^{-\Delta t/\tau}, & P = 0, \end{cases} \quad (7.7)$$

which, due to the linear character of the model, is functionally equivalent to (7.4). For simplicity, we also assume $\rho_{\alpha, \xi} = 1$, so that:

$$\sigma_{\theta} = \sigma_{\vartheta} + \sigma_{\xi}. \quad (7.8)$$

Through our formulation we ensure perfect rank stability of point-scale soil moisture (i.e., temporal persistence in the spatial pattern), which is required in order not to violate the assumption that $\rho_{\alpha, \vartheta} = 1$. The existence of rank (or time) stability in surface soil moisture fields was shown by Jacobs *et al.* (2004). Since changes in $\bar{\theta}$ and σ_{θ} in (7.4) and (7.7), respectively, are both proportional to P , the relation between $\bar{\theta}$ and σ_{θ} is linear:

$$\sigma_{\theta}(\bar{\theta}) = CV_{\alpha} (\bar{\theta} - \bar{\xi}) + \sigma_{\xi}, \quad \bar{\theta} \geq \bar{\xi}. \quad (7.9)$$

where $CV_{\alpha} = \sigma_{\alpha}/\bar{\alpha}$ is the coefficient of variation of α .

The parameter values are given in Table 7.1. First, $\bar{\xi}$ was taken as the average observed values of $\bar{\theta}$ before the first rainfall (here DOY 306), τ was taken from Kurc and Small (2004), and $\bar{\alpha}$ was optimized such that the amplitude of $\bar{\theta}$ was in correspondence with the observations. Next, σ_{α} and σ_{ξ} were adjusted such that (7.9) corresponds to the linear regression $\sigma_{\theta} = a\bar{\theta} + b$ between all observed $\bar{\theta}$ and σ_{θ} ($\sigma_{\alpha} = a\bar{\alpha}$ and $\sigma_{\xi} = b + \bar{\xi}\sigma_{\alpha}/\bar{\alpha}$). Initial conditions for $\bar{\vartheta}$ and σ_{ϑ} are $\bar{\xi}$ and σ_{ξ} , respectively. We use $\Delta t = 20 \text{ min}$.

The simultaneous increase of $\bar{\theta}$ and σ_{θ} during storms of low intensity, and their subsequent decrease during interstorm periods, is apparent in both the simulations and observations (Fig. 7.2B). The decay timescale of Kurc and Small (2004) works well for the NAFE'06 conditions, with the observed amplitude and dynamics of $\bar{\theta}$ and σ_{θ} captured by the model. Regional scale precipitation variability induces only small variability in the field-scale responses of $\bar{\theta}$, which is also suggested by the similar pattern of observed $\bar{\theta}$ and σ_{θ} . The changes in top 5 cm soil moisture were found to account for over half of the precipitation ($\bar{\alpha} = 0.53$).

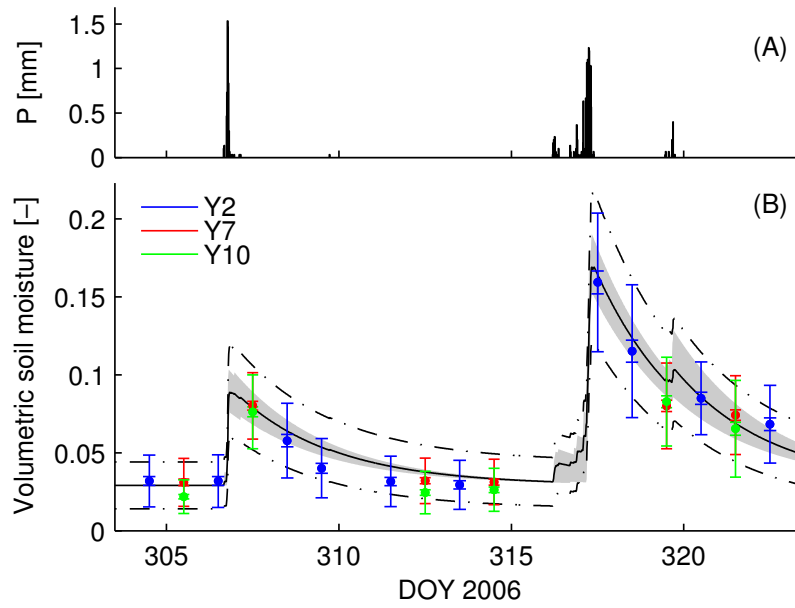


Figure 7.2. Precipitation and soil moisture during NAFE'06. (A) Regional average precipitation (20 min). (B) Soil moisture dynamics. Points are observed field-scale means, inner bounds the 95% confidence bounds for $\bar{\theta}$, and outer bounds $\bar{\theta} \pm \sigma_{\theta}$. Solid line is simulated $\bar{\theta}$ with (7.4) forced with regional average P , dash-dotted lines are $\bar{\theta} \pm \sigma_{\theta}$ with (7.7). Grey area marks the range in $\bar{\theta}$ in response to regional-scale variability in P .

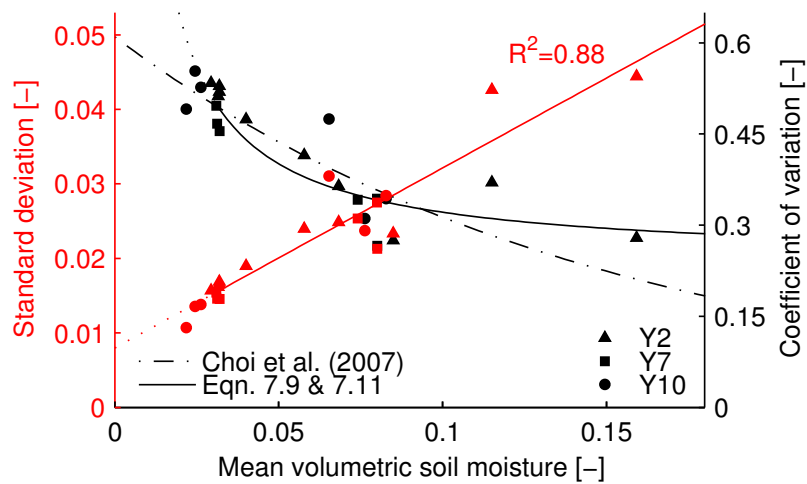


Figure 7.3. Relation between field-scale spatial mean and spatial variability of surface soil moisture.

Table 7.1. Parameters and their values.

Parameter	Symbol	Value	Units
Surface layer depth	L	50	mm
Infiltration fraction (mean)	$\bar{\alpha}$	0.53	-
Infiltration fraction (SD)	σ_{α}	0.13	-
Evaporation decay time	τ	2.8 ^a	d
Residual moisture content (mean)	$\bar{\xi}$	0.029	-
Residual moisture content (SD)	σ_{ξ}	0.015	-
Mean storm depth	η	2.1	mm
Mean storm arrival rate	λ	0.50	d ⁻¹

^a Taken from *Kurc and Small (2004)* for semiarid grassland.

7.4. Mean versus variability

The relation between the spatial mean and variability is of interest for scaling. The modeled relation between $\bar{\theta}$ and σ_{θ} is given by (7.9). Note that (7.9) is independent of the interstorm decay time τ . Recently, *Choi et al. (2007)* investigated the relation between the spatial mean soil moisture and coefficient of variation (CV_{θ}) for a number of datasets. They optimized the parameters A and B in the empirical model:

$$CV_{\theta}(\bar{\theta}) = Ae^{B\bar{\theta}}. \quad (7.10)$$

Here, this relation is hyperbolic:

$$CV_{\theta}(\bar{\theta}) = CV_{\alpha} + \frac{1}{\bar{\theta}} \left(\sigma_{\xi} - \bar{\xi} CV_{\alpha} \right), \quad \bar{\theta} \geq \bar{\xi}. \quad (7.11)$$

Figure 7.3 shows the observed and simulated relation between $\bar{\theta}$ and σ_{θ} . Overall, the (linear) model explains 88% of the variance in all observed σ_{θ} . Separate analysis of Y2, Y7, and Y10, yields R^2 values of 0.92, 0.86, and 0.83, respectively. The regressions are similar for all sites, confirming the validity of our assumption that the field-scale soil moisture within the region responds similarly to a given precipitation input.

The relative variability CV_{θ} decreases with increasing $\bar{\theta}$ (Fig. 7.3). Since the absolute variability increases with $\bar{\theta}$, the decrease of CV_{θ} can be attributed to the increase in $\bar{\theta}$. For the exponential *Choi et al.* model, we find parameters $A = 0.61$ and $B = -0.067$ (with soil moisture expressed in % as in *Choi et al., 2007*). The difference between the models increases for $\bar{\theta} > 0.10$, partly due to the different fitting procedures (i.e., fitting CV_{θ} or σ_{θ}). Although there is an obvious physical limit to the increase of σ_{θ} with $\bar{\theta}$ due to the presence of the upper bound at porosity, this limit was not reached during NAFE'06. The added value of our model (7.11) with respect to the *Choi et al.* model lies in the fact that it can be interpreted in terms of the underlying processes.

7.5. Steady state distribution

The dynamics of soil moisture is governed by the occurrence and amount of rainfall (Fig. 7.2), which are both stochastic. We investigate the impact of climate variability (through P) on the steady-state soil moisture distribution $f(\vartheta)$ (or $f(\vartheta)$) by including a stochastic representation of rainfall pulses in the model. Here, storms occur instantaneously, and can be described by a marked Poisson process. The depth of storm events and the interarrival times are considered independent random variables. Both are exponentially distributed with mean η and λ^{-1} , respectively. The mean rain rate $\langle P \rangle$ equals $\eta\lambda$. We estimate λ from the (spatial) average number of non-interrupted rainless sequences during NAFE'06 at the 20 min resolution, and η from the corresponding total rainfall over the same period (Table 7.1). In this simplified case, the resulting steady-state distribution is a shifted Gamma pdf (App. G):

$$f(\vartheta) = \frac{(\bar{\vartheta})^{\lambda\tau-1} \exp(-c\bar{\vartheta})}{c^{-\lambda\tau} \Gamma(\lambda\tau)}, \quad (7.12)$$

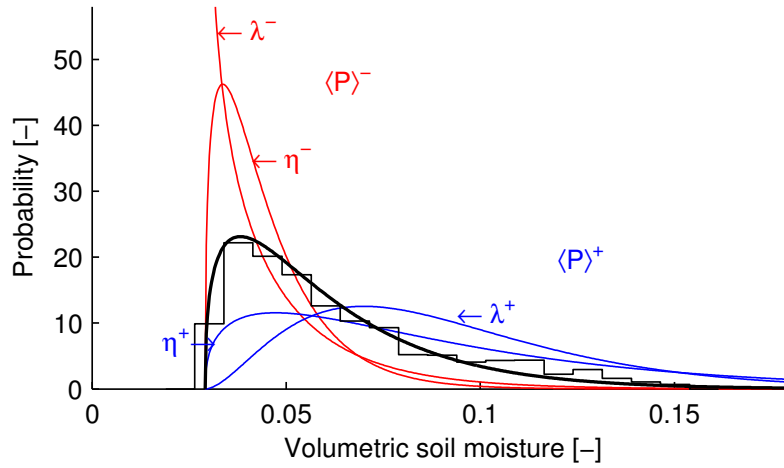


Figure 7.4. Steady-state distribution of field-scale mean soil moisture during NAFE'06 and its sensitivity to precipitation characteristics. Histogram shows the distribution of 20 min resolution point-scale soil moisture (0–5 cm) at Y10 for DOY 298–327.

where $c = (\bar{\alpha}\eta/L)^{-1}$. This distribution has mean $\bar{\xi} + \lambda\tau c^{-1}$ and standard deviation $(\lambda\tau)^{1/2}c^{-1}$. For $\lambda\tau = 1$, (7.12) reduces to a shifted exponential distribution. While our solution with linear losses is more realistic than previous “minimalistic” models with constant losses (Milly, 2001; Calanca, 2004), it is valid for a smaller range of climate conditions than the more complex models of (Rodríguez-Iturbe et al., 1999; Laio et al., 2001). Although (7.12) is written in terms of field-scale averages, it is equally valid at the point-scale by using the appropriate α . Figure 7.4 shows the resulting $f(\bar{\theta})$ and its sensitivity to climate scenarios. In the wet scenario $\langle P \rangle^+$, $\langle P \rangle$ is doubled either by an increase in η or λ (η^+ and λ^+ , respectively). Similarly, we assume $\langle P \rangle$ to be halved in the dry scenario $\langle P \rangle^-$.

For the NAFE'06 conditions, which were below the climatic average, the mean and standard deviation of the steady-state soil moisture distribution are 0.061 and 0.027, respectively. Its distribution is unimodal and positively skewed. The positive skew is due to the decreasing evaporation towards $\bar{\xi}$, corresponding to smaller $d\bar{\vartheta}/dt$, and subsequently larger $f(\bar{\vartheta})$. Independent high resolution point-scale observations at Y10 (Fig. 7.4) confirm the validity of the model. Their distribution is also unimodal and positively skewed, with mean 0.064 and standard deviation 0.028. The wet scenario $\langle P \rangle^+$ results in a mean soil moisture of 0.093, the dry scenario $\langle P \rangle^-$ in 0.045. While the mean soil moisture depends on $\langle P \rangle$ and not on its temporal structure (i.e., on the balance between η and λ), this structure does influence the steady state variability. When changes in $\langle P \rangle$ are caused by changes in mean storm depth η (i.e., η^+ and η^-), the temporal variability is largest. Since the temporal standard deviation is proportional to η , it is twice as high under η^+ than under NAFE'06 conditions (0.054 and 0.027, respectively). A reduction in mean storm frequency (λ^-) causes a shift in the mode of $f(\bar{\theta})$ towards $\bar{\xi}$.

7.6. Discussion and Conclusions

An analytical model to study daily surface soil moisture variability dynamics in the dry-end of the soil moisture range has been developed. Under the low intensity rainfall encountered during NAFE'06, the dynamics of soil moisture are well reproduced by a linear relationship between soil moisture and daily evaporation. We found that the spatial mean and standard deviation rapidly increased during rainfall, and slowly decreased during interstorm periods. The temporal distribution of surface soil moisture was found to be highly sensitive to the amount and structure of precipitation. The results are consistent with previous experiments (Kurc and Small, 2004; Reynolds, 1970; Famiglietti et al., 1998), and allow for a more quantitative (water balance-based) approach to surface soil moisture variability. More comprehensive models, for instance those utilized by Albertson and Montaldo (2003) and in Chaps. 6 and 8, are valid at the full soil moisture range, but require numerical solution.

8. Climate variability effects on spatial soil moisture dynamics*

We investigate the role of interannual climate variability on spatial soil moisture variability dynamics for a field site in Louvain-la-Neuve, Belgium. Observations were made during 3 years under intermediate (1999), wet (2000), and extremely dry conditions (2003). Soil moisture variability dynamics are simulated with a comprehensive model for the period 1989–2003. The results show that climate variability induces non-uniqueness and two distinct hysteresis modes in the yearly relation between the spatial mean soil moisture and its variability. We demonstrate that the direction of hysteresis is related to a yearly climate index that does not require soil moisture observations.

8.1. Introduction

Soil moisture is an important variable in many land surface models since it controls the partitioning of fluxes of both water and energy. However soil moisture shows a large spatial variability, and the relation between soil moisture dynamics at a point (i.e., the scale of most observations) and that of a larger area (field, region) are still poorly understood. Over the past decades, field experiments have quantified the variability of soil moisture, its intra-seasonal dependence on the mean soil moisture state (*Bell et al.*, 1980; *Famiglietti et al.*, 1998), and its dependence on external factors such as soil, vegetation, and topography (e.g., *Western et al.*, 1999; *Wilson et al.*, 2004). *Western et al.* (2003) analyzed spatial root zone soil moisture variability dynamics from 13 study areas around the globe (their Fig. 8.6). Their analysis revealed that “variance increases with average moisture in dry catchments and it decreases in wet catchments. Where the spatial mean moisture has a sufficiently large range over time, the variance peaks at intermediate values”. While climate conditions are known to affect soil moisture variability dynamics (Chap. 6), little attention has been paid to the role of interannual climate variability on the dynamics of spatial soil moisture variability.

Here we analyze the impact of both intra-annual climate dynamics and interannual climate variability on soil moisture variability at the field scale. We employ an extension of the comprehensive soil moisture variability model used in Chap. 6. The advantage of this approach is that the number of parameters (with generally unknown covariability) is small, while the parameters still reflect observable properties. Models of similar complexity have been shown to correctly simulate root zone soil moisture dynamics under different climatic conditions (*Albertson and Kiely*, 2001, Chaps. 2 and 6).

8.2. Data

Soil moisture variability was measured at multiple occasions during the growing seasons of 1999, 2000, and 2003 in a 1 ha agricultural field located in Louvain-la-Neuve, Belgium. The measurements were part of a campaign that aimed at investigating within-field variability of transpiration (*Hupet and Vanclooster*, 2002). The same instruments were used, but in a different experimental setup (Fig. 8.1). Detailed information on the 1999 and 2003 data can be found in *Hupet and Vanclooster* (2002) and *Hupet and Vanclooster* (2005), respectively. The 2000 data has not been analyzed before. The soils in the field can be classified as well-drained silty-loam and there is little relief. During the campaigns the field was cropped with maize (*Zea Mays* L.). The

*This chapter is an edited version of: Teuling, A. J., F. Hupet, R. Uijlenhoet, and P. A. Troch (2007), Climate variability effects on spatial soil moisture dynamics, *Geophys. Res. Lett.*, 34(6), L06406, doi:10.1029/2006GL029080. Copyright 2007 American Geophysical Union.

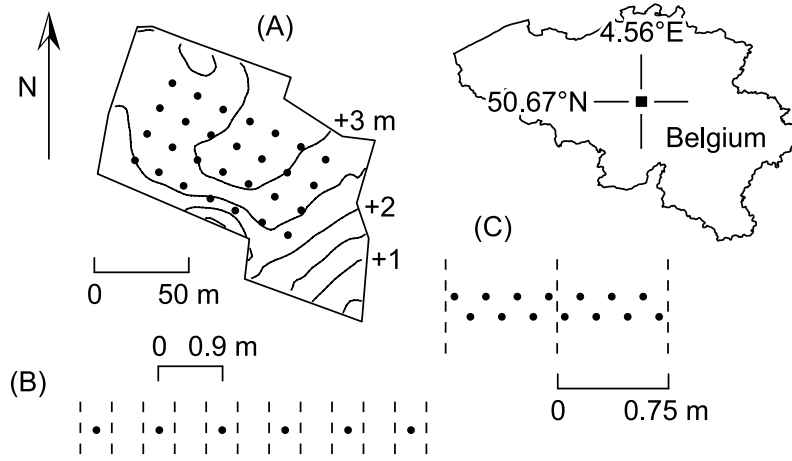


Figure 8.1. Location of the field and experimental setup. (A) 1999, with 0.5 m contour lines, (B) 2000 (detail of 45 m long transect), and (C) 2003, both with location of maize rows (dashed lines).

climate is temperate humid. Meteorological observations made in the vicinity of the field are available for the period 1 January 1989 until 28 August 2003.

8.3. Model

We assume that the point-scale soil moisture dynamics are spatially unconnected. Vertical redistribution of soil moisture is assumed to occur instantaneously (at the daily time step). We solve the daily water balance for a number of independent soil columns of depth L :

$$\frac{d\theta}{dt} = \frac{1}{L}(T - S - E - R - q), \quad (8.1)$$

where θ is the volumetric soil moisture content, T the throughfall, S the root water uptake, E the evaporation from the soil surface, R the saturation excess runoff, and q the deep drainage. Here $L = 0.65$ m. Although roots can penetrate deeper than 0.65 m, most of the water uptake occurs above this depth. The number of columns is taken the same as the 1999 setup (28, Fig. 8.1A). Throughfall is rainfall that is not intercepted by vegetation. The size of the interception reservoir is taken proportional to the leaf area index ξ (with a constant of 0.2 mm). Root water uptake is thought to be proportional to a maximum transpiration rate E_m , a soil moisture stress $\beta(\theta)$, and a function accounting for leaf area index following *Al-Kaisi et al.* (1989):

$$S = \beta(\theta)E_m = \beta(\theta) \left[1 - e^{-c\xi} \right] ET_0, \quad (8.2)$$

where c is a light use efficiency parameter (0.55), and ET_0 the potential evapotranspiration calculated by the FAO Penman-Monteith method (*Allen et al.*, 1998). The positive relation between ξ and S was confirmed by *Hupet and Vanclooster* (2004). Soil moisture stress is modeled as:

$$\beta(\theta) = \begin{cases} 0, & \theta \leq \theta_w \\ \frac{\theta - \theta_w}{\theta_c - \theta_w}, & \theta_w < \theta \leq \theta_c \\ 1, & \theta_c < \theta \leq \theta_s, \end{cases} \quad (8.3)$$

where the critical moisture content θ_c defines the transition between unstressed and stressed transpiration, θ_s is the porosity, and the wilting point θ_w corresponds to a pressure head of -150 m. To account for the effect of different E_m on θ_c (e.g., *Denmead and Shaw*, 1962), we determine θ_c dynamically from:

$$\frac{E_m}{E_s} = \frac{\theta_c - \theta_w}{\theta_f - \theta_w}, \quad (8.4)$$

where θ_f is the field capacity and $E_s = 10 \text{ mm d}^{-1}$ the maximum sustainable uptake at θ_f . The field capacity corresponds to a hydraulic conductivity k of 1 mm d^{-1} and is derived from:

$$k(\theta) = k_s \left(\frac{\theta}{\theta_s} \right)^{2b+3}, \quad (8.5)$$

where k_s is the value of k at saturation, and b a pore size distribution parameter. We assume E to be proportional to the remaining fraction bare soil ($\exp(-c\xi)$), ET_0 , and the inverse of the square root of time since the last rainfall event ($\geq 10 \text{ mm}$). E is included for a correct water balance when ξ is small, but it has little effect on the soil moisture variability. Leaf area index ξ is modeled as:

$$\xi(t) = \begin{cases} 0, & t \leq t_s \\ \frac{\xi_{max}}{2} \left[1 - \cos \left(2\pi \frac{t-t_s}{t_d} \right) \right], & t_s < t \leq t_h \\ 0, & t > t_h, \end{cases} \quad (8.6)$$

where the sowing and harvest days t_s and t_h are taken as 119 and 283, respectively, and $t_d = 260$ for all years. This implies that both the dynamics and variability of ξ are considered to be the same for all years. Runoff R is the part of T that causes oversaturation of the soil. Drainage q is assumed to be driven only by gravity, i.e., $q = k$ with $k(\theta)$ defined by (8.5) and adjusted for daily timescales (App. A).

The spatial distribution of ξ_{max} is assumed to be normal, with mean 3.6 and standard deviation 0.5 derived from observations (*Hupet and Vanclooster, 2002*). The spatial distribution of $\ln(k_s)$ is also assumed to be normal, with parameters 5.6 and 0.4 fitted from observed k_s at the site. As in Chap. 6, we relate θ_s and b to k_s by regressions derived from the data in *Clapp and Hornberger (1978)*. These are $\theta_s = -0.0147 \ln(k_s) + 0.545$ and $b = -1.24 \ln(k_s) + 15.3$. Since soil and vegetation properties can show spatial correlation, we need to specify the (linear) correlation coefficient of the joint spatial distribution of $\ln(k_s)$ and ξ_{max} . Due to the positive effect of high k_s on canopy growth through better aeration, soil temperature and water transport to roots, we assume a positive correlation of 0.8. Impacts of correlation between soil and vegetation fields are discussed by *Montaldo and Albertson (2003)*. For every year, the soil moisture field was initialized at θ_f .

8.4. Analysis and Results

It is of interest to identify the processes that are responsible for the temporal changes in spatial variability of the simulated soil moisture field (here expressed as a variance σ_s^2 or standard deviation σ_s). *Albertson and Montaldo (2003)* showed how the temporal changes in σ_s^2 are related to the covariances of the different water balance terms and the soil moisture field. For our water balance (8.1) this yields:

$$\frac{d\sigma_s^2}{dt} = \underbrace{\frac{2}{L} (\overline{\theta'T'} - \overline{\theta'E'} - \overline{\theta'S'})}_{\text{Vegetation}} - \underbrace{\frac{2}{L} (\overline{\theta'R'} + \overline{\theta'q'})}_{\text{Soil}}, \quad (8.7)$$

where the horizontal bars indicate spatial averaging, and the prime a deviation from the spatial average. For convenience, the different terms in (8.7) have been grouped by vegetation and soil effects on $d\sigma_s^2/dt$. E is listed in the vegetation group since in the model it depends on ξ rather than soil characteristics.

An important variable that characterizes soil moisture dynamics in (sub)humid areas is Ψ (Chap. 2). It is defined as the maximum precipitation deficit during the growing season (D_P , calculated with respect to E_m) and scaled by the storage available for “unstressed” plant uptake:

$$\Psi = \frac{D_P}{L(\theta_f - \theta_c)}, \quad (8.8)$$

where $\overline{\theta_c}$ is taken at $E_m = 3 \text{ mm d}^{-1}$. Ψ not only depends on climate (through D_P), but also on soil and vegetation characteristics. Deeper rooting vegetation will have lower Ψ , but also a more damped soil moisture dynamics. In Chap. 2 it is shown that the expected value of this index can explain differences in observed soil moisture dynamics. Here we determine Ψ for each year separately.

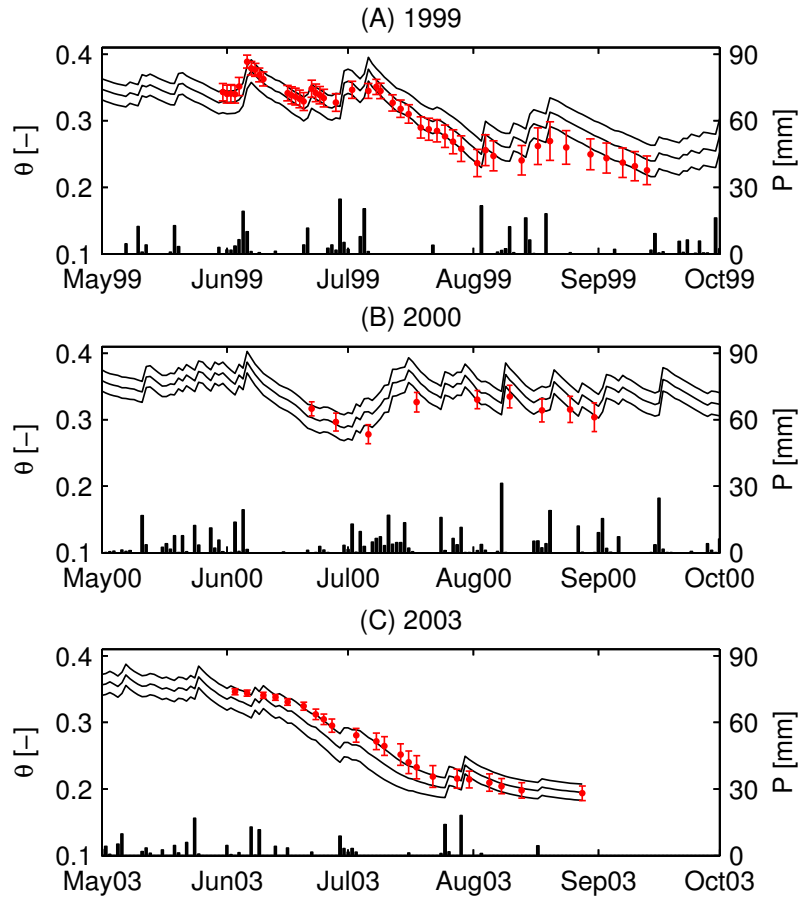


Figure 8.2. Observed (σ_o) and simulated (σ_s) soil moisture variability versus spatial mean soil moisture ($\bar{\theta}$) for the years 1999, 2000, and 2003. The middle line indicates $\bar{\theta}$, the outer lines $\bar{\theta} \pm \sigma_s$.

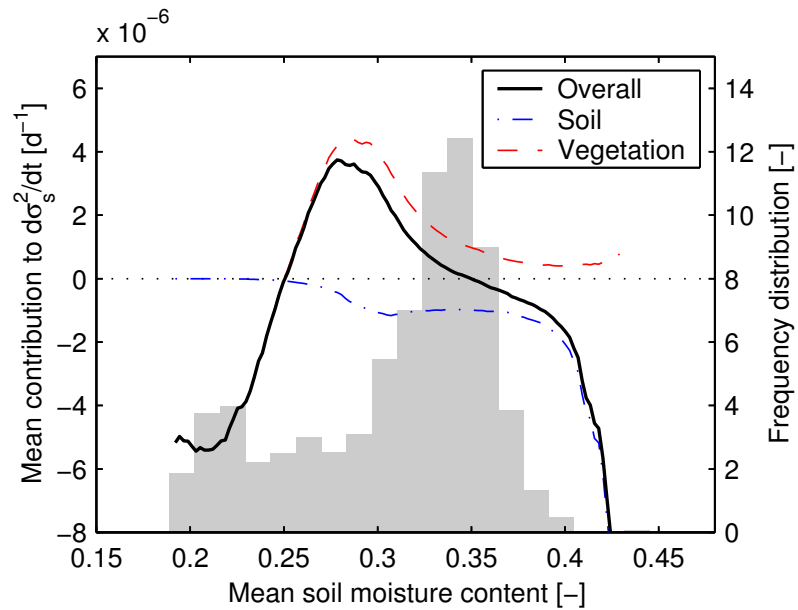


Figure 8.3. Dependence of the vegetation and soil contributions to $d\sigma_s^2/dt$ on mean soil moisture $\bar{\theta}$, and frequency distribution of $\bar{\theta}$ for the growing season (1989–2003).

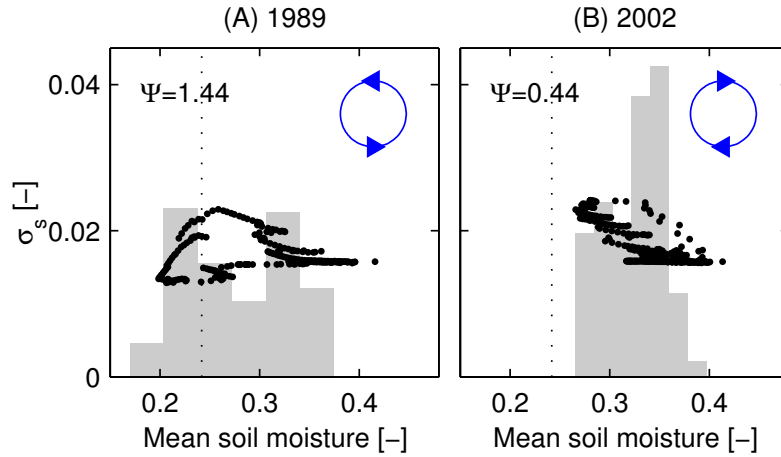


Figure 8.4. Relation between $\bar{\theta}$ and σ_s and direction of hysteresis for the years 1989 and 2002. The grey area indicates the corresponding frequency distribution of $\bar{\theta}$ for the growing season, and dotted line $\bar{\theta}_c$ for $E_m = 3 \text{ mm d}^{-1}$.

The upper panels in Fig. 8.2 show the observed soil moisture variability dynamics for the root zone (here $\sim 0.65 \text{ m}$). Although the observations were made at different spatial scales (Fig. 8.1), we argue that the effect of spatial scale is reflected in the magnitude of σ_o rather than in its trend. In 1999, σ_o showed an increasing trend with decreasing $\bar{\theta}$, while during the extremely dry summer of 2003, a similar initial increase in σ_o was followed by a strong decrease at low $\bar{\theta}$. In 2000, neither $\bar{\theta}$ nor σ_o showed strong dynamics. A more comprehensive analysis of soil moisture variability in the years 1999 and 2003 can be found in *Hupet and Vanclooster (2002)* and *Hupet and Vanclooster (2005)*, respectively. Since the observations are limited in extent (namely 3 growing seasons) and temporal resolution, they show only partly the hysteresis associated with rapid rewetting after rainfall. This is further investigated using simulations.

The lower panels in Fig. 8.2 show the relation between the simulated mean soil moisture and its standard deviation σ_s . In contrast to the observations, the simulations for the different years apply to the same spatial scale, and are not limited to the growing season. An important element of the simulated soil moisture field is that its variability near $\bar{\theta}_f$ is nearly constant. This is the soil “footprint”, which corresponds to the variability that accommodates a spatially uniform q . For all three years, the simulations show behavior similar to the observations. Both the range in $\bar{\theta}$ and the different trends in σ_o are realistically simulated. While the observations do not cover the rewetting to θ_f after the growing season, the simulations reveal that the relation between $\bar{\theta}$ and σ_s does not only show different trends, but is also subject to hysteresis. Interestingly, the direction of this hysteresis can vary.

First we focus on the question what causes the non-uniqueness in the relation between $\bar{\theta}$ and σ_s . Figure 8.3 shows the average vegetation and soil contributions to the variance rate of change budget in (8.7) as a function of $\bar{\theta}$. It should be noted that the soil and vegetation groups are dominated by $\bar{\theta}'q'$ and $\bar{\theta}'S'$, respectively. There is a clear structure in the vegetation contributions to $d\sigma_s^2/dt$. If $\bar{\theta}$ is above ~ 0.25 , then the spatial variability in S (which for $\theta \geq \theta_c$ is not sensitive to soil moisture) causes σ_s to increase. The spatial variability in S is due to the spatial variability in leaf area index. At lower $\bar{\theta}$, the vegetation contributions switch sign (S becomes a strong function of θ) and their magnitude increases. This can be explained by the fact that when soil moisture is limiting, roots take up more water in wet soil columns than in dry ones. By doing so, they decrease the spatial (inter-column) variability.

The transition between these two states is relatively fast, as is indicated by the corresponding local minimum at 0.25 in the bimodal frequency distribution of $\bar{\theta}$. Soil contributions are only significant near $\bar{\theta}_f$ (~ 0.35), and counteract the vegetation effects ($d\sigma_s^2/dt \approx 0$). Vegetation effects are limited to the growing season. Negative vegetation contributions do not occur early in the growing season when $\bar{\theta}$ is high. In this period, the counteracting effect of the soil contributions is also highest. Occasional positive soil contributions occur directly after the end of the growing season. Figure 8.3 also shows that $d\sigma_s^2/dt$ converges to the vegetation or soil contributions in the dry or wet soil moisture range, respectively. This confirms the strong dependency of the different soil

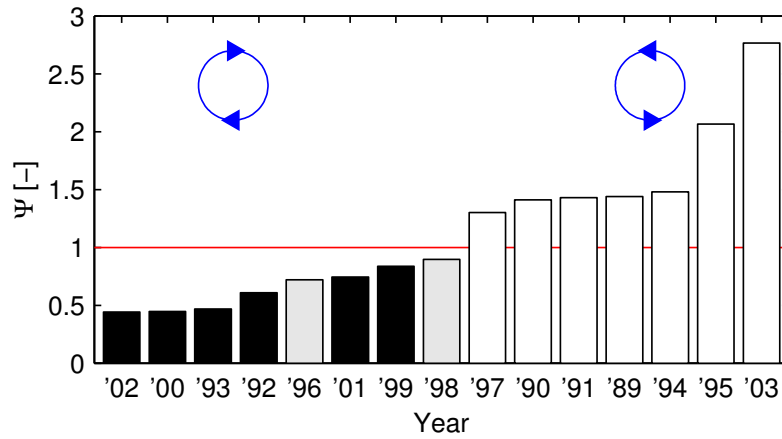


Figure 8.5. Index Ψ for the 15 years of simulation, sorted in increasing order. Small values ($\Psi < 1$) result in clockwise hysteresis (black), while large values ($\Psi > 1$) result in anti-clockwise hysteresis (white). Years in grey have no clear hysteresis direction.

moisture variability controls on $\bar{\theta}$.

The different trends in σ_s (increasing or increasing followed by decreasing) with decreasing spatial mean soil moisture lead to different hysteresis loops in the relation between $\bar{\theta}$ and σ_s , since the soil contributions that counteract the previous vegetation effects on σ_s become significant only once the soil is rewetted to near $\bar{\theta}_f$ (Fig. 8.3). This is illustrated in Fig. 8.4 for the years 1989 (dry) and 2002 (wet). The bimodal growing season soil moisture frequency distribution in 1989 illustrates that during a large part of the season, $\bar{\theta}$ is below $\bar{\theta}_c$, and vegetation destroys spatial variance. This does not occur in 2002, when the distribution is unimodal. This shows that $\bar{\theta}_c$ acts as a threshold that controls soil moisture variability dynamics. The yearly climate index Ψ , which does not require information on soil moisture status, is a good predictor for the crossing of the threshold. Figure 8.5 confirms that low $\Psi (< 1)$ is associated with clockwise hysteresis in the relation between $\bar{\theta}$ and σ_s , and high $\Psi (> 1)$ with anti-clockwise hysteresis. Note that the crossing not necessarily occurs exactly at $\Psi = 1$, due to variability in θ_c and the initial soil moisture content at the start of the period over which D_p is determined.

8.5. Discussion and Conclusions

While spatial patterns of soil moisture are known to reflect patterns in soil and vegetation, they are also affected by climate variability. We conclude that the yearly relation between spatial mean soil moisture and its standard deviation is non-unique, and is subject to hysteresis. The direction of hysteresis in time is clockwise for relatively wet years, and anti-clockwise for dry years. Starting from field capacity, both types of hysteresis loops share a similar initial increase in standard deviation with decreasing mean soil moisture.

The dynamic nature of soil moisture variability has important implications for current approaches to aggregation and scaling of soil moisture. For instance, the fact that vegetation effects on soil moisture fields are affected by climate variability might explain observed differences in scaling of surface soil moisture fields for the same region during different field campaigns (Oldak *et al.*, 2002). Furthermore in many aggregation studies, soil moisture variability is assumed to be constant or to be uniquely related to mean soil moisture. These assumptions might not be appropriate.

In this study we prescribe the seasonal development of leaf area index rather than to model its development dynamically in response to atmospheric and soil moisture conditions. Our reasons for doing so are twofold: a) we could not validate its interannual variability, and b) we had no information on the processes that caused its observed spatial variability. Although including vegetation dynamics might affect the interannual variability of soil moisture (Montaldo *et al.*, 2005), we assume these effects to be small for the vegetation and climate at Louvain-la-Neuve.

9. Epilogue

9.1. General discussion

In this thesis, simple models of soil moisture and evapotranspiration are used. Obviously, more complex models have the advantage of more detailed process description, but they require detailed a priori knowledge about the system. For instance, it is known that without calibration, models of intermediate complexity often perform better than more complex models (*Hogue et al.*, 2006). The required model complexity can, among other factors, also depend on climate conditions (*Atkinson et al.*, 2002). Especially when used to investigate field-scale spatial variability (as in Chaps. 6 and 8), more complex models (i.e., with more parameters) result in an extremely complex (and generally unknown) spatial covariance structure between the parameters. Simple models have the additional advantage that their behavior is readily understood, providing easier insight into many issues.

The use of simple models is justified by the fact that variability in, for instance, evapotranspiration, is almost fully explained by radiation and/or soil moisture alone (*Abramowitz*, 2005, see also Fig. 4.2), limiting the potential for more complex models to outperform simple models. Based on the results of Chaps. 2 and 4, one might argue that land surface modelers have been developing more complex instead of more robust models. In Fig. 4.3, the decay times (the key characteristic of the soil moisture reservoir) between the different GSWP-2 land surface models for Rheindahlen range from less than 5 to over 200 days. It is of interest to compare this range between different models for one site to the range in observations for all sites (Table 4.1). Curiously, this latter range is (much) smaller: 12.4 to 118 days. While model “validation” is common practice in hydrology, the null hypothesis that a model (or one of its process parameterizations) is correct is hardly ever rejected.

Chapter 2 shows that even sparse soil moisture observations contain useful information on the shape of the loss curve. Since the observed bimodality is apparent in simulations with a partly flat loss curve, but not when a continuously increasing curve is used, the bimodality does suggest that the former curve is more realistic. Some further indications that the loss curve has a domain with little sensitivity of the losses to soil moisture is provided in Chaps. 6 and 8. If the loss function would be monotonically increasing, the system would behave dissipative with respect to spatial soil moisture anomalies during interstorm periods. However, the opposite is observed for intermediate mean soil moisture. The initial increase in spatial variability during drydown is well-reproduced by a model where the losses have little sensitivity to soil moisture at intermediate values. Knowledge about the shape of the loss curve is of relevance to land surface modeling, since in many land surface models the losses are currently not well represented (*Lohmann and Wood*, 2003). The frequency distribution of soil moisture might therefore function as a valuable additional diagnostic for land surface model validation.

It is also interesting to compare the timescales in Table 4.1 to autocorrelation timescales for soil moisture anomalies from the literature. Following the original framework of *Delworth and Manabe* (1988), the time constant of soil moisture autocorrelation decay under white noise rainfall anomalies equals the ratio between potential evapotranspiration and soil moisture storage capacity in case of a linear relation between soil moisture and evapotranspiration. In this case, the time constant of autocorrelation decay is also the time constant of evapotranspiration decay in absence of rainfall forcing. Using the *Delworth and Manabe* framework, *Vinnikov et al.* (1996) reported timescales in the order of 3 months for the Russian Valdai basin. While later studies have reported somewhat smaller timescales of 1–2 months for other regions (*Entin et al.*, 2000; *Amenu et al.*, 2005), these timescales are generally much longer than the evapotranspiration decay timescales in Table 4.1.

Two explanations can readily be given for the differences in autocorrelation decay and evapotranspiration decay times. Firstly, the relation between soil moisture and evapotranspiration might not be linear but convex (see Chap. 3). In the wet soil moisture range, this will lead to a slower dissipation of soil moisture anomalies. Secondly, soil moisture autocorrelation decay times represent the persistence in the coupled land-atmosphere system, while the evaporation decay times are a property of the “uncoupled” land surface only. Hence, evaporation decay times are not affected by a possible non-whiteness of rainfall anomalies.

Chapters 5, 6, and 8 provide a consistent first-order picture of the temporal dynamics of the spatial variability

of soil moisture. Near field capacity, the variability is constant and there is near-perfect rank stability (Fig. 5.6). During drydown, this rank stability breaks down and a new pattern is established. In Chaps. 6 and 8, a perfect respectively high positive correlation between saturated hydraulic conductivity and leaf area index is assumed. This assumption results in high rank stability. However, Fig. 5.6 also reveals that reality is more heterogeneous. This is likely due to small-scale heterogeneous processes (see *Hupet and Vanclooster, 2005*) that are not included in the model. This also implies the following contradiction: as long as the mean soil moisture remains constant, there is near-perfect rank stability. However, as soon as mean soil moisture changes, then also its spatial pattern changes (and with it, rank stability). As a result, perfect rank stability under changing soil moisture conditions is extremely unlikely.

A matter of significant scientific interest is how parameterizations change with scale as a result of small scale variabilities. This matter is well-studied for the relation between soil moisture and evapotranspiration (e.g. *Crow and Wood, 2002*). Most of these studies derive aggregated soil moisture-evapotranspiration relationships assuming only variability in soil moisture, but not in land surface properties. This will often result in an over- rather than underestimation of the effects of spatial variability. When land surface properties are considered, the spatial correlation structure between soil and vegetation fields plays a central role in closure schemes for sub-grid soil moisture variability (*Montaldo and Albertson, 2003*). In the simple soil moisture variability model that was applied in this thesis, this structure is represented by a single linear correlation coefficient. In more complex models, this structure would be represented by a high dimensional correlation matrix. Despite its importance to land surface modeling, surprisingly little is known about this structure. Apparently, its importance to land surface modeling has not yet been fully recognized.

The issue of spatial scale also applies to the vertical discretization (or resolution). With the exception of Chap. 3, this thesis treats the root zone as a single reservoir. However, it has been argued that the upscaling from a vertically discretized (1-D) model to a single layer (0-D) model results in non-uniqueness of the upscaled parameterizations (*Guswa, 2005*). The fact that there is little observational evidence that supports the use of 1-D models over 0-D models when evapotranspiration is concerned, favors the use of the low-dimensional 0-D models such as those used throughout this thesis. This might not be the case when fast processes such as runoff are concerned (*Kim et al., 1996; Downer and Ogden, 2004*).

9.2. Directions for further research

Unrealistic land surface process representation, especially the sensitivity of evapotranspiration to soil moisture, is known to impact the simulated feedback with the atmosphere through its effect on the magnitude and dynamics of evapotranspiration (*Koster and Suarez, 1996*). Hence, it is important that land surface models have the correct response, or coupling, to atmospheric conditions (*Abramowitz, 2005; Lawrence and Slingo, 2005; Dirmeyer et al., 2006b*). When the soil moisture component in land surface models is “validated”, it is often rescaled to soil wetness (relative moisture content). This procedure, however, also removes the physical dimensions of the soil moisture dynamics (i.e., the direct linkage between soil moisture storage and evapotranspiration as in Chap. 4). Future land surface model calibration/validation should therefore focus on changes in soil moisture storage rather than soil wetness. This is likely to result in more robust models.

In Chaps. 6 and 8, the key determinant of the spatial-temporal evolution of the soil moisture distribution is the correlation structure between different land surface characteristics. This correlation is also the central parameter in the closure schemes for sub-grid soil moisture variability (*Montaldo and Albertson, 2003*). Given the complex interactions between vegetation, soil, and soil moisture, it seems unlikely that this correlation can be derived a priori (i.e., from theory). Future field experiments would provide valuable insight into soil moisture variability if, besides soil moisture observations, also accompanying observations of soil and vegetation characteristics would be made that allow for a complete observation-based characterization of the controls on soil moisture variability. One other possible solution to this problem is to investigate whether this correlation can be derived soil moisture observations only, for example the intensive soil moisture observations described in Chap. 5.

A. Time integration of gravitational drainage

Using the assumption of gravitational drainage, the instantaneous downward flux of water q is equal to the unsaturated hydraulic conductivity k . *Campbell (1974)* proposed the following parameterization of $k(\theta)$:

$$k(\theta) = k_s \left(\frac{\theta}{\theta_s} \right)^{2b+3}, \quad (\text{A.1})$$

where k_s is the hydraulic conductivity at saturation, θ_s the saturated moisture content or porosity, and b a pore size distribution parameter. Assuming that all changes in soil moisture are caused by drainage q , the water balance becomes:

$$\frac{d\theta}{dt} = -\frac{q}{L} \quad (\text{A.2})$$

so that by using $q = k$, the rate of change in soil moisture storage due to drainage can now be written as:

$$\frac{d\theta}{dt} = -\frac{k_s}{L} \left(\frac{\theta}{\theta_s} \right)^{2b+3}. \quad (\text{A.3})$$

Since this equation is highly nonlinear for most realistic b , it cannot be used directly to predict the change in θ due to drainage over longer time intervals. Rewriting (A.3) yields:

$$dt = -\frac{L}{k_s} \left(\frac{\theta}{\theta_s} \right)^{-2b-3} d\theta. \quad (\text{A.4})$$

Integration over a time interval $\Delta t = t_e - t_0$ yields:

$$\int_0^{\Delta t} dt = -\int_{\theta_0}^{\theta_{\Delta t}} \frac{L}{k_s} \left(\frac{\theta}{\theta_s} \right)^{-2b-3} d\theta, \quad (\text{A.5})$$

where θ_0 and $\theta_{\Delta t}$ are the values of θ at $t = 0$ and $t = \Delta t$, respectively. Performing the integration yields:

$$\Delta t = \frac{1}{2b+2} \frac{\theta_s L}{k_s} \left[\left(\frac{\theta_0}{\theta_s} \right)^{-2b-2} - \left(\frac{\theta_{\Delta t}}{\theta_s} \right)^{-2b-2} \right]. \quad (\text{A.6})$$

Rearranging the different terms in (A.6), and using $q_{\Delta t} = (\theta_0 - \theta_{\Delta t})L$ yields an expression for q over any time interval Δt :

$$q_{\Delta t} = L\theta_0 - L\theta_s \left[\left(\frac{\theta_0}{\theta_s} \right)^{-2b-2} + \frac{(2b+2)k_s \Delta t}{\theta_s L} \right]^{-\frac{1}{2b+2}}. \quad (\text{A.7})$$

B. Integration of double exponential with linear term

Depth integration of (3.6) requires integration of the following term between 0 and z_c :

$$\lambda' E_m \int_0^{z_c} \frac{\theta'(z,t)}{\theta'_c} e^{-\lambda z} dz = \lambda' E_m \int_0^{z_c} \exp\left(\frac{\theta'_0 - \theta'_c}{\theta'_c} - \frac{\lambda' e^{-\lambda z} E_m t}{\theta'_c}\right) e^{-\lambda z} dz. \quad (\text{B.1})$$

The integral on the right hand side can also be written as:

$$\int_0^{z_c} \exp\left(\frac{\theta'_0 - \theta'_c}{\theta'_c} - \frac{\lambda' e^{-\lambda z} E_m t}{\theta'_c}\right) e^{-\lambda z} dz = \exp\left(\frac{\theta'_0 - \theta'_c}{\theta'_c}\right) \int_0^{z_c} \exp\left(-\frac{\lambda' e^{-\lambda z} E_m t}{\theta'_c} - \lambda z\right) dz. \quad (\text{B.2})$$

Hence, solving (B.1) is equivalent to solving the double exponential integral I:

$$I = \lambda' E_m \exp\left(\frac{\theta'_0 - \theta'_c}{\theta'_c}\right) \int_0^{z_c} \exp\left(-\frac{\lambda' e^{-\lambda z} E_m t}{\theta'_c} - \lambda z\right) dz. \quad (\text{B.3})$$

By application of the chain rule it can be seen that:

$$\frac{d}{dz} \exp\left(-\frac{\lambda' e^{-\lambda z} E_m t}{\theta'_c}\right) = \exp\left(-\frac{\lambda' e^{-\lambda z} E_m t}{\theta'_c}\right) \cdot \frac{\lambda' E_m t}{\theta'_c} \lambda e^{-\lambda z} = \frac{\lambda' E_m t}{\theta'_c} \lambda \exp\left(-\frac{\lambda' e^{-\lambda z} E_m t}{\theta'_c} - \lambda z\right). \quad (\text{B.4})$$

The integral I can now be written as:

$$I = E_m \exp\left(\frac{\theta'_0 - \theta'_c}{\theta'_c}\right) \left[\frac{\theta'_c}{E_m t \lambda} \exp\left(-\frac{\lambda' e^{-\lambda z} E_m t}{\theta'_c}\right) \right]_0^{z_c}. \quad (\text{B.5})$$

By substituting the expression for z_c in (3.5) and the expressions $f = \theta'_c/\theta'_0$, $b = \lambda'/\lambda$, and $\tau = \lambda E_m t/\theta'_0$, the integral I becomes:

$$I/E_m = \frac{f}{\tau} \exp\left(\frac{1-f}{f}\right) \left[\exp\left(-\frac{1-f}{f}\right) - \exp\left(-\frac{b\tau}{f}\right) \right] = -\frac{f}{\tau} \exp\left(\frac{1-f}{f} - \frac{b\tau}{f}\right). \quad (\text{B.6})$$

For $z_c = L$, i.e., the third case in (3.6) for $t \geq t_c(L)$, the integral I becomes:

$$I/E_m = \frac{f}{\tau} \exp\left(\frac{1-f}{f}\right) \left[\exp\left(-\frac{b\tau}{f} e^{-c}\right) - \exp\left(-\frac{b\tau}{f}\right) \right], \quad (\text{B.7})$$

where $c = \lambda L$.

C. Integration of double exponential without linear term

Depth integration of (3.4) requires integration of a double exponential term between 0 and z_c (here I):

$$I = \frac{1}{L} \int_0^{z_c} \theta'(z, t) dz = \frac{\theta'_c}{L} \exp\left(\frac{\theta'_0 - \theta'_c}{\theta'_c}\right) \int_0^{z_c} \exp\left(-\frac{\lambda' e^{-\lambda z} E_m t}{\theta'_c}\right) dz. \quad (C.1)$$

The main difference with (B.1) is the absence of a linear term in the exponent. In order to solve (C.1), we change variable: $x = e^{-\lambda z} \Leftrightarrow z = -\lambda^{-1} \ln(x)$, so that $dz = -(\lambda x)^{-1} dx$. The integral I can now be written as:

$$I = \frac{\theta'_c}{\lambda L} \exp\left(\frac{\theta'_0 - \theta'_c}{\theta'_c}\right) \int_{e^{\lambda z_c}}^1 x^{-1} \exp\left(-\frac{\lambda' E_m t}{\theta'_c} x\right) dx. \quad (C.2)$$

By introducing the new variable y :

$$y = \frac{\lambda' E_m t}{\theta'_c} x \Leftrightarrow x = \frac{\theta'_c y}{\lambda' E_m t}, \quad (C.3)$$

dx can be written as:

$$dx = \frac{\theta'_c dy}{\lambda' E_m t}. \quad (C.4)$$

The integral I can now be written as:

$$I = \frac{\theta'_c}{\lambda L} \exp\left(\frac{\theta'_0 - \theta'_c}{\theta'_c}\right) \int_{\frac{\lambda' E_m t}{\theta'_c} e^{-\lambda z_c}}^{\frac{\lambda' E_m t}{\theta'_c}} \frac{e^{-y}}{y} dy. \quad (C.5)$$

This integral can be solved with the help of the exponential integral function $Ei(x)$:

$$E_1(x) = -Ei(-x) = \int_x^\infty \frac{e^{-t}}{t} dt. \quad (C.6)$$

The integral I now becomes:

$$I = \frac{\theta'_c}{\lambda L} \exp\left(\frac{\theta'_0 - \theta'_c}{\theta'_c}\right) \left[E_1\left(\frac{\lambda' E_m t}{\theta'_c} e^{-\lambda z_c}\right) - E_1\left(\frac{\lambda' E_m t}{\theta'_c}\right) \right]. \quad (C.7)$$

By substituting the expression for z_c in (3.5) and the dimensionless groups $f = \theta'_c/\theta'_0$, $b = \lambda'/\lambda$, and $\tau = \lambda E_m t/\theta'_0$, the integral I becomes:

$$I/\theta'_0 = \frac{f}{c} \exp\left(\frac{1-f}{f}\right) \left[E_1\left(\frac{1-f}{f}\right) - E_1\left(\frac{b\tau}{f}\right) \right]. \quad (C.8)$$

For $z_c = L$, i.e., the third case in (3.6) for $t \geq t_c(L)$, the integral I becomes:

$$I/\theta'_0 = \frac{f}{c} \exp\left(\frac{1-f}{f}\right) \left[E_1\left(\frac{b\tau}{f} e^{-c}\right) - E_1\left(\frac{b\tau}{f}\right) \right], \quad (C.9)$$

where $c = \lambda L$.

D. Regression results for GSWP-2 simulations

Table D.1. GSWP-2 e -folding times (λ) and corresponding R^2 for Rheindahlen (1990, 1991, and 1995 dry spells) and SEBEX. Non-significant regressions (95% level) are italicized.

Model ^a	RD 1990		RD 1991		RD 1995		SB 1989	
	λ [d]	R^2	λ [d]	R^2	λ [d]	R^2	λ [d]	R^2
BUCKETIIS	7.0	0.86	6.2	0.93	5.4	0.92	6.0	0.87
CLM2-TOP	19.8	0.60	14.0	0.89	11.3	0.88	26.7	0.95
HySSiBLIS	18.5	0.79	21.4	0.78	18.3	0.76	65.1	0.84
ISBA	5.2	0.88	20.2	0.40	4.9	0.83	20.3	0.96
LaD	19.0	0.60	11.4	0.80	19.6	0.69	4.4	0.93
MOSES2	28.0	0.62	18.0	0.79	19.3	0.73	32.3	0.91
MosLIS	46.6	0.27	31.8	0.58	<i>231.</i>	<i>0.02</i>	6.9	0.96
NOAH	16.6	0.67	9.6	0.81	18.6	0.52	44.6	0.97
NSIPP-Catchment	29.2	0.41	11.6	0.75	42.9	0.37	22.7	0.92
ORCHIDEE	17.9	0.65	18.2	0.68	21.6	0.61	36.6	0.96
SiBUC	16.5	0.68	35.9	<i>0.10</i>	15.4	0.71	87.9	0.91
SSiB-COLA	5.7	0.75	<i>10.8</i>	<i>0.03</i>	3.5	0.95	21.0	0.66
SWAP	18.2	0.77	17.9	0.72	20.9	0.71	28.0	0.95
VISA	<i>116.</i>	<i>0.04</i>	14.1	0.76	<i>1450.</i>	<i>0.00</i>	26.6	0.89
TESSEL ^b	17.2	0.51	32.4	0.24	22.3	0.44	34.0	0.69
Multi-model analysis ^c	17.8	0.77	17.1	0.82	16.1	0.92	29.2	0.94
Observations	19.1	0.84	20.3	0.80	21.0	0.63	66.2 ^d	0.63

^a Abbreviations from the GSWP-2 website.

^b The ECMWF LSM TESSEL, did not participate in GSWP-2.

^c Does not include TESSEL.

^d Based on average ET for tigerbush and fallow sites.

E. Mean and variance for sum of densities

Here, an expression is derived for the mean and variance of a random selection from n densities of the same random variable X , $f_i(X)$, with $i = \{1, 2, \dots, n\}$. Each density $f_i(X)$ has a mean $E[X|i] = \mu_i$ and variance $\text{Var}[X|i] = \sigma_i^2$. Here we assume i to be a discrete random variate with uniform probability of n^{-1} . The mean of X is:

$$E[X] = E[E(X|i)] = \frac{1}{n} \sum_{i=1}^n E[X|i] \quad (\text{E.1})$$

The variance of X can be calculated from:

$$\text{Var}[X] = E[X^2] - E^2[X]. \quad (\text{E.2})$$

Since

$$E[X^2] = \frac{1}{n} \sum_{i=1}^n E[X^2|i] = \frac{1}{n} \sum_{i=1}^n \{\text{Var}[X|i] + E^2[X|i]\}, \quad (\text{E.3})$$

the variance of X can also be written as:

$$\text{Var}[X] = \frac{1}{n} \sum_{i=1}^n \text{Var}[X|i] + \frac{1}{n} \sum_{i=1}^n E^2[X|i] - \left\{ \frac{1}{n} \sum_{i=1}^n E[X|i] \right\}^2. \quad (\text{E.4})$$

The last term of this equation is expanded as:

$$\left\{ \frac{1}{n} \sum_{i=1}^n E[X|i] \right\}^2 = \frac{1}{n^2} \sum_{i=1}^n E^2[X|i] + \frac{2}{n^2} \sum_{i=1}^n \sum_{j=1}^{i-1} E[X|i] E[X|j], \quad (\text{E.5})$$

so that combining (E.4) and (E.5) yields an expression that allows $\text{Var}[X]$ to be calculated from the individual $E[X|i]$ and $\text{Var}[X|i]$:

$$\text{Var}[X] = \frac{1}{n} \sum_{i=1}^n \sigma_i^2 + \frac{n-1}{n^2} \sum_{i=1}^n \mu_i^2 - \frac{2}{n^2} \sum_{i=1}^n \sum_{j=1}^{i-1} \mu_i \mu_j. \quad (\text{E.6})$$

Finally, if $E[X|i] = E[X|j] \quad \forall \quad j \neq i$, then simply

$$\text{Var}[X] = \frac{1}{n} \sum_{i=1}^n \sigma_i^2. \quad (\text{E.7})$$

F. Summary of the NAFE'06 soil moisture observations

Table F.1. Field-scale mean ($\bar{\theta}$) and standard deviation (σ_{θ}) of the field-scale soil moisture surveys during NAFE'06 for the non-irrigated field sites Y2, Y7, and Y10.

Date	Y2 ^a		Y7 ^b		Y10 ^b	
	$\bar{\theta}$ [-]	σ_{θ} [-]	$\bar{\theta}$ [-]	σ_{θ} [-]	$\bar{\theta}$ [-]	σ_{θ} [-]
31 October 2007	0.0319	0.0166				
1 November 2007			0.0310	0.0154	0.0218	0.0107
2 November 2007	0.0319	0.0169				
3 November 2007			0.0801	0.0213	0.0763	0.0237
4 November 2007	0.0578	0.0240				
5 November 2007	0.0400	0.0190				
6 November 2007 ^c						
7 November 2007	0.0315	0.0162				
8 November 2007			0.0320	0.0146	0.0245	0.0135
9 November 2007	0.0294	0.0157				
10 November 2007			0.0312	0.0146	0.0262	0.0138
11 November 2007 ^c						
12 November 2007 ^c						
13 November 2007	0.1592	0.0444				
14 November 2007	0.1151	0.0426				
15 November 2007			0.0800	0.0275	0.0828	0.0284
16 November 2007	0.0849	0.0234				
17 November 2007			0.0741	0.0253	0.0654	0.0310
18 November 2007	0.0683	0.0249				

^a Regular 12×12 grid, 250 m spacing (3×3 km²).

^b Regular 46×5 grid, 50 m spacing (2.3×0.25 km²).

^c No sampling.

G. Derivation of soil moisture distribution

Let an instantaneous rainfall event contribute an exponentially distributed amount I with mean μ ($= c^{-1}$) to transformed soil moisture ϑ . Furthermore, let ϑ_- be the value of ϑ immediately preceding, and ϑ_+ directly after the event ($\vartheta_+ = \vartheta_- + I$, see Fig. G.1). In the steady state, the pdf of ϑ_- ($f_{\vartheta_-}(\vartheta)$) equals the pdf of soil moisture at the end of the drydown following the event. In addition, if rainfall occurrence follows a Poisson process, then $f_{\vartheta}(\vartheta)$ equals $f_{\vartheta_-}(\vartheta)$.

We have to show that:

$$f_{\vartheta_-}(\vartheta) = \frac{\vartheta^{\lambda\tau-1} \exp\left(-\frac{\vartheta}{\mu}\right)}{\mu^{\lambda\tau} \Gamma(\lambda\tau)}, \quad (\text{G.1})$$

is the steady state pdf of ϑ . Because soil moisture decays exponentially (with constant τ) during drydown, and the duration of drydown periods follows an exponential pdf with mean $1/\lambda$, the conditional pdf $f_{\vartheta_-|\vartheta_+}(\vartheta)$ is:

$$f_{\vartheta_-|\vartheta_+}(\vartheta) = \frac{\lambda\tau}{\vartheta} \left(\frac{\vartheta}{\vartheta_+}\right)^{\lambda\tau}. \quad (\text{G.2})$$

Hence the unconditional pdf of ϑ_- becomes:

$$f_{\vartheta_-}(\vartheta) = \int_{\vartheta}^{\infty} f_{\vartheta_-|\vartheta_+}(\vartheta) f_{\vartheta_+}(\vartheta_+) d\vartheta_+. \quad (\text{G.3})$$

Because ϑ_- and I are independent random variables, $f_{\vartheta_+}(\vartheta)$ is the convolution of $f_I(I)$ and $f_{\vartheta_-}(\vartheta)$:

$$f_{\vartheta_+}(\vartheta) = \frac{1}{\mu} \int_0^{\vartheta} \exp\left(-\frac{\vartheta-I}{\mu}\right) f_{\vartheta_-}(I) dI \quad (\text{G.4})$$

Substituting (G.1) in (G.4) leads to $f_{\vartheta_+}(\vartheta)$. Subsequently substituting this result in (G.3) again produces (G.1). This completes the demonstration.

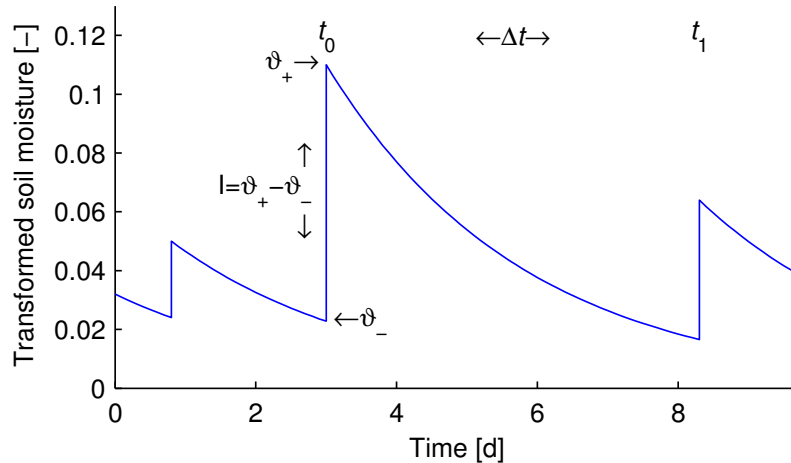


Figure G.1. Definition of the model and notation.

Summary

Soil moisture is the amount of moisture in the upper part of the soil, where plant roots can be found. It plays a central role in the hydrological cycle by controlling the exchange of water and energy between the land surface and the atmosphere. Therefore, it is a key variable in models of, for instance, rainfall-runoff, the weather, climate, or crop growth. Up to present, the possibilities to monitor soil moisture from space are limited. Fluxes to and from the soil moisture reservoir, as well as physical properties of the soil and vegetation, are difficult to measure and can be subject to large spatial variability. Hence, improvement of land surface models is important. This thesis investigates the linkage between spatial and temporal soil moisture variability on the one hand, and evapotranspiration and climate on the other hand. The different chapters treat several aspects of this linkage.

Chapter 2 describes the impact of non-linearities in the relation between soil moisture and fluxes from the soil moisture reservoir (the so-called loss-function) on the temporal distribution of soil moisture. This study utilizes soil moisture data from Illinois (U.S.). The climate in this region is characterized by wet, cold winters, and hot, dry summers. Previous studies have used the bimodality in the temporal soil moisture distribution as evidence for a strong feedback between soil moisture and precipitation. However, a different explanation is more plausible. The loss function has a domain with little sensitivity of the losses to soil moisture itself: there where the losses are equal to the maximum (potential) evaporation. As a result, the probability of soil moisture values in this domain is smaller than the probability of values in the wet or dry domain. It is shown that soil moisture dynamics in land surface models are directly related to the shape of the loss-function.

Chapter 3 describes the effect of different root water uptake parameterizations on the dynamics of evapotranspiration and soil moisture. Two different strategies are distinguished: a static strategy where the local uptake at any depth primarily depends on the local availability of moisture, and an adaptive strategy where the uptake also depends on the total root zone soil moisture. Starting from similar initial soil moisture, these strategies lead to a completely different characteristic drydown. During drydown, the difference in evapotranspiration between the strategies can be as high as 50%. The corresponding differences in soil moisture are smaller (since soil moisture integrates the preceding evaporation), but are still as high as 25%. Observations suggest the adaptive strategy to be a better model for the real uptake.

Chapter 4 describes the typical timescales of evapotranspiration decay during drydown of a vegetated land surface. These timescales reflect the sensitivity of evapotranspiration for soil moisture storage and are an important characteristic for the dynamics of both. In land surface models, this sensitivity depends on several soil and vegetation parameters. The values of these parameters are often uncertain. Knowledge about the sensitivity can contribute to more robust estimates of, primarily, effective rooting depth. From an extensive analysis of evapotranspiration observations during drydown, the sensitivity is found to range from less than 0.03 to 0.1 per day. In all investigated cases, the timescales exceeded the typical timescale for agricultural crops from literature. The shortest timescales were found for grasslands; in general forests were characterized by longer timescales. In two cases it was tested how well models participating in the Global Soil Wetness Project (GSWP-2) reproduced the observed drydown. The considerable inter-model differences indicate that the dependence of evapotranspiration to soil moisture storage in land surface models can be improved.

Chapter 5 describes different methods to estimate spatial average soil moisture in the root zone from point-scale observations. This problem is relevant since root zone soil moisture is observed at the point-scale, while many applications need the spatial average at the grid or pixel scale. The relation between soil moisture at the point scale and its spatial average depends on the spatial variability of point-scale soil moisture, but also on the temporal persistence in the spatial distribution. For this reason, two groups of strategies are considered for the sampling of spatial soil moisture fields: one with the objective to monitor the spatial mean itself, and one with the objective to monitor only the dynamics (i.e., temporal changes) of the spatial mean. The accuracy of different strategies was investigated using three different datasets. The accuracy with which the dynamics of the spatial mean can be estimated is in all cases higher than for the spatial mean itself. When a series of spatial fields is available, there appear to be sites that are more representative for the spatial mean than others. However it is shown to be impossible to identify these sites based on a single spatial survey or on vegetation or

SUMMARY

landscape characteristics only.

Chapter 6 describes how the existence of different relations between spatial mean soil moisture and its associated spatial variability in different datasets can be explained. Knowledge on the origin of the different relations will aid the upscaling of models and parameterizations that are often applied beyond their spatial validity scale (typically the point scale). It appears to be possible to simulate the temporal dynamics of the spatial distribution by applying a simple soil moisture model to a large number of points in space. For each point, the parameter values are taken from a spatial distribution. If necessary, a topographic correction is applied. Based on the covariances between the soil moisture field and the different fluxes, it is determined what processes (fluxes) cause the spatial soil moisture variance to either increase or decrease. By accounting for effects of spatial variability in soil and vegetation characteristics, in combination with atmospheric forcing (precipitation and potential evapotranspiration), different observed relations between spatial mean soil moisture and its variability are explained.

Chapter 7 describes an analysis of intensive soil moisture observations made in the Australian Murrumbidgee catchment during the National Airborne Field Experiment (NAFE'06). During the three-week long campaign, surface (0–5 cm) soil moisture variability was monitored in six field sites. Due to the dry background conditions in combination with several minor rainfall events, the dynamics of the spatial soil moisture distribution could be described by a simple analytical model. After long rainless periods, soil moisture approached the residual moisture content. During rainfall, spatially variable infiltration caused a proportional increase in both the spatial mean and its standard deviation. Both decrease exponentially during interstorm periods due to spatially variable evaporation. The time constant of this process is in the order of 2 to 3 days. The moments of the steady state probability distribution of soil moisture depend both on the amount and structure of precipitation.

Chapter 8 describes the effect of climate variability on the yearly relation between spatial mean soil moisture and its associated spatial variability for a field in Louvain-la-Neuve (Belgium). In this study, observations made during three growing seasons have been compared to simulations over a longer 15-year period (1989–2003). The observations were available for the years 1999 (average with respect to precipitation), 2000 (wet), and 2003 (dry). For each year, the observations show an initial increase in spatial variability with decreasing mean soil moisture (1999 and 2000), followed by a strong decrease in the event of very low soil moisture conditions (2003). The simulations show a similar pattern. Since the simulations also cover the period of rewetting after the growing season, they reveal a hysteresis in the relation between spatial mean soil moisture and its variability. The direction of the hysteresis loop differs for wet and dry years, and can be predicted by a simple climate index which is the ratio between the maximum precipitation deficit and the available soil moisture storage above the critical moisture content.

This thesis shows that relatively simple models are sufficient to capture the essence of soil moisture and evapotranspiration dynamics. Since more complex models often fail to reproduce the observed processes, it can be concluded that the focus should be on improving key land surface characteristics such as root distribution and depth, rather than increasing model complexity. The spatial variability of soil moisture is shown to be related to variability in soil, vegetation, and landscape characteristics, and should therefore only be considered in conjunction with these characteristics. Evapotranspiration is shown to be insensitive to soil moisture for soil moisture values around and just below field capacity. For lower soil moisture, the relation between soil moisture and evapotranspiration is approximately linear. A correct representation of these processes in land surface models is important, especially in conditions of increasing climate variability and drought.

Samenvatting

Bodemvocht is de hoeveelheid vocht in het bovenste gedeelte van de bodem, daar waar planten hun wortels kunnen hebben. Het vervult een centrale rol in de hydrologische cyclus door de controle op de uitwisseling van water en energie tussen het landoppervlak en de atmosfeer. Het is daarom een belangrijke variabele in modellen van bijvoorbeeld neerslag-afvoer, het weer, het klimaat, of gewasgroei. De mogelijkheden van satelliet bodemvochtmetingen zijn tot op heden beperkt. Ook het modelleren van bodemvocht kent de nodige moeilijkheden. Veel fluxen van en naar het bodemvocht reservoir, alsmede fysieke kenmerken van de bodem en vegetatie, zijn lastig te meten en kunnen bovendien een grote ruimtelijke variatie vertonen. Dit maakt het verbeteren van landoppervlaktemodellen belangrijk. Dit proefschrift onderzoekt de link tussen de ruimtelijke en temporele variaties van bodemvocht enerzijds, en verdamping en klimaat anderszijds. In verschillende hoofdstukken worden een aantal aspecten daarvan behandeld.

Hoofdstuk 2 beschrijft de invloed van niet-lineariteiten in de relatie tussen bodemvocht en de fluxen uit het bodemvochtreservoir (de zgn. verliesfunctie) op de temporele verdeling van bodemvocht. Voor deze studie zijn gegevens gebruikt uit Illinois (V.S.). Het klimaat in deze regio wordt gekenmerkt door natte, koude winters, en hete, droge zomers. Eerdere studies hebben de bimodaliteit in de temporele verdeling van bodemvochtgegevens uit deze regio gebruikt als bewijs voor een sterke terugkoppeling tussen bodemvocht en neerslag. Een andere verklaring blijkt echter aannemelijker. De verliesfunctie heeft een domein waarin de verliezen van bodemvocht relatief ongevoelig zijn voor bodemvocht zelf, namelijk precies daar waar de verliezen gelijk zijn aan de maximaal mogelijke (potentiële) verdamping. Als gevolg daarvan is de kans op bodemvocht waarden in dit domein kleiner dan de kans op waarden in het natte of droge domein. Het blijkt dat bodemvochtdynamiek in landoppervlaktemodellen direct gerelateerd is aan de vorm van de verliesfunctie.

Hoofdstuk 3 beschrijft het effect van verschillen in de parameterisatie van wateropname door wortels op de dynamiek van verdamping en bodemvocht. Hierbij worden twee verschillende strategieën onderscheiden: een statische strategie waarbij de lokale opname op elke diepte voornamelijk afhangt van de lokale vochtbeschikbaarheid en een adaptieve strategie waarbij de lokale wortelopname juist afhankelijk is van de totale hoeveelheid bodemvocht in de wortelzone. Deze twee strategieën hebben een totaal verschillende karakteristieke uitdroging bij een gelijk initieel bodemvocht tot gevolg. Tijdens uitdroging kunnen de verschillen in verdamping tussen de twee strategieën oplopen tot meer dan 50%. De corresponderende verschillen in bodemvocht zijn kleiner (omdat bodemvocht een integrator is van alle voorafgaande verdamping), maar bedragen nog altijd meer dan 25%. Uit waarnemingen blijkt dat de adaptieve strategie een beter model is voor de werkelijke opname.

Hoofdstuk 4 beschrijft de typische tijdschalen van verdampingsafname tijdens uitdroging van een met vegetatie begroeid landoppervlak. Deze tijdschalen weerspiegelen de gevoeligheid van verdamping voor de totale bodemvochtberging en zijn een belangrijke karakteristiek van de dynamiek van beiden. In landoppervlakte modellen is deze gevoeligheid afhankelijk van diverse bodem- en vegetatieparameters. De waarden van deze parameters is echter veelal onzeker. Kennis van de gevoeligheid kan bijdragen tot een betere schatting van met name effectieve worteldiepte. Uit een uitgebreide analyse van verdampingswaarnemingen tijdens uitdroging blijkt deze gevoeligheid te variëren van minder dan 0.03 tot 0.1 per dag. In alle onderzochte gevallen waren de corresponderende tijdschalen groter dan de tijdschaal voor landbouwgewassen uit de literatuur. De kortste tijdschalen werden gevonden voor graslanden; bossen werden over het algemeen gekenmerkt door langere tijdschalen. In twee gevallen is getoetst hoe goed verschillende modellen uit het Global Soil Wetness Project (GSWP-2) de uitdroging reproduceren. De gevonden verschillen geven aan dat met name de gevoeligheid van verdamping voor bodemvocht in landoppervlaktemodellen voor verbetering vatbaar is.

Hoofdstuk 5 beschrijft verschillende manieren om voor een bepaald gebied het ruimtelijk gemiddelde bodemvocht in de wortelzone te schatten uit puntwaarnemingen. Dit is een relevant probleem omdat bodemvocht in de wortelzone op puntschaal waargenomen wordt, terwijl een ruimtelijk gemiddelde op grid- of pixelschaal vaak het doel is. De relatie tussen bodemvocht op puntschaal en het ruimtelijk gemiddelde hangt in eerste instantie af van de ruimtelijke variatie op de puntschaal, maar ook van de temporele persistentie van de ruimtelijke verdeling. Er worden dan ook twee groepen van strategieën onderscheiden voor het bemonsteren

van een ruimtelijk bodemvochtveld: één waarbij het doel is het gemiddelde zelf te schatten en één waarbij het doel is om alleen de dynamiek van het gemiddelde te schatten. Voor drie datasets is onderzocht hoe goed het ruimtelijk gemiddelde geschat kan worden met de verschillende strategieën. De nauwkeurigheid waarmee de dynamiek geschat kan worden is in alle gevallen groter dan die van het gemiddelde. Wanneer een serie van ruimtelijke velden beschikbaar is blijken er plekken te zijn die meer representatief zijn voor het ruimtelijk gemiddelde dan andere. Het blijkt echter niet mogelijk te zijn om deze plek a priori aan te wijzen op basis van een enkele ruimtelijke meetcampagne, of enkel op basis van vegetatie van landschap kenmerken.

Hoofdstuk 6 beschrijft verschillen in de relatie tussen ruimtelijk gemiddeld bodemvocht en de onderliggende variatie op puntschaal zoals die geobserveerd zijn tijdens verschillende meetcampagnes. Kennis over hoe deze verschillen ontstaan is van belang voor onder andere het opschalen van modellen en voor parameterisaties, die meestal worden toegepast op een grotere ruimtelijke schaal dan waarop ze geldig zijn (vaak de puntschaal). Het blijkt mogelijk om de temporele dynamiek van de ruimtelijke variatie te simuleren. Hiervoor is met behulp van een eenvoudig model bodemvocht gesimuleerd voor een groot aantal lokaties. De parameters van het model zijn voor elk punt getrokken uit een ruimtelijke verdeling. Indien nodig is een topografische correctie toegepast. Aan de hand van de covarianties tussen het bodemvochtveld en de verschillende fluxen is bepaald welke processen (fluxen) tot een toe- dan wel afname van de ruimtelijke variatie leiden. Door rekening te houden met effecten van ruimtelijke variatie in bodem- en vegetatie-eigenschappen in combinatie met de atmosferische forcering (in de vorm van neerslag en potentiële verdamping), zijn de verschillende geobserveerde trends in de grootte van de ruimtelijke variatie als functie van het gemiddelde bodemvocht verklaard.

Hoofdstuk 7 beschrijft een analyse van uitgebreide oppervlaktebodemvocht metingen in het Murrumbidgee stroomgebied (Australië) tijdens het National Airborne Field Experiment (NAFE'06). Tijdens deze drie weken durende campagne werd in een zestal gebieden van enkele vierkante kilometers de ruimtelijke verdeling van bodemvocht in de bovenste 5 cm van de bodem gemeten. De zeer droge achtergrondomstandigheden, in combinatie met lichte neerslag, maken dat de dynamiek van de ruimtelijke verdeling (gemiddelde en standaardafwijking) met een zeer eenvoudig analytisch model beschreven kunnen worden. Na een lange periode zonder neerslag is er geen verandering in bodemvocht waarneembaar: bodemvocht benadert dan het residueel vochtgehalte. Door ruimtelijke variatie in infiltratie van neerslag was er tijdens buien een evenredige toename van het ruimtelijke gemiddelde en de ruimtelijke variatie (standaardafwijking) van bodemvocht. Door ruimtelijke variatie in verdamping tijdens uitdroging nemen beide exponentieel af in periodes zonder neerslag. De tijdconstante van dit proces is in de orde van 2 tot 3 dagen. De momenten van de stationaire kansverdeling van bodemvocht onder deze omstandigheden zijn zowel afhankelijk van de hoeveelheid als van de structuur van de neerslag.

Hoofdstuk 8 beschrijft het effect van klimaatvariëaties op de jaarlijkse relatie tussen gemiddeld bodemvocht en de onderliggende variatie op veldschaal voor een veld in Louvain-la-Neuve (België). Hierbij zijn observaties voor drie groeiseizoenen vergeleken met simulaties over een langere periode van 15 jaren (1989–2003). De observaties waren beschikbaar voor de jaren 1999 (een gemiddeld jaar qua neerslag), 2000 (nat) en 2003 (droog). De observaties laten aanvankelijk een toename van de ruimtelijke variatie zien bij een afname van gemiddeld bodemvocht (1999 en 2000), eventueel gevolgd door een sterke afname van de ruimtelijke variatie bij een zeer laag gemiddeld bodemvocht (2003). De simulaties laten een zelfde patroon zien. Omdat de simulaties ook de periode na het groeiseizoen beslaan, blijkt dat de relatie tussen gemiddeld bodemvocht en de onderliggende variatie hysteresis vertoont. De richting van de hysteresis lus is verschillend voor droge en natte jaren, en kan voorspeld worden aan de hand van een eenvoudige klimaatsindex die de verhouding weergeeft tussen het maximale neerslagtekort tijdens het groeiseizoen enerzijds, en de hoeveelheid beschikbaar bodemvocht boven het kritiek vochtgehalte anderzijds.

Uit dit proefschrift blijkt dat de essentie van de dynamiek van bodemvocht en verdamping al met zeer eenvoudige modellen goed beschreven kan worden. Gezien de moeite die meer complexe modellen hebben met deze processen kan worden geconcludeerd dat de aandacht voor modelcomplexiteit ten koste is gegaan van kennis over de primaire kenmerken zoals wortelverdeling en -diepte. De ruimtelijke variatie in bodemvocht blijkt gerelateerd aan de variaties in bodem- en vegetatie-eigenschappen, en hebben door deze relatie minder invloed dan voorheen gedacht op het opschalen van model parameterisaties. Bij bodemvochtwaarden rond en net beneden veldcapaciteit blijkt verdamping ongevoelig te zijn voor bodemvocht. Een juiste representatie van deze processen in landoppervlaktmodellen is van groot belang, zeker wanneer deze modellen gebruikt worden onder condities van toenemende klimaatvariëaties en droogte.

Bibliography

- Abramowitz, G. (2005), Towards a benchmark for land surface models, *Geophys. Res. Lett.*, 32, L22702, doi: 10.1029/2005GL024419.
- Adiku, S. G. K., C. W. Rose, R. D. Braddock, and H. Ozier-Lafontaine (2000), On the simulation of root water extraction: examination of a minimum energy hypothesis, *Soil Sci.*, 165(3), 226–236.
- Al-Kaisi, M., L. J. Brun, and J. W. Enz (1989), Transpiration and evapotranspiration from maize as related to leaf area index, *Agr. Forest Meteorol.*, 48, 111–116.
- Albertson, J. D., and G. Kiely (2001), On the structure of soil moisture time series in the context of land surface models, *J. Hydrol.*, 243, 101–119.
- Albertson, J. D., and N. Montaldo (2003), Temporal dynamics of soil moisture variability: 1. Theoretical basis, *Water Resour. Res.*, 39(10), 1274, doi:10.1029/2002WR001616.
- Allen, R. G., L. S. Pereira, D. Raes, and M. Smith (1998), Crop evapotranspiration - guidelines for computing crop water requirements, *FAO Irrigation and drainage paper 56*, FAO, Rome.
- Amenu, G. G., P. Kumar, and X. Liang (2005), Interannual variability of deep-layer hydrologic memory and mechanisms of its influence on surface energy fluxes, *J. Climate*, 18(23), 5024–5045, doi: 10.1175/JCLI3590.1.
- Anderson, M. G., and P. E. Kneale (1980), Topography and hillslope soil water relationships in a catchment of low relief, *J. Hydrol.*, 47, 115–128.
- Atkinson, S. E., R. A. Woods, and M. Sivapalan (2002), Climate and landscape controls on water balance model complexity over changing timescales, *Water Resour. Res.*, 38(12), 1314.
- Baldocchi, D., et al. (2001), Fluxnet: A new tool to study the temporal and spatial variability of ecosystem-scale carbon dioxide, water vapor, and energy flux densities, *Bull. Am. Meteorol. Soc.*, 82(11), 2415–2434.
- Baldocchi, D. D., L. Xu, and N. Kiang (2004), How plant functional-type, weather, seasonal drought, and soil physical properties alter water and energy fluxes of an oak-grass savanna and an annual grassland, *Agr. Forest Meteorol.*, 123, 13–39, doi:10.1016/j.agrformet.2003.11.006.
- Bárdossy, A., and W. Lehmann (1998), Spatial distribution of soil moisture in a small catchment. Part 1: Geostatistical analysis, *J. Hydrol.*, 206, 1–15.
- Beljaars, A. C. M., P. Viterbo, M. J. Miller, and A. K. Betts (1996), The anomalous rainfall over the United States during July 1993: Sensitivity to land surface parameterization and soil moisture anomalies, *Mon. Weather Rev.*, 124(3), 362–382.
- Bell, K. R., B. J. Blanchard, T. J. Schmugge, and M. W. Witzak (1980), Analysis of surface moisture variations within large-field sites, *Water Resour. Res.*, 16(4), 796–810.
- Bierkens, M. F. P., and B. J. J. M. van den Hurk (2007), Groundwater convergence as a possible mechanism for multi-year persistence in rainfall, *Geophys. Res. Lett.*, 34(2), L02402, doi:10.1029/2006GL028396.
- Bosilovich, M. G., and W. Sun (1999), Numerical simulation of the 1993 Midwestern flood: Land-atmosphere interactions, *J. Climate*, 12(5), 1490–1505.
- Brubaker, K. L., D. Entekhabi, and P. S. Eagleson (1993), Estimation of continental precipitation recycling, *J. Climate*, 6(6), 1077–1089.
- Bruno, R. D., H. R. da Rocha, H. C. de Freitas, M. L. Goulden, and S. D. Miller (2006), Soil moisture dynamics in an eastern Amazonian tropical forest, *Hydrol. Process.*, 20, 2477–2489, doi:10.1002/hyp.6211.
- Brutsaert, W. (2005), *Hydrology — An introduction*, Cambridge Univ. Press.
- Brutsaert, W., and D. Chen (1995), Desorption and the two stages of drying of natural tallgrass prairie, *Water Resour. Res.*, 31(5), 1305–1313.
- Calanca, P. (2004), Interannual variability of summer mean soil moisture conditions in Switzerland during the 20th century: A look using a stochastic soil moisture model, *Water Resour. Res.*, 40, W12502, doi: 10.1029/2004WR003254.

BIBLIOGRAPHY

- Calvet, J., J. Noilhan, and P. Bessemoulin (1998), Retrieving the root-zone soil moisture from surface soil moisture or temperature estimates: A feasibility study based on field measurements, *J. Appl. Meteorol.*, 37(4), 371–386.
- Campbell, G. S. (1974), A simple method for determining unsaturated conductivity from moisture retention data, *Soil Sci.*, 117(6), 311–314.
- Cantón, Y., A. Solé-Benet, and F. Domingo (2004), Temporal and spatial patterns of soil moisture in semiarid badlands of SE Spain, *J. Hydrol.*, 285, 199–214.
- Capehart, W. J., and T. N. Carlson (1997), Decoupling of surface and near-surface soil water content: A remote sensing perspective, *Water Resour. Res.*, 33(6), 1383–1395.
- Charpentier, M. A., and P. M. Groffman (1992), Soil moisture variability within remote sensing pixels, *J. Geophys. Res.*, 97(D17), 18,987–18,995.
- Chen, Y. (2006), Letter to the Editor on “rank stability or temporal stability”, *Soil Sci. Soc. Am. J.*, 70(1), 306, doi:10.2136/sssaj2005.0290l.
- Choi, M., J. M. Jacobs, and M. Cosh (2007), Scaled spatial variability of soil moisture fields, *Geophys. Res. Lett.*, 34(1), L01401, doi:10.1029/2006GL028247.
- Clapp, R. B., and G. M. Hornberger (1978), Empirical equations for some soil hydraulic properties, *Water Resour. Res.*, 14(4), 601–604.
- Coelho, E. F., and D. Or (1999), Root distribution and water uptake patterns of corn under surface and subsurface drip irrigation, *Plant Soil*, 206(2), 123–136.
- Comegna, V., and A. Basile (1994), Temporal stability of spatial patterns of soil water storage in a cultivated Vesuvian soil, *Geoderma*, 62, 299–310.
- Cosh, M. H., J. R. Stedinger, and W. Brutsaert (2004), Variability of surface soil moisture at the watershed scale, *Water Resour. Res.*, 40, W12513, doi:10.1029/2004WR003487.
- Crave, A., and C. Gascuel-Oudoux (1997), The influence of topography on time and space distribution of soil surface water content, *Hydrol. Process.*, 11, 203–210.
- Crow, W. T., and E. F. Wood (2002), Impact of soil moisture aggregation on surface energy flux prediction during SGP’97, *Geophys. Res. Lett.*, 29(1), doi:10.1029/2001GL013796.
- Dardanelli, J. L., J. T. Ritchie, M. Calmon, J. M. Andriani, and D. J. Collino (2004), An empirical model for root water uptake, *Field Crop. Res.*, 87, 59–71, doi:10.1016/j.fcr.2003.09.008.
- Delworth, T. L., and S. Manabe (1988), The influence of potential evaporation on the variabilities of simulated soil wetness and climate, *J. Climate*, 1(5), 523–547.
- Denmead, O. T., and R. H. Shaw (1962), Availability of soil water to plants as affected by soil moisture content and meteorological conditions, *Agron. J.*, 54, 385–390.
- Desborough, C. E. (1997), The impact of root weighting on the response of transpiration to moisture stress in land surface schemes, *Mon. Weather Rev.*, 125(8), 1920–1930.
- Dirmeyer, P. A., X. Gao, M. Zhao, Z. Guo, T. Oki, and N. Hanasaki (2006a), The Second Global Soil Wetness Project (GSWP-2): Multi-model analysis and implications for our perception of the land surface, *Bull. Am. Meteorol. Soc.*, 87(10), 1381–1397, doi:10.1175/bams-87-10-1381.
- Dirmeyer, P. A., R. D. Koster, and Z. Guo (2006b), Do global models properly represent the feedback between land and atmosphere?, *J. Hydrometeorol.*, 7(6), 1177–1198, doi:10.1175/JHM532.1.
- D’Odorico, P., and A. Porporato (2004), Preferential states in soil moisture and climate dynamics, *P. Natl. Acad. Sci. USA*, 101(24), 8848–8851, doi:10.1073/pnas.0401428101.
- Dolman, A. J., and D. Gregory (1992), The parameterization of rainfall interception in GCMs, *Q. J. Roy. Meteor. Soc.*, 118(505), 455–467.
- Downer, C. W., and F. L. Ogden (2004), Appropriate vertical discretization of Richards’ equation for two-dimensional watershed-scale modelling, *Hydrol. Process.*, 18, 1–22, doi:10.1002/hyp.1306.
- Ek, M. B., and A. A. M. Holtslag (2004), Influence of soil moisture on boundary layer cloud development, *J. Hydrometeorol.*, 5(1), 86–99.
- Engelbrecht, B. M. J., L. S. Comita, R. Condit, T. A. Kursar, M. T. Tyree, B. L. Turner, and S. P. Hubbell (2007), Drought sensitivity shapes species distribution patterns in tropical forests, *Nature*, 447(7140), 80–83, doi:10.1038/nature05747.

- Entin, J. K., A. Robock, K. Y. Vinnikov, S. E. Hollinger, S. Liu, and A. Namkhai (2000), Temporal and spatial scales of observed soil moisture variations in the extratropics, *J. Geophys. Res.*, *105*(D9), 11,865–11,877.
- Falge, E., et al. (2005), *FLUXNET Marconi Conference Gap-Filled Flux and Meteorology Data, 1992–2000*. Data set. Available on-line [<http://mercury.ornl.gov/ornl daac/>] from Oak Ridge National Laboratory Distributed Active Archive Center, Oak Ridge, Tennessee, USA.
- Famiglietti, J. S., J. W. Rudnicki, and M. Rodell (1998), Variability in surface moisture content along a hillslope transect: Rattlesnake Hill, Texas, *J. Hydrol.*, *210*, 259–281.
- Famiglietti, J. S., J. A. Devereaux, C. A. Laymon, T. Tsegaye, P. R. Houser, T. J. Jackson, S. T. Graham, M. Rodell, and P. J. van Oevelen (1999), Ground-based investigation of soil moisture variability within remote sensing footprints during the Southern Great Plains 1997 (SGP97) Hydrology Experiment, *Water Resour. Res.*, *35*(6), 1839–1851.
- Feddes, R. A., et al. (2001), Modeling root water uptake in hydrological and climate models, *Bull. Am. Meteorol. Soc.*, *82*(12), 2797–2809.
- Findell, K. L., and E. A. B. Eltahir (1997), An analysis of the soil moisture-rainfall feedback, based on direct observations from Illinois, *Water Resour. Res.*, *33*(4), 725–735.
- Findell, K. L., and E. A. B. Eltahir (2003), Atmospheric controls on soil moisture-boundary layer interactions. Part II: Feedbacks within the continental United States, *J. Hydrometeorol.*, *4*(3), 570–583.
- Fitzjohn, C., J. L. Ternan, and A. G. Williams (1998), Soil moisture variability in a semi-arid gully catchment: implications for runoff and erosion control, *Catena*, *32*, 55–70.
- Gerwitz, A., and E. R. Page (1974), An empirical mathematical model to describe plant root systems, *J. Appl. Ecol.*, *11*(2), 773–781.
- Giorgi, F., and R. Avissar (1997), Representation of heterogeneity effects in earth system modeling: experience from land surface modeling, *Rev. Geophys.*, *35*(4), 413–438.
- Giorgi, F., L. O. Mearns, C. Shields, and L. Meyer (1996), A regional model study of the importance of local versus remote controls of the 1988 drought and the 1993 flood over the central United States, *J. Climate*, *9*(5), 1150–1162.
- Gómez-Plaza, A., J. Alvarez-Rogel, J. Albaladejo, and V. M. Castillo (2000), Spatial patterns and temporal stability of soil moisture across a range of scales in a semi-arid environment, *Hydrol. Process.*, *14*, 1261–1277.
- Gower, S. T. (2000–2004), *LAI field measurements for BigFoot MODIS land product validation, KONZ, 2001/2002*. Data set. Available on-line [<http://mercury.ornl.gov/ornl daac/>] from Oak Ridge National Laboratory Distributed Active Archive Center, Oak Ridge, Tennessee, USA.
- Grant, L., M. Seyfried, and J. McNamara (2004), Spatial variation and temporal stability of soil water in a snow-dominated, mountain catchment, *Hydrol. Process.*, *18*, 3493–3511, doi:10.1002/hyp.5798.
- Grayson, R. B., and A. W. Western (1998), Towards areal estimation of soil water content from point measurements: time and space stability of mean response, *J. Hydrol.*, *207*, 68–82.
- Grayson, R. B., A. W. Western, F. H. S. Chiew, and G. Blöschl (1997), Preferred states in spatial soil moisture patterns: Local and nonlocal controls, *Water Resour. Res.*, *33*(12), 2897–2908.
- Green, S. R., and B. E. Clothier (1995), Root water uptake by kiwifruit vines following partial wetting of the root zone, *Plant Soil*, *173*, 317–328.
- Guswa, A. J. (2005), Soil-moisture limits on plant uptake: an upscaled relationship for water-limited ecosystems, *Adv. Water Resour.*, *28*, doi:10.1016/j.advwatres.2004.08.016.
- Guswa, A. J., M. A. Celia, and I. Rodríguez-Iturbe (2002), Models of soil moisture dynamics in ecohydrology: A comparative study, *Water Resour. Res.*, *38*(9), 1166.
- Gutmann, E. D., and E. E. Small (2007), A comparison of land surface model soil hydraulic properties estimated by inverse modeling and pedotransfer functions, *Water Resour. Res.*, *43*(5), W05418, doi: 10.1029/2006WR005135.
- Hasler, N., and R. Avissar (2007), What controls evapotranspiration in the Amazon Basin? *J. Hydrometeorol.*, *8*, 380–395, doi:10.1175/JHM587.1.
- Hawley, M. E., T. J. Jackson, and R. H. McCuen (1983), Surface soil moisture variation on small agricultural watersheds, *J. Hydrol.*, *62*, 179–200.

BIBLIOGRAPHY

- Hetherington, A. M., and F. I. Woodward (2003), The role of stomata in sensing and driving environmental change, *Nature*, 424, 901–908.
- Hogue, T. S., L. A. Bastidas, H. V. Gupta, and S. Sorooshian (2006), Evaluating model performance and parameter behavior for varying levels of land surface model complexity, *Water Resour. Res.*, 42, W08430, doi:10.1029/2005WR004440.
- Hollinger, S. E., and S. A. Isard (1994), A soil moisture climatology of Illinois, *J. Climate*, 7, 822–833.
- Homaei, M., R. A. Feddes, and C. Dirksen (2002), Simulation of root water uptake II. Non-uniform transient water stress using different reduction functions, *Agric. Wat. Mngt.*, 57, 111–126.
- Hong, S., and E. Kalnay (2000), Role of sea surface temperature and soil-moisture feedback in the 1998 Oklahoma-Texas drought, *Nature*, 408(6814), 842–844, doi:10.1038/35048548.
- Hoogland, J. C., R. A. Feddes, and C. Belmans (1981), Root water uptake model depending on soil water pressure head and maximum extraction rate, *Acta Hort. (ISHS)*, 119, 123–136.
- Hunt, J. E., F. M. Kelliher, T. M. McSeveny, and J. N. Byers (2002), Evaporation and carbon dioxide exchange between the atmosphere and a tussock grassland during a summer drought, *Agr. Forest Meteorol.*, 111, 65–82.
- Hupet, F., and M. Vanclooster (2002), Intraseasonal dynamics of soil moisture variability within a small agricultural maize cropped field, *J. Hydrol.*, 261, 86–101.
- Hupet, F., and M. Vanclooster (2004), Sampling strategies to estimate field areal evapotranspiration fluxes with a soil water balance approach, *J. Hydrol.*, 292, 262–280, doi:10.1016/j.jhydrol.2004.01.006.
- Hupet, F., and M. Vanclooster (2005), Micro-variability of hydrological processes at the maize row scale: implications for soil water content measurements and evapotranspiration estimates, *J. Hydrol.*, 303, 247–270, doi:10.1016/j.jhydrol.2004.07.017.
- Hupet, F., P. Bogaert, and M. Vanclooster (2004), Quantifying the local-scale uncertainty of estimated actual evapotranspiration, *Hydrol. Process.*, 18, 3415–3434, doi:10.1002/hyp.1504.
- Huxman, T. E., et al. (2004), Convergence across biomes to a common rain-use efficiency, *Nature*, 429(6992), 651–654, doi:10.1038/nature02561.
- Jackson, R. B., J. S. Sperry, and T. E. Dawson (2000), Root water uptake and transport: Using physiological processes in global predictions. *Trends Plant Sci.*, 5(11), 482–488.
- Jacobs, J. M., B. P. Mohanty, E. Hsu, and D. Miller (2004), SMEX02: Field scale variability, time stability and similarity of soil moisture, *Remote Sens. Environ.*, 92, 436–446, doi:10.1016/j.rse.2004.02.017.
- Jarvis, N. J. (1989), A simple empirical model of root water uptake, *J. Hydrol.*, 107, 57–72.
- Kachanoski, R. G., and E. de Jong (1988), Scale dependence and the temporal persistence of spatial patterns of soil water storage, *Water Resour. Res.*, 24(1), 85–91.
- Kerr, Y. H. (2007), Soil moisture from space: Where are we?, *Hydrogeol. J.*, 15(1), 117–200, doi:10.1007/s10040-006-0095-3.
- Kerr, Y. H., P. Waldteufel, J. Wigneron, J. Martinuzzi, J. Font, and M. Berger (2001), Soil moisture retrieval from space: the Soil Moisture and Ocean Salinity (SMOS) mission, *IEEE T. Geosci. Remote Sens.*, 39(8), 1729–1735.
- Kim, C. P., and J. N. M. Stricker (1996), Influence of spatially variable soil hydraulic properties and rainfall intensity on the water budget, *Water Resour. Res.*, 32(6), 1699–1712.
- Kim, C. P., J. N. M. Stricker, and P. J. J. F. Torfs (1996), An analytical framework for the water budget of the unsaturated zone, *Water Resour. Res.*, 32(12), 3475–3484.
- Kim, C. P., J. N. M. Stricker, and R. A. Feddes (1997), Impact of soil heterogeneity on the water budget of the unsaturated zone, *Water Resour. Res.*, 33(5), 991–999.
- Kleidon, A., and M. Heimann (1998), Optimised rooting depth and its impacts on the simulated climate of an Atmospheric General Circulation Model, *Geophys. Res. Lett.*, 25(3), 345–348.
- Kochendorfer, J. P., and J. A. Ramírez (2005), The impact of land-atmosphere interactions on the temporal variability of soil moisture at the regional scale, *J. Hydrometeorol.*, 6(1), 53–67, doi:10.1175/JHM-401.1.
- Koster, R. D., and M. J. Suarez (1996), The influence of land surface moisture retention on precipitation statistics, *J. Climate*, 9(10), 2551–2567.
- Koster, R. D., and M. J. Suarez (2001), Soil moisture memory in climate models, *J. Hydrometeorol.*, 2(6), 558–570.

- Koster, R. D., M. J. Suarez, R. W. Higgins, and H. M. van den Dool (2003), Observational evidence that soil moisture variations affect precipitation, *Geophys. Res. Lett.*, *30*(5), 1241, doi:10.1029/2002GL016571.
- Koster, R. D., et al. (2004), Regions of strong coupling between soil moisture and precipitation, *Science*, *305*(5687), 1138–1140, doi:10.1126/science.1100217.
- Koster, R. D., et al. (2006), GLACE: The Global Land-Atmosphere Coupling Experiment. Part 1: Overview, *J. Hydrometeorol.*, *7*(4), 590–610.
- Kurc, S. A., and E. E. Small (2004), Dynamics of evapotranspiration in semiarid grassland and shrubland ecosystems during the summer monsoon season, central New Mexico, *Water Resour. Res.*, *40*, W09305, doi:10.1029/2004WR003068.
- Lai, C., and G. Katul (2000), The dynamic role of root-water uptake in coupling potential to actual transpiration, *Adv. Water Resour.*, *23*(4), 427–439.
- Laio, F., A. Porporato, L. Ridolfi, and I. Rodríguez-Iturbe (2001), Plants in water-controlled ecosystems: Active role in hydrologic processes and response to water stress II. Probabilistic soil moisture dynamics, *Adv. Water Resour.*, *24*(7), 707–723.
- Lawrence, D. M., and J. M. Slingo (2005), Weak land-atmosphere coupling strength in HadAM3: The role of soil moisture variability, *J. Hydrometeorol.*, *6*(5), 670–680, doi:10.1175/JHM445.1.
- Lee, T. R., and G. M. Hornberger (2006), Inferred bimodality in the distribution of soil moisture at Big Meadows, Shenandoah National Park, Virginia, *Geophys. Res. Lett.*, *33*, L06407, doi:10.1029/2005GL025536.
- Li, K. Y., R. De Jong, and J. B. Boisvert (2001), An exponential root-water-uptake model with water stress compensation, *J. Hydrol.*, *252*, 189–204.
- Loague, K. (1992), Soil water content at R-5. Part 1. Spatial and temporal variability, *J. Hydrol.*, *139*, 233–251.
- Lohmann, D., and E. F. Wood (2003), Timescales of land surface evapotranspiration response in the PILPS phase 2(c), *Global Planet. Change*, *38*, 81–91.
- Mahfouf, J. (1991), Analysis of soil moisture from near-surface parameters: A feasibility study., *J. Appl. Meteorol.*, *30*, 1534–1547.
- Manfreda, S., and I. Rodríguez-Iturbe (2006), On the spatial and temporal sampling of soil moisture fields, *Water Resour. Res.*, *42*, W05409, doi:10.1029/2005WR004548.
- Martínez-Fernández, J., and A. Ceballos (2005), Mean soil moisture estimation using temporal stability analysis, *J. Hydrol.*, *312*, 28–38, doi:10.1016/j.jhydrol.2005.02.007.
- Metselaar, K., and Q. de Jong van Lier (2007), The shape of the transpiration reduction function under plant water stress, *Vadose Zone J.*, *6*, 124–139, doi:10.2136/vzj2006.0086.
- Meyers, T. P. (2001), A comparison of summertime water and CO₂ fluxes over rangeland for well watered and drought conditions, *Agr. Forest Meteorol.*, *106*, 205–214.
- Miller, G. R., D. B. Baldocchi, B. E. Law, and T. Meyers (2007), An analysis of soil moisture dynamics using multi-year data from a network of micrometeorological observation sites, *Adv. Water Resour.*, *30*, 1065–1081, doi:10.1016/j.advwatres.2006.10.002.
- Milly, P. C. D. (1997), Sensitivity of greenhouse summer dryness to changes in plant rooting characteristics, *Geophys. Res. Lett.*, *24*(3), 269–271.
- Milly, P. C. D. (2001), A minimalist probabilistic description of root zone soil water, *Water Resour. Res.*, *37*(3), 457–463.
- Mohanty, B. P., and T. H. Skaggs (2001), Spatio-temporal evolution and time-stable characteristics of soil moisture within remote sensing footprints with varying soil, slope, and vegetation, *Adv. Water Resour.*, *24*, 1051–1067.
- Montaldo, N., and J. D. Albertson (2003), Temporal dynamics of soil moisture variability: 2. Implications for land surface models, *Water Resour. Res.*, *39*(10), 1275, doi:10.1029/2002WR001618.
- Montaldo, N., R. Rondena, J. D. Albertson, and M. Mancini (2005), Parsimonious modeling of vegetation dynamics for ecohydrologic studies of water-limited ecosystems, *Water Resour. Res.*, *41*(10), W10416, doi:10.1029/2005WR004094.
- Nepstad, D. C., et al. (1994), The role of deep roots in the hydrological and carbon cycles of Amazonian forests and pastures, *Nature*, *372*(6507), 666–669.

BIBLIOGRAPHY

- Njoku, E. G., and D. Entekhabi (1996), Passive microwave remote sensing of soil moisture, *J. Hydrol.*, *184*, 101–129.
- Nyberg, L. (1996), Spatial variability of soil water content in the covered catchment at Gårdsjön, Sweden, *Hydrol. Process.*, *10*, 89–103.
- Oglesby, R. J., and D. J. Erickson (1989), Soil moisture and the persistence of North American drought, *J. Climate*, *2*(11), 1362–1380.
- Oki, T., and S. Kanae (2006), Global hydrological cycles and world water resources, *Science*, *313*, 1068–1072, doi:10.1126/science.1128845.
- Oldak, A., Y. Pachepsky, T. J. Jackson, and W. J. Rawls (2002), Statistical properties of soil moisture images revisited, *J. Hydrol.*, *255*, 12–24.
- Owe, M., E. B. Jones, and T. J. Schmugge (1982), Soil moisture variation patterns observed in Hand County, South Dakota, *Water Resour. Bull.*, *18*(6), 949–954.
- Pachepsky, Y. A., A. K. Guber, and D. Jacques (2005), Temporal persistence in vertical distributions of soil moisture contents, *Soil Sci. Soc. Am. J.*, *69*(2), 347–352.
- Pal, J. S., and E. A. B. Eltahir (2002), Teleconnections of soil moisture and rainfall during the 1993 Midwest summer flood, *Geophys. Res. Lett.*, *29*(18), 1865, doi:10.1029/2002GL014815.
- Pancieria, R., O. Merlin, R. Young, and J. Walker (2006), *The Hydraprobe Data Acquisition System: User guide*, Department of Civil and Environmental Engineering, The University of Melbourne, Melbourne, Australia.
- Petrone, R. M., J. S. Price, S. K. Carey, and J. M. Waddington (2004), Statistical characterization of the spatial variability of soil moisture in a cutover peatland, *Hydrol. Process.*, *18*, 41–52, doi:10.1002/hyp.1309.
- Price, A. G., and B. O. Bauer (1984), Small-scale heterogeneity and soil-moisture variability in the unsaturated zone, *J. Hydrol.*, *70*, 277–293.
- Qiu, Y., B. Fu, J. Wang, and L. Chen (2001), Spatial variability of soil moisture content and its relation to environmental indices in a semi-arid gully catchment of the Loess Plateau, China, *J. Arid Environ.*, *49*, 723–750.
- Regianni, P., S. M. Hassanizadeh, M. Sivapalan, and W. G. Gray (1999), A unifying framework for watershed thermodynamics: Constitutive relationships, *Adv. Water Resour.*, *23*(1), 15–39.
- Reynolds, S. G. (1970), The gravimetric method of soil moisture determination, Part III, An examination of factors influencing soil moisture variability, *J. Hydrol.*, *11*(3), 288–300.
- Robock, A., K. Y. Vinnikov, G. Srinivasan, J. K. Entin, S. E. Hollinger, N. A. Speranskaya, S. Liu, and A. Namkhai (2000), The global soil moisture data bank, *Bull. Am. Meteorol. Soc.*, *81*(6), 1281–1299.
- Rodríguez-Iturbe, I., and A. Porporato (2004), *Ecohydrology of water-controlled ecosystems*, Cambridge Univ. Press.
- Rodríguez-Iturbe, I., D. Entekhabi, and R. L. Bras (1991), Nonlinear dynamics of soil moisture at climate scales 1. Stochastic analysis, *Water Resour. Res.*, *27*(8), 1899–1906.
- Rodríguez-Iturbe, I., A. Porporato, L. Ridolfi, V. Isham, and D. R. Cox (1999), Probabilistic modelling of water balance at a point: The role of climate, soil and vegetation, *Proc. R. Soc. Lond. A*, *455*, 3789–3805.
- Ryu, D., and J. S. Famiglietti (2005), Characterization of footprint-scale surface soil moisture variability using Gaussian and beta distribution functions during the Southern Great Plains 1997 SGP97 hydrology experiment, *Water Resour. Res.*, *41*, W12433, doi:10.1029/2004WR003835.
- Salvucci, G. D. (1998), Limiting relations between soil moisture and soil texture with implications for measured, modeled and remotely sensed estimates, *Geophys. Res. Lett.*, *25*(10), 1757–1760.
- Salvucci, G. D. (2001), Estimating the soil moisture dependence of root zone water loss using conditionally averaged precipitation, *Water Resour. Res.*, *37*(5), 1357–1365.
- Salvucci, G. D., J. A. Saleem, and R. Kauffmann (2002), Investigating soil moisture feedback on precipitation with tests of Granger causality, *Adv. Water Resour.*, *25*(8–12), 1305–1312.
- Sankaran, M., et al. (2005), Determinants of woody cover in African savannas, *Nature*, *438*, 846–849, doi:10.1038/nature04070.
- Savenije, H. H. G. (1995), New definitions for moisture recycling and the relationship with land-use changes in the Sahel, *J. Hydrol.*, *167*, 57–78.

- Savenije, H. H. G. (2004), The importance of interception and why we should delete the term evapotranspiration from our vocabulary, *Hydrol. Process.*, 18(8), 1507–1511, doi:10.1002/hyp.5563.
- Scanlon, B. R., D. G. Levitt, R. C. Reedy, K. E. Keese, and M. J. Sully (2005), Ecological controls on water-cycle response to climate variability in deserts, *P. Natl. Acad. Sci. USA*, 102(17), 6033–6038, doi:10.1073/pnas.0408571102.
- Schenk, H. J., and R. B. Jackson (2002), The global biogeography of roots, *Ecol. Monogr.*, 72(3), 311–328.
- Schmugge, T. J., T. J. Jackson, and H. L. McKim (1980), Survey of methods for soil moisture determination, *Water Resour. Res.*, 16(6), 961–979.
- Schneider, J. M., D. K. Fisher, R. L. Elliott, G. O. Brown, and C. P. Bahrman (2003), Spatiotemporal variations in soil water: First results from the ARM SGP CART network, *J. Hydrometeorol.*, 4(1), 106–120.
- Schubert, S. D., M. J. Suarez, P. J. Pegion, R. D. Koster, and J. T. Bacmeister (2004), On the cause of the 1930s dust bowl, *Science*, 303(5665), 1855–1859, doi:10.1126/science.1095048.
- Schulz, K., and K. Beven (2003), Data-supported robust parameterisations in land surface-atmosphere flux predictions: Towards a top-down approach, *Hydrol. Process.*, 17, 2259–2277.
- Schume, H., G. Jost, and K. Katzensteiner (2003), Spatial-temporal analysis of the soil water content in a mixed Norway spruce (*picea abies* (L.) Karst.)-European beech (*fagus sylvatica* L.) stand, *Geoderma*, 112, 273–287.
- Schüttemeyer, D., A. F. Moene, A. A. M. Holtslag, H. A. R. de Bruin, and N. van de Giesen (2006), Surface fluxes and characteristics of drying semi-arid terrain in West Africa, *Bound.-Lay. Meteorol.*, 118(3), 583–612, doi:10.1007/s10546-005-9028-2.
- Scott, D. W. (1979), On optimal and data-based histograms, *Biometrika*, 66(3), 605–610.
- Scott, R., D. Entekhabi, R. Koster, and M. Suarez (1997), Timescales of land surface evapotranspiration response, *J. Climate*, 10, 559–566.
- Seneviratne, S. I., P. Viterbo, D. Lüthi, and C. Schär (2004), Inferring changes in terrestrial water storage using ERA-40 reanalysis data: The Mississippi River basin, *J. Climate*, 17(11), 2039–2057.
- Seneviratne, S. I., D. Lüthi, M. Litschi, and C. Schär (2006a), Land-atmosphere coupling and climate change in Europe, *Nature*, 443(7108), 205–209, doi:10.1038/nature05095.
- Seneviratne, S. I., et al. (2006b), Soil moisture memory in AGCM simulations: Analysis of Global Land-Atmosphere Coupling Experiment (GLACE) data, *J. Hydrometeorol.*, 7(5), 1090–1112, doi:10.1175/JHM533.1.
- Seyfried, M. (1998), Spatial variability constraints to modeling soil water at different scales, *Geoderma*, 85, 231–254.
- Seyfried, M. S., and M. D. Murdock (2004), Measurement of soil water content with a 50-MHz soil dielectric sensor, *Soil Sci. Soc. Am. J.*, 68, 394–403.
- Sharp, R. E., and W. J. Davies (1985), Root growth and water uptake by maize plants in drying soil, *J. Exp. Bot.*, 36(170), 1441–1456.
- Shukla, J., and Y. Mintz (1982), Influence of land-surface evapotranspiration on the Earth's climate, *Science*, 215(4539), 1498–1501.
- Soet, M., and J. N. M. Stricker (2003), Functional behaviour of pedotransfer functions in soil water flow simulation, *Hydrol. Process.*, 17, 1659–1670.
- Soet, M., R. J. Ronda, J. N. M. Stricker, and A. J. Dolman (2000), Land surface scheme conceptualisation and parameter values for three sites with contrasting soils and climate, *Hydrol. Earth Syst. Sci.*, 4(2), 283–294.
- Starks, P. J., G. C. Heathman, T. J. Jackson, and M. H. Cosh (2006), Temporal stability of soil moisture profile, *J. Hydrol.*, 324, 400–411, doi:10.1016/j.jhydrol.2005.09.024.
- Svetlitchnyi, A. A., S. V. Plotnitskiy, and O. Y. Stepovaya (2003), Spatial distribution of soil moisture content within catchments and its modelling on the basis of topographic data, *J. Hydrol.*, 277, 50–60, doi:10.1016/S0022-1694(03)00083-0.
- Taylor, C. M., and R. J. Ellis (2006), Satellite detection of soil moisture impacts on convection at the mesoscale, *Geophys. Res. Lett.*, 33, L03404, doi:10.1029/2005GL025252.
- Vachaud, G., A. Passerat De Silans, P. Balabanis, and M. Vauclin (1985), Temporal stability of spatially measured soil water probability density function, *Soil Sci. Soc. Am. J.*, 49, 822–828.

BIBLIOGRAPHY

- van den Hurk, B. J. J. M., P. Viterbo, A. C. M. Beljaars, and A. K. Betts (2000), Offline validation of the ERA40 surface scheme, *Tech. Rep. 295*, ECMWF, Reading, UK.
- van den Hurk, B. J. J. M., P. Viterbo, and S. O. Los (2003), Impact of leaf area index seasonality on the annual land surface evaporation in a global circulation model, *J. Geophys. Res.*, *108*(D6), 4191, doi: 10.1029/2002JD002846.
- Verhoef, A., S. J. Allen, and C. R. Lloyd (1999), Seasonal variation of surface energy balance over two Sahelian surfaces, *Int. J. Climatol.*, *19*(11), 1267–1277.
- Vinnikov, K. Y., A. Robock, N. A. Speranskaya, and C. A. Schlosser (1996), Scales of temporal and spatial variability of midlatitude soil moisture, *J. Geophys. Res.*, *101*(D3), 7163–7174.
- Walker, J. P., G. R. Willgoose, and J. D. Kalma (2004), In situ measurement of soil moisture: A comparison of techniques, *J. Hydrol.*, *293*, 85–99.
- Wan, C., I. Yilmaz, and R. E. Sosebee (2002), Seasonal soil-water availability influences snakeweed root dynamics, *J. Arid Environ.*, *51*, 255–264, doi:10.1016/j.jare.2001.0942.
- Wang, A., X. Zeng, S. S. P. Shen, Q. Zeng, and R. E. Dickinson (2006), Time scales of land surface hydrology, *J. Hydrometeorol.*, *7*(5), 868–879, doi:10.1175/JHM527.1.
- Western, A. W., and G. Blöschl (1999), On the spatial scaling of soil moisture, *J. Hydrol.*, *217*, 203–224.
- Western, A. W., and R. B. Grayson (1998), The Tarrawarra data set: Soil moisture patterns, soil characteristics, and hydrological flux measurements, *Water Resour. Res.*, *34*(10), 2765–2768.
- Western, A. W., G. Blöschl, and R. B. Grayson (1998), Geostatistical characterisation of soil moisture patterns in the Tarrawarra catchment, *J. Hydrol.*, *205*, 20–37.
- Western, A. W., R. B. Grayson, G. Blöschl, G. R. Willgoose, and T. A. McMahon (1999), Observed spatial organization of soil moisture and its relation to terrain indices, *Water Resour. Res.*, *35*(3), 797–810.
- Western, A. W., R. B. Grayson, and G. Blöschl (2002), Scaling of soil moisture: A hydrologic perspective, *Annu. Rev. Earth Planet. Sci.*, *30*, 149–180, doi:10.1146/annurev.earth.30.091201.140434.
- Western, A. W., R. B. Grayson, G. Blöschl, and D. J. Wilson (2003), Spatial variability of soil moisture and its implications for scaling, in *Scaling methods in soil physics*, edited by Y. Percepisky, M. Selim, and D. Radcliffe, chap. 8, CRC Press.
- Western, A. W., S. Zhou, R. B. Grayson, T. A. McMahon, G. Blöschl, and D. J. Wilson (2004), Spatial correlation of soil moisture in small catchments and its relationship to dominant spatial hydrological processes, *J. Hydrol.*, *286*, 113–134, doi:10.1016/j.jhydrol.2003.09.014.
- Williams, C. A., and J. D. Albertson (2004), Soil moisture controls on canopy-scale water and carbon fluxes in an African savanna, *Water Resour. Res.*, *40*(9), W09302, doi:10.1029/2004WR003208.
- Wilson, D. J., A. W. Western, and R. B. Grayson (2004), Identifying and quantifying sources of variability in temporal and spatial soil moisture observations, *Water Resour. Res.*, *40*(2), W02507, doi: 10.1029/2003WR002306.
- Wilson, D. J., A. W. Western, and R. B. Grayson (2005), A terrain and data-based method for generating the spatial distribution of soil moisture, *Adv. Water Resour.*, *28*, 43–54, doi:10.1016/j.advwatres.2004.09.007.
- Wood, E. F. (1997), Effects of soil moisture aggregation on surface evaporative fluxes, *J. Hydrol.*, *190*, 397–412.
- Xu, C., and D. Chen (2005), Comparison of seven models for estimation of evapotranspiration and ground-water recharge using lysimeter measurement data in Germany, *Hydrol. Process.*, *19*, 3717–3734, doi: 10.1002/hyp.5853.
- Zeng, X., Y. Dai, R. E. Dickinson, and M. Shaikh (1998), The role of root distribution for climate simulation over land, *Geophys. Res. Lett.*, *25*(24), 4533–4536.

Curriculum Vitae

Adriaan Josephus (Ryan) Teuling, 21 mei 1976, Eindhoven

juni 1994

diploma Vrije School Brabant, Eindhoven
inclusief diploma Middelbaar Algemeen Voortgezet Onderwijs (IVO-MAVO)

juni 1995

diploma Voorbereidend Wetenschappelijk Onderwijs (VWO), Dag-/Avondcollege Eindhoven

augustus 1996

propedeuse Bodem, Water en Atmosfeer, Landbouwniversiteit Wageningen (cum laude)

augustus 2002

ingenieurs-diploma Bodem, Water en Atmosfeer, Wageningen Universiteit (cum laude)
specialisatie hydrologie en waterbeheer
afstudeervakken hydrologie en hydraulica

september 2002 – juli 2007

assistent in opleiding, leerstoelgroep Hydrologie en Kwantitatief Waterbeheer, Wageningen Universiteit

maart 2007 – april 2007

technical expert, Department of Hydrology and Water Resources, University of Arizona

augustus 2007 – heden

post doc, Institute of Atmospheric and Climate Science, ETH Zürich
subsidie toegekend door de Nederlandse Organisatie voor Wetenschappelijk Onderzoek (NWO) in het kader van het Rubicon programma

oktober 2007

diploma Netherlands Research School for the Socio-Economic and Natural Sciences of the Environment (SENSE)

belangrijkste activiteiten:

deelname aan de cursus *Uncertainty modelling & analysis* (Wageningen, 2004)

organisatie van de CAHMDA-II international workshop (Princeton, 2004)

deelname aan de cursus *Climate and the hydrological cycle* (Utrecht, 2005)

bezoek aan Institute of Atmospheric and Climate Science ETH (Zürich, 2005)

deelname aan het National Airborne Field Experiment (Melbourne, 2006)

List of publications

- Teuling, A. J., and P. A. Troch (2004), Simulating soil moisture variability dynamics. *Workshop Proceedings, 2nd international workshop on CAatchment-scale Hydrological Modeling and Data Assimilation (CAHMDA)*, 25–27 Oct. 2004, Princeton, NJ, USA.
- Jacobs, C., E. Moors, H. Ter Maat, and A. J. Teuling (2004), Validation of ELDAS products using in situ observations, *Workshop Proceedings, ECMWF/ELDAS workshop on Land Surface Assimilation*, 167–177, 8–11 Nov. 2004, Reading, UK.
- Teuling, A. J., and P. A. Troch (2005), Improved understanding of soil moisture variability dynamics, *Geophys. Res. Lett.*, 32(5), L05404, doi:10.1029/2004GL021935.
- Teuling, A. J., R. Uijlenhoet, and P. A. Troch (2005), On bimodality in warm season soil moisture observations, *Geophys. Res. Lett.*, 32(13), L13402, doi:10.1029/2005GL023223.
- Teuling, A. J., (2005), Aspecten van bodemvochtdynamiek en implicaties voor procesparameterisatie, *Stromingen*, 11(3), 32–36. (in Dutch)
- Teuling, A. J., R. Uijlenhoet, F. Hupet, and P. A. Troch (2006), Impact of plant water uptake strategy on soil moisture and evapotranspiration dynamics during drydown, *Geophys. Res. Lett.*, 33(3), L03401, doi:10.1029/2005GL025019.
- Teuling, A. J., R. Uijlenhoet, F. Hupet, E. E. van Loon, and P. A. Troch (2006), Estimating spatial mean soil moisture from point-scale observations, *Hydrol. Earth Syst. Sci.*, 10(5), 755–767.
- Teuling, A. J., S. J. van Andel, P. A. Troch, and A. J. F. Hoitink (2006), Entropy and river meander planform. *River Flow 2006: Proceedings of the International Conference on Fluvial Hydraulics*, 1137–1146, 6–8 Sept. 2006, Lisbon, Portugal.
- Teuling, A. J., S. I. Seneviratne, C. Williams, and P. A. Troch (2006), Observed timescales of evapotranspiration response to soil moisture, *Geophys. Res. Lett.*, 33(23), L23403, doi:10.1029/2006GL028178.
- Teuling, A. J., F. Hupet, R. Uijlenhoet, and P. A. Troch (2007), Climate variability effects on spatial soil moisture dynamics, *Geophys. Res. Lett.*, 34(6), L06406, doi:10.1029/2006GL029080.
- Teuling, A. J., R. Uijlenhoet, R. Hurkmans, O. Merlin, R. Panciera, J. P. Walker, and P. A. Troch (2007), Dry-end surface soil moisture variability during NAFE'06, *Geophys. Res. Lett.*, 34(17), L17402, doi:10.1029/2007GL031001.
- Troch, P. A., M. Durcik, S. I. Seneviratne, M. Hirschi, A. J. Teuling, R. Hurkmans, and S. Hasan (2007), New datasets to improve terrestrial water storage change estimation. Submitted to *EOS T. Am. Geophys. Un.*
- Jacobs, C. M. J., E. J. Moors, H. W. Ter Maat, A. J. Teuling, G. Balsamo, K. Bergaoui, J. Ettema, M. Lange, B. J. J. M. van den Hurk, P. Viterbo, and W. Wergen (2007), Validation of European Land Data Assimilation System (ELDAS) products using in situ observations. Submitted to *Tellus A*.
- Bogaart, P. W., A. J. Teuling, and P. A. Troch (2007), A state-dependent parameterization for saturated-unsaturated zone interaction. Submitted to *Water Resour. Res.*
- Lyon, S., F. Dominguez, D. Gochis, N. Brunzell, C. Castro, F. Chow, D. Fuka, Y. Hong, P. Kucera, S. Nesbitt, Y. Fan, N. Salzmann, J. Schmidli, P. Snyder, A. Teuling, T. Twine, G. Lee, S. Levis, J. Lundquist, G. Salvucci, A. Sealy, T. Walter (2007), Coupling terrestrial and atmospheric water dynamics to improve prediction in a changing environment. *in preparation*